Temporal Decomposition of EEG into Stimulus- and Response-locked Components

刺激及び反応に時間同期した脳波信号の分離手法の開発

by

Yusuke Takeda

武田　祐輔

Department of Physical and Health Education
Graduate School of Education
The University of Tokyo

Acknowledgements

I would like to express my sincere appreciation of Professor Yoshiharu Yamamoto for supervising me throughout my graduate studies. He constantly and patiently encouraged me to complete my studies, made many constructive comments and provided much theoretical input on a wide range. I greatly appreciate all the help from him. I would also like to thank him for carefully reading this thesis and making many valuable comments on writing in English, as well as on research.

I would like to thank Associate Professor Gentaro Taga for supervising me during my graduate studies. He made many valuable comments and suggestions about my studies.

I would like to thank Associate Professor Daichi Nozaki for supervising me during my graduate studies. He gave me with much theoretical advice, and improved my studies considerably.

I would also like to thank Assistant Professor Kentaro Yamanaka for supervising me throughout my graduate studies. He always gave me much valuable advice, encouraged me to study diligently, and taught me many things about research: how to make a research plan, conduct experiments, analyse experimental data, write a paper, and submit it. I greatly appreciate all the help from him. I would also like to thank him for carefully reading this thesis and making many valuable comments.

I would like to thank all the other staff at the laboratory, Professor Yoshiteru Muto, Professor Shigeru Kitazawa, Associate Professor Mitsuaki Shibawaka, Associate Professor Zbigniew R. Struzik, and Assistant Professor Rika Soma, for their support in my graduate studies.

I would like to thank Dr. Ken Kiyono of Nihon University and Dr. Ryoya Saji of Tamagawa University for teaching me physics and mathematics, and making many valuable comments on

my studies.

Thanks also to my colleagues at the laboratory, especially Mr. Takatsugu Aihara and Mr. Tsuyoshi Ikegami, for discussing various problems of academic life with me.

Finally, I thank my family for all of the long-term support they have given to me, visible and invisible.

Contents

Chapter 1

Introduction

1.1 Motivation

In our daily life, we make two types of responses to sensory stimuli. One is an externally observable "overt" response, which is executed by muscular activity. The other is an externally unobservable "covert" response, which occurs only within the brain. For example, let us imagine that you are driving a car. You approach some traffic lights, and the light turns red. Then, you push down the brake pedal. In this case, it is considered that you make an "overt" response to the visual stimulus of the traffic light by pushing the brake pedal. On the other hand, let us imagine that you are climbing a mountain. You reach the top and view a beautiful landscape. Then, you feel "Great!". In this case, it is considered that you make a "covert" response to the visual stimulus of the beautiful landscape by feeling "Great!".

It is considered that the responses, pushing the brake pedal and feeling "Great!" occur with variable delays after the onset of sensory stimuli. In this thesis, therefore, I define a "response" as an event which involves a fixed brain activity and of which delays after stimulus onsets fluctuate with every response. Note that not all events driven by a stimulus are referred to as "responses" in this thesis, although they are in a broad sense. For example, stimulus-locked changes in the brain activity are not referred to as "responses". Further, I divide responses into "overt responses" and "covert responses" according to whether the responses are observable or not. Pushing the brake pedal is categorized as an "overt response", because the response, pushing the pedal, is

observable. Feeling "Great!" is categorized as a "covert response", because the response, the feeling, covertly occurs in the brain and is not observable.

In brain research, what should be examined in such stimulus-response situations is how the brain operates during the time period from a stimulus onset to a response onset. Because there are two events, receiving a stimulus and making a response, it is considered that the two kinds of brain processes occur, related to the two events respectively. For example, in the case of pushing the brake pedal, the brain process related to looking at the traffic light (stimulus-related activity) and that related to pushing the pedal (response-related activity) occur. To examine such brain activity in detail, we need to separate the stimulus- and response-related activity and examine the two activities separately. By separating the brain activities, we can identify which activity is responsible for different response patterns, e.g., reaction times (RTs), in different situations. To separate the brain activity, we need data analysis methods to decompose brain signals, such as an electroencephalography (EEG) signal, into stimulus- and response-related components.

This thesis deals with data analysis methods which decompose brain signals into the stimulus- and response-related components.

1.2 EEG as Target Signal

The target signals of my analysis are human scalp EEG signals, and I propose methods for decomposing EEG data.

Electroencephalography (EEG) is a non-invasive neurophysiologic measurement of the electrical activity of the brain recorded from electrodes placed on the scalp. Electroencephalography represents a summation of post-synaptic potentials from a large number of neurons under the electrodes. Electroencephalography has the limitation of poor spatial resolution. This is because the meninges, cerebrospinal fluid and the skull smear the EEG signal and obscure its intracranial source. On the other hand, the advantage of EEG is its high time resolution (on the level of a single millisecond). This advantage is due to the fact that EEG measures the brain's electrical activity directly. Other methods of looking at brain activity, such as positron emission tomogra-

phy (PET) and functional magnetic resonance imaging (fMRI), have lower time resolutions (on the level of seconds and minutes), because these methods record changes in metabolic activity (e.g., PET) or blood flow (e.g., fMRI), which are indirect markers of brain electrical activity. The high time resolution of EEG makes it possible to investigate rapid changes in the brain activity. Because the interval between a stimulus and a response is usually shorter than 1 s, EEG is a suitable measure for investigating the brain activity during a stimulus-response situation.

In order to propose methods for decomposing EEG into the stimulus- and response-related components, we need to know how the stimulus- and response-related brain activities appear in the EEG. Figure 1.1 shows a color-coded representation of the EEG potentials at the midline-central electrode (Cz) during a simple reaction time task in which human subjects were instructed to press a button as soon as possible after beeps (described in Chapter 4). In this figure, the EEG epochs are sorted in the order of RTs, and the stimulus and response onsets are represented by solid and dotted lines respectively[1]. Two types of fluctuations appear in this image (see also

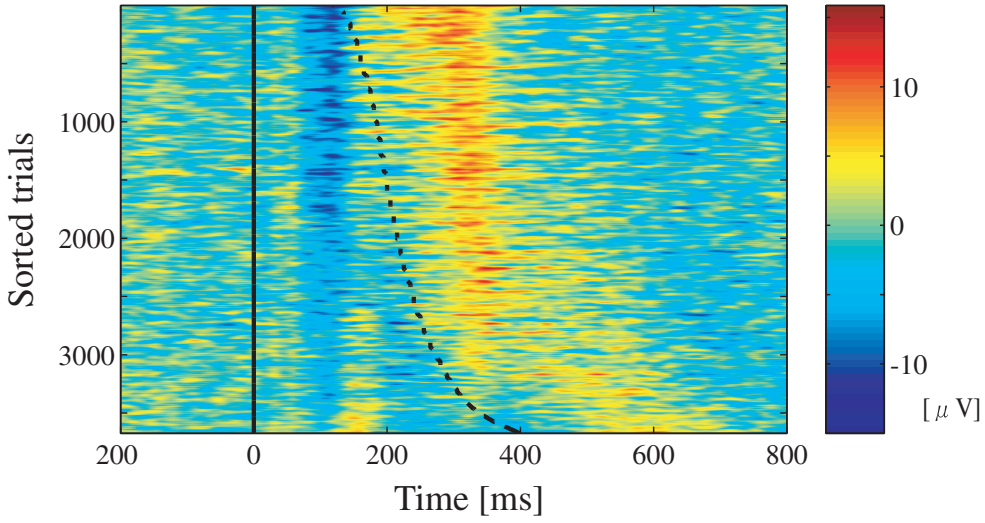

Figure 1.1: Time-trial image of EEG during a simple reaction time task. The solid line represents stimulus onsets, and the dotted line represents the response onsets.

Fig. 2.6, A). One is fluctuations parallel to the stimulus onsets (stimulus-locked fluctuations),

[1]In this thesis, I refer to this kind of image as a time-trial image.

and the other is fluctuations parallel to the response onsets (response-locked fluctuations). This indicates that the stimulus- and response-related brain activity respectively appear in stimulus- and response-locked ways. Further, the stimulus- and response-locked fluctuations are overlapping in the trials with fast RTs. This indicates that the stimulus- and response-related brain processes can be temporally overlapping.

To summarize these observations, stimulus- and response-related EEG activities are respectively stimulus- and response-locked, and these two EEG activities can be temporally overlapping. Therefore, to separate the stimulus- and response-related EEG activities, we need to propose methods for temporally decomposing EEG into the stimulus- and response-locked components. The schematic representation of the EEG activity in a stimulus-response situation is shown in Fig. 1.2.

1.3 Proposed Methods

In this thesis, I propose two methods for decomposing EEG into stimulus- and response-locked components, and the two methods are used when responses are overt and covert respectively.

When responses are overt, the stimulus- and overt response-locked components have conventionally been extracted by averaging EEG epochs with respect to either stimulus or overt response onset to increase the signal to noise ratio. However, when the two components are temporally overlapping, the conventional stimulus- or overt response-triggered average EEG does not reflect exactly pure stimulus- or overt response-locked brain activity, because, by the averaging procedure, each component is contaminated by the other component. Here, I propose a method to extract the uncontaminated stimulus- and overt response-locked components. In this method, the two components are extracted from single-channel EEG epochs and RTs using a discrete Fourier transform.

When responses are covert, conventionally, only the stimulus-locked component has been extracted by the averaging procedure. This is because the onset of the covert response-locked component is unknown, and the response-triggered averaging procedure, or even the above-mentioned

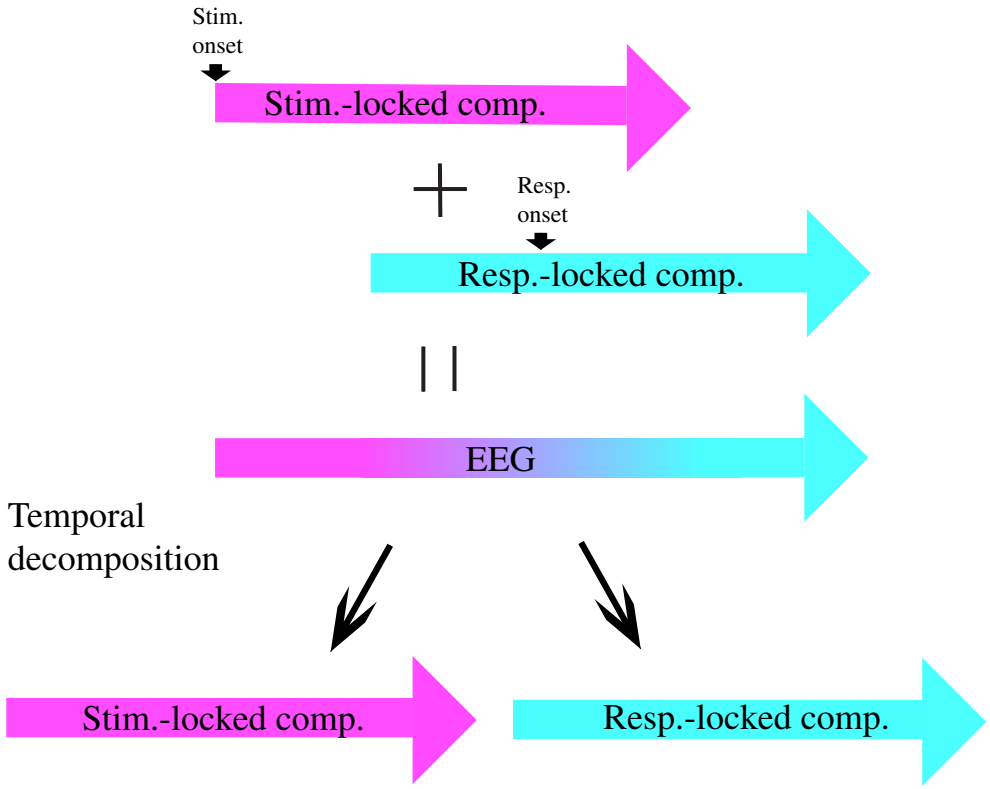

Figure 1.2: Schematic representation of the EEG including the stimulus- and response-locked components. I propose methods for temporally decomposing the EEG into the two components.

method for overt responses, cannot be used. Here, I propose a method to obtain the stimulus-locked component, the covert response-locked component and its delays of individual trials only from single-channel EEG epochs. In this method, I estimate the delays of the covert response-locked component, and extract the two components simultaneously using the above method for overt responses.

1.4 Organization of Thesis

The organization of this thesis is as follows.

In Chapters 2–4, I deal with the decomposition of EEG into the stimulus- and overt response-locked components. In Chapter 2, I introduce previous reports on the brain activity during tasks which require overt responses, and discuss the previous methods for extracting the stimulus- and overt response-locked components. In Chapter 3, I propose a method for decomposing EEG into stimulus- and overt response-locked components by using RTs, and examine the performance of the proposed method by two types of simulation tests with artificial and EEG data. In Chapter 4, I apply the proposed method to the EEG during a simple reaction time task, and examine the contamination by the conventional averaging procedure.

In Chapters 5–7, I deal with the decomposition of EEG into the stimulus- and covert response-locked components. In Chapter 5, I introduce previous reports on the brain activity during the cognitive tasks which induce covert responses, and discuss the previous methods for extracting the covert response-locked component. In Chapter 6, I propose a method for estimating the delays of the covert response-locked component and decomposing EEG into the stimulus- and covert response-locked components, and examine the performance of the method by two types of simulation tests with artificial and EEG data. In Chapter 7, I apply the proposed method to the EEG during NoGo trials of a Go/NoGo task.

In Chapter 8, I summarize the proposed methods and the presented results, and discuss the further development of the proposed methods.

1.5 Glossary

Stimulus-locked component: The EEG component time-locked to stimulus onsets.

Overt response-locked component: The EEG component time-locked to overt response onsets.

Covert response-locked component: The EEG component which has a fixed waveform and of which the delay fluctuates from trial to trial.

Method for overt responses: The proposed method for obtaining the stimulus- and overt response-locked components from EEG epochs and RTs.

Method for covert responses: The proposed method for obtaining the stimulus-locked component, the covert response-locked component and its delays of individual trials from EEG epochs.

Simple reaction time task: A reaction time task in which a specified overt response is required on the presentation of a stimulus.

Go/NoGo task: A choice reaction time task in which a specified overt response is required on the presentation of a "Go" signal (Go trial) but is not to a "NoGo" signal (NoGo trial).

Some of the studies in this thesis are based on papers, published or in press, as below:

1. Takeda, Y., Yamanaka, K., Yamamoto, Y., 2008. Temporal decomposition of EEG during a simple reaction time task into stimulus- and response-locked components. NeuroImage 39, 742-754.

2. Takeda, Y., Yamanaka, K., Nozaki, D., Yamamoto, Y., 2008. Extracting a stimulus-unlocked component from EEG during NoGo trials of a Go/NoGo task. NeuroImage (in press).

Chapter 2

EEG during Tasks with Overt Responses

In this chapter, I firstly introduce reports on the brain activity during tasks which require overt responses (i.e., reaction time tasks). Then, based on the reports, I mathematically formulate the EEG during the reaction time tasks. Finally, I discuss the previous methods for extracting the stimulus- and overt response-locked components from the EEG, and discuss the necessity of a novel method for extracting the two components.

2.1 Brain Activity during Tasks with Overt Responses

The brain activity during the period from a stimulus presentation to an overt response was examined in cats, monkeys and humans by using various reaction time tasks, and the stimulus-locked activity and/or the overt response-locked activity was observed [1–5].

As expected, the stimulus-locked activity was observed from the sensory cortex. For example, Nelson [2] investigated single unit activity in the somatosensory cortex in monkeys during a paradigm with wrist movements in response to vibration of their hands, and showed that some neurons exhibit the stimulus-locked activities (Fig. 2.1).

The overt response-locked activity was observed from the motor cortex. For example, Tanji and Kurata [5] investigated single unit activity in the precentral motor cortex in monkeys during a paradigm with wrist extension in response to three types of stimuli: visual, auditory and tactile

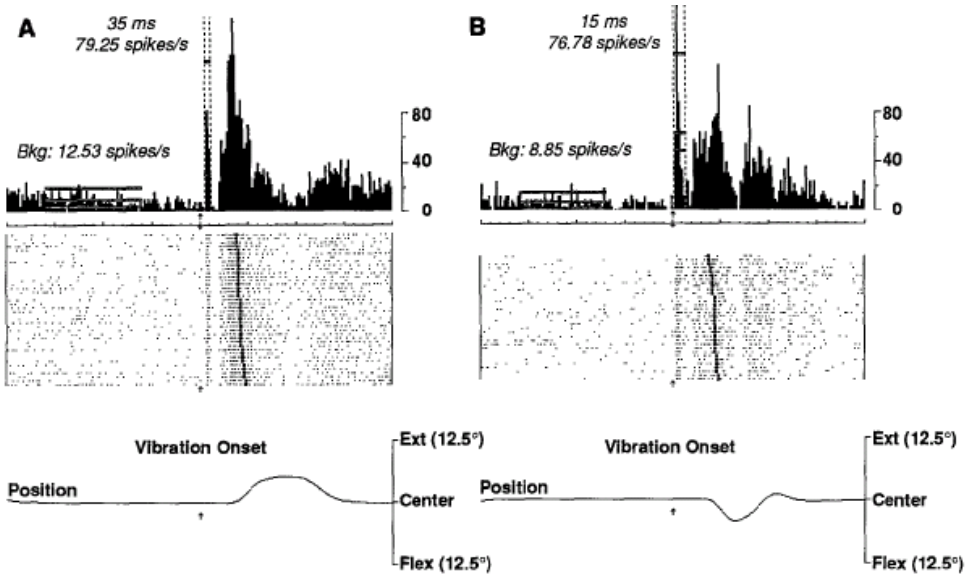

Figure 2.1: Activity of an area 3b QA neuron (A) and an area 1 QA neuron (B) showing the stimulus-locked activity. The activity of the neurons is presented as histograms (top) and raster plots (bottom). Discharges are aligned at the onset of the vibratory cue and ordered by reaction times (dark marks in the raster plots signify movement onset). (Adapted from [2])

stimuli. They showed that some neurons exhibit similar response-locked activities regardless of the modality of the sensory stimuli (Fig. 2.2).

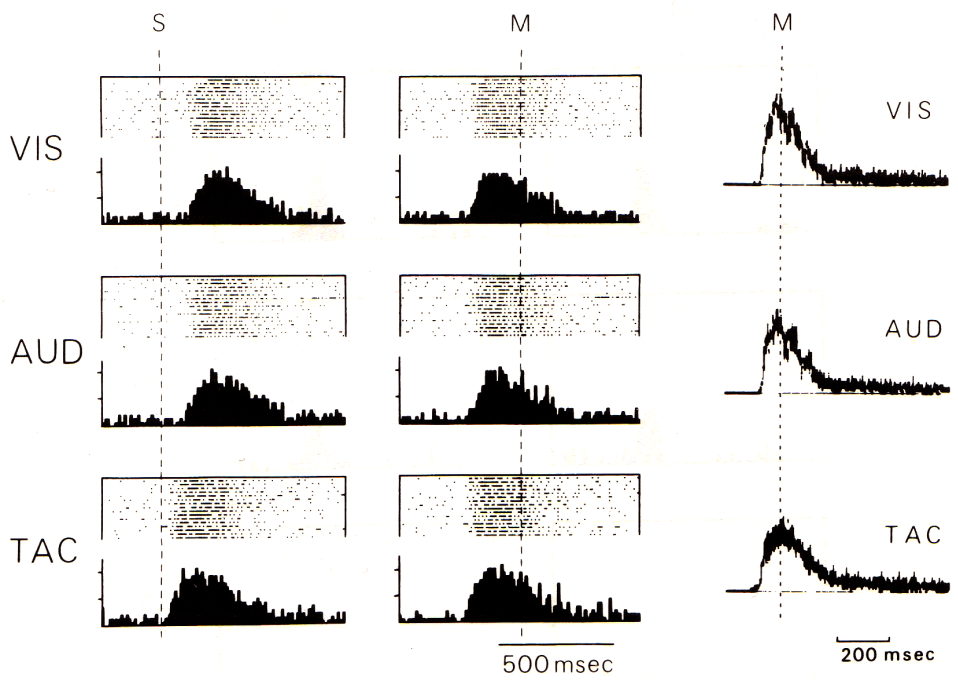

Figure 2.2: Activity of a neuron showing response-locked activities. In the left and middle columns of this figure, the activities of the neuron are presented as a raster histogram. **Left column**: Discharges are aligned at the onset of visual, auditory, and tactile stimuli (indicated with a dotted line labeled S). **Middle column**: Discharges are aligned at the onset of the wrist extension movement (indicated with a dotted line labeled M). **Right column**: EMG activity recorded from m. extensor carpi radialis. (Adapted from [5])

On the other hand, there are reports showing that the same neurons exhibit both stimulus- and overt response-locked activities. For example, Pefiliev [4] investigated single unit activity in the forelimb area of the motor cortex (area 4γ) in cats during target-reaching with the contralateral limb for a morsel of food, and showed that some neurons exhibit both stimulus- and overt response-locked activities (Fig. 2.3).

These reports indicate that the stimulus- and overt response-locked brain activities occur during tasks which require overt responses, and further that, in some cases, the same neuron

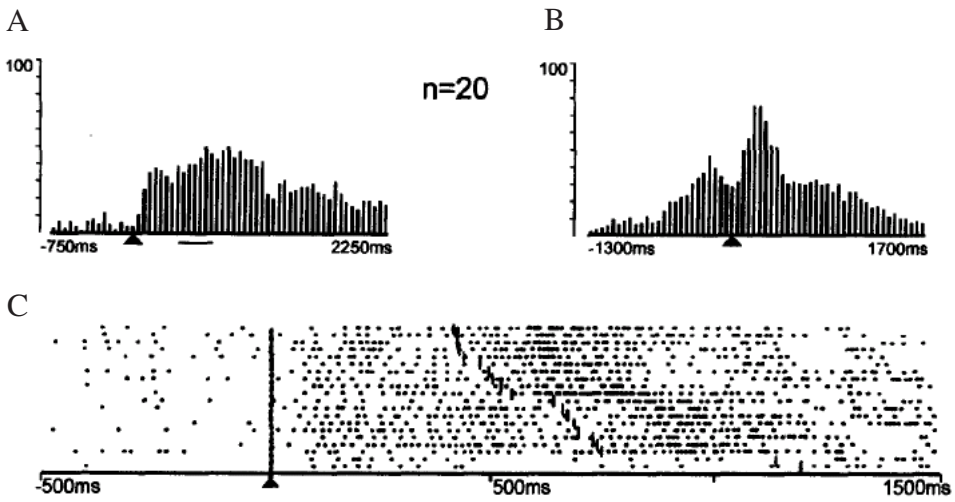

Figure 2.3: Activity of a neuron clearly showing two components in relation to target-reaching. **A**: Histogram which is aligned with the stimulus onset indicated by a triangle. The horizontal line below the histogram indicates the range of the response onsets. **B**: Histogram which is aligned with the response onset indicated by a triangle. The activity of the cell is presented as a raster histogram (**C**), where each dot indicates one spike and each line one trial. The trials are arranged in the order of increasing RTs indicated by short vertical lines and aligned with the stimulus onset (triangle). (Adapted from [4])

exhibits both of the two activities.

By using EEG or magnetoencephalography (MEG), human brain activities during reaction time tasks have been examined non-invasively, and the stimulus- and overt response-locked components have been observed [6–9]. For example, Jung et al. [7] spatially decomposed the multichannel EEG during a choice reaction time task using independent component analysis (ICA) [10], and showed some stimulus- and overt response-locked independent components (Fig. 2.4).

From the above reports, it is considered that the human scalp EEG during tasks with overt responses includes the stimulus- and overt response-locked components, and that both of the components are spatially overlapping. Because of the spatial overlapping, the two components are temporally overlapping when intervals between stimulus and response onsets are short.

2.2 Mathematical Formulation

Here, let me mathematically formulate the EEG during tasks which require overt responses. By formulating the EEG, we can consider the problem in its simplest form. As a result, I can clearly describe the limitations of the previous methods for extracting the stimulus- and overt response-locked components, and can propose a novel method for the extraction by simple mathematical operations as shown in Chapter 3.

It is reported that brain activity during a reaction time task consists of stimulus-locked activity, overt response-locked activity shifted by the RT of an individual trial, and noise. Therefore, observed single-channel EEG data during a reaction time task can be expressed by:

$$y_n(t) = s(t) + or(t - \tau_n) + v_n(t) \quad (t = 0, \cdots, T-1;\ n = 1, \cdots, N), \tag{2.1}$$

where $y_n(t)$: observed EEG data in trial n; $s(t)$: stimulus-locked component; $or(t)$: overt response-locked component; τ_n: RT in trial n; $v_n(t)$: noise in trial n. This implies that ongoing EEG activity and trial-to-trial variability of stimulus- and overt response-locked activity are included in $v_n(t)$.

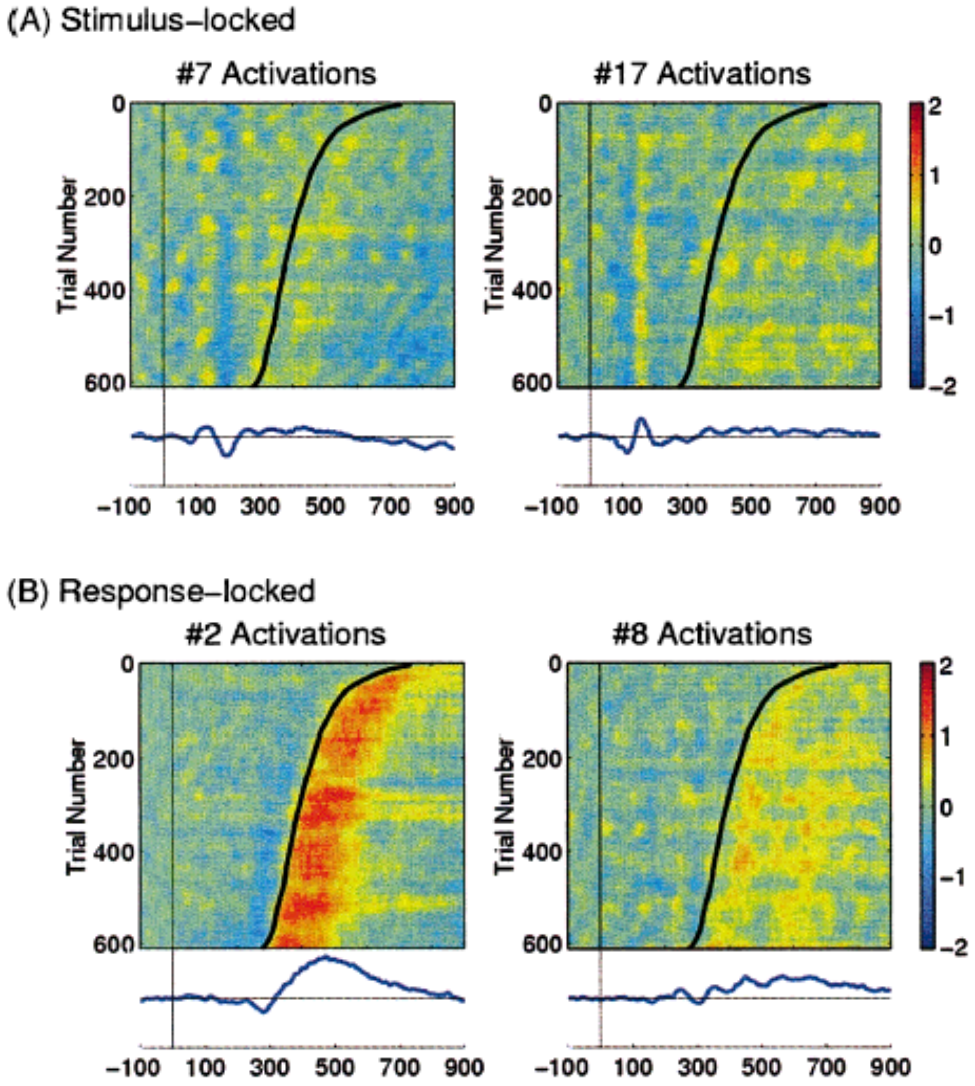

Figure 2.4: Stimulus-locked independent components and overt response-locked independent components obtained by ICA. **A**: Time-trial images of stimulus-locked independent components. **B**: Time-trial images of overt response-locked independent components. Thin vertical lines represent stimulus onsets, and thick oblique lines represent response onsets. (Adapted from [7])

2.3 Previous Methods

2.3.1 Stimulus-/Overt Response-triggered Averaging Procedure

Conventionally, the stimulus- and overt response-locked components have been extracted by averaging EEG epochs with respect to either stimulus or overt response onset to increase the signal to noise ratio. Indeed, when the EEG includes either the stimulus- or overt response-locked component, the averaging procedure is a suitable means. However, when the EEG includes both the two components and these are temporally overlapping, the conventional stimulus- or overt response-triggered average EEG is not appropriate. This is because, by the averaging procedure, the stimulus-/overt response-locked component is contaminated by the other component. With the contamination, the peak amplitudes and latencies in the stimulus-/overt response-triggered average EEG become more or less different from the original stimulus-/overt response-locked component, leading to wrong conclusions about the stimulus/overt response-locked brain activity. Figure 2.5 is a simulation result showing how the contamination occurs in the stimulus-/overt response-triggered average EEG. The waveform of the stimulus-triggered average in the late part is different from that of the stimulus-locked component, indicating that the contamination is large in the late part of the stimulus-triggered average (Fig. 2.5, C, indicated by the arrow). The waveform of the overt response-triggered average in the early part is different from that of the overt response-locked component, indicating that the contamination is large in the early part of the overt response-triggered average (Fig. 2.5, D, indicated by the arrow).

The contamination effects in the stimulus-/overt response-triggered average EEG are quantitatively described as follows. Under the assumption of Eq. (2.1), the stimulus-triggered average EEG $\bar{y}_s(t)$ is expressed by:

$$\bar{y}_s(t) = s(t) + \frac{1}{N}\sum_{\tau=0}^{t} h(\tau) or(t-\tau) + \frac{1}{N}\sum_{n=1}^{N} v_n(t), \tag{2.2}$$

where $h(\tau)$ represents the distribution of RTs. In this equation, the contamination by the overt response-locked component is expressed by $1/N \sum_{\tau=0}^{t} h(\tau) or(t-\tau)$. Similarly, the overt response-

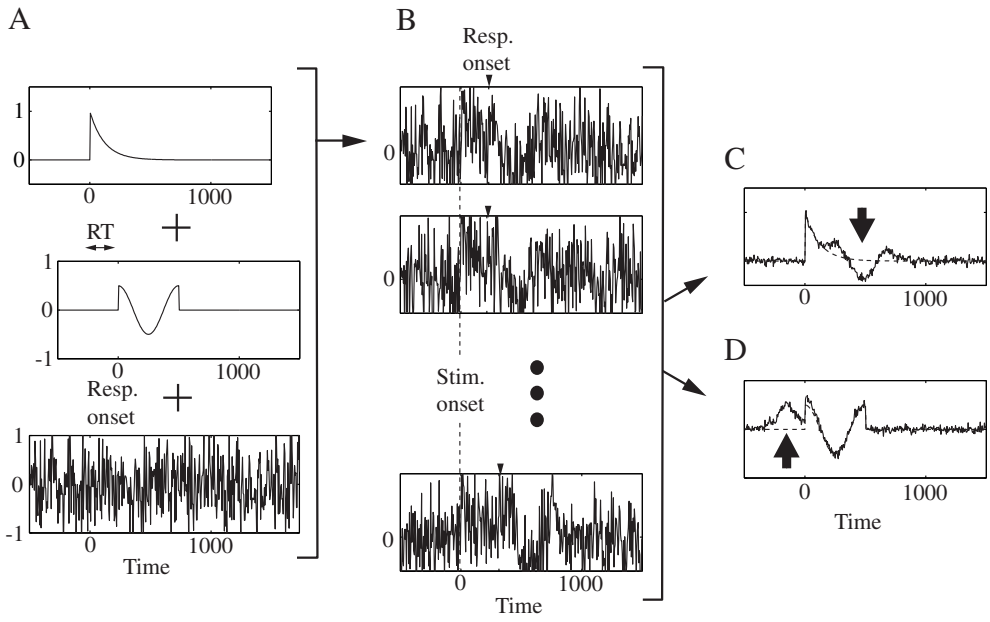

Figure 2.5: Simulation with artificial data. **A**: Original stimulus-locked component (top), overt response-locked component (middle), and noise (bottom). **B**: Simulated data obtained by Eq. (2.1) using the real RTs of a simple reaction time task (described in Chapter 4). **C**: Stimulus-triggered average of the simulated data (solid line) and the original stimulus-locked component (dotted line). **D**: Overt response-triggered average of the simulated data (solid line) and the original overt response-locked component (dotted line). Arrows in **C** and **D** indicate the parts around which the contamination occurs.

triggered average EEG $\bar{y}_{or}(t)$ is expressed by:

$$\bar{y}_{or}(t) = or(t) + \frac{1}{N}\sum_{\tau=0}^{T-t-1} h(\tau)s(t+\tau) + \frac{1}{N}\sum_{n=1}^{N} v_n(t+\tau_n), \tag{2.3}$$

and in this equation the contamination by the stimulus-locked component is expressed by $1/N\sum_{\tau=0}^{T-t-1} h(\tau)s(t+\tau)$. Obviously, the terms for the contamination include stimulus- and overt response-locked components, indicating that we need these components to identify the level of the contamination. In other words, whether the contamination is large or small should be unclear only from the contaminated average EEG.

When the effect of the contamination is unclear, we cannot distinguish whether different waveforms of the stimulus/overt response-triggered average EEG in different task conditions are attributable to the difference in the level of the contamination due to a change in the RTs or to the difference in the stimulus/overt response-locked EEG activity itself. Therefore, we cannot discuss the brain activity in detail from the stimulus/overt response-triggered average EEG.

2.3.2 Spatial Decomposition

Other methods for extracting the stimulus- and overt response-locked components have been spatial decompositions by principal component analysis (PCA) [11] and ICA [7,12]. For example, as mentioned above, Jung et al. [7] spatially decomposed the EEG during a choice reaction time task into the stimulus- and the overt response-locked independent components by ICA (Fig. 2.4). The PCA and ICA are computational methods for decomposing multi-channel data into orthogonal components or independent components respectively [13,14]. Therefore, to decompose EEG data into the two components by PCA or ICA, the EEG needs to satisfy the following two conditions.

1. Time series of stimulus- and overt response-locked components are orthogonal (for PCA) or independent (for ICA).

2. Stimulus- and overt response-locked components have different scalp distributions.

Unless the condition 1 is satisfied, obviously, PCA/ICA should not separate the stimulus- and overt response-locked components. Considering that RTs are not distributed uniformly but

within a fixed range after stimulus onsets, the overt response-locked components tend to occur at a certain phase of the stimulus-locked components. This indicates that the occurrences of the two components tend to be correlated and the time series of the two components also tend to be correlated; that is, condition 1 is rarely satisfied.

Further, unless condition 2 is satisfied, PCA/ICA should not separate the stimulus- and overt response-locked components. This is because PCA/ICA does not distinguish components attributable to the same sources. In animal studies, as mentioned above, the same neurons in the sensory and motor cortices exhibit both the stimulus- and overt response-locked activities, indicating that the sources of the stimulus- and overt response-locked activities are the same in some cases. Of course, these reports do not directly lead to the same scalp distributions of human scalp EEG signals. Nevertheless, these reports suggest that EEG does not always satisfy condition 2.

To sum up, we cannot guarantee that EEG always satisfies the two conditions, indicating that PCA/ICA does not always separate the stimulus- and overt response-locked components. In fact, I applied ICA to the EEG during the auditory simple reaction time task (described in Chapter 4), and found that some independent components exhibited both the stimulus- and overt response-locked fluctuations in their time-trial images (Fig. 2.6), indicating that ICA was not able to separate the two components completely.

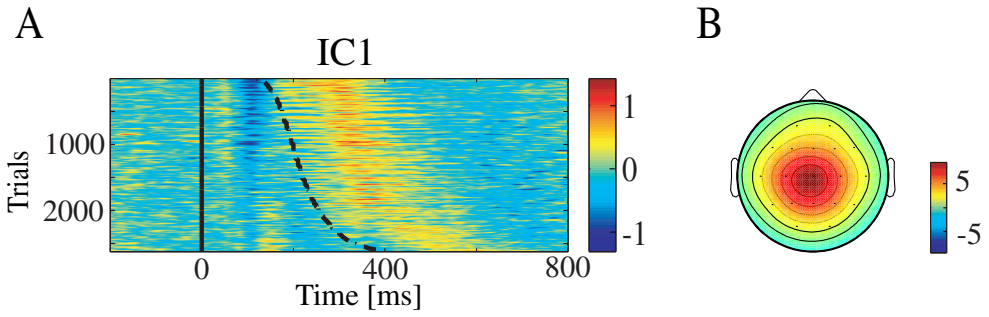

Figure 2.6: An independent component (IC1) exhibiting both the stimulus- and overt response-locked fluctuations. **A**: Time-trial image of IC1. Solid line represents stimulus onsets, and dotted line represents overt response onsets. **B**: Scalp distribution of IC1.

2.4 Conclusions

From previous reports, it is shown that the EEG during tasks which require overt responses consists of the stimulus- and overt response-locked components. To extract the two components, the stimulus-/overt response-triggered averaging procedure and the spatial decomposition methods (PCA and ICA) have been used. However, these methods are not adequate. Therefore, it is necessary to propose a novel method which can always be used for extracting the uncontaminated stimulus- and overt response-locked components. In the next chapter, I propose such a method for the extraction.

Chapter 3

Proposed Method for Overt Responses

In the previous chapter, I describe the necessity of a novel method for temporally decomposing EEG into the stimulus- and overt response-locked components. In this chapter, therefore, I propose a method for the temporal decomposition. We can consider two types of methods for the decomposition; parametric methods and non-parametric methods. With parametric methods, parametric models for the stimulus- and overt response-locked components are assumed and identified. With non-parametric methods, the stimulus- and overt response-locked components are extracted without the assumption of parametric models for these components. In this thesis, I propose a non-parametric method, because the non-parametric method does not need a priori knowledge of parametric models themselves, in contrast to the parametric method, and is better than the parametric method.

3.1 Decomposition Method

I assume that the EEG activity consists of the stimulus- and overt response-locked components, and is expressed by Eq. (2.1). Here, the objective is to obtain $s(t)$ and $or(t)$ from $y_n(t)$ and τ_n $(n = 1, \cdots, N)$ (Fig. 3.1).

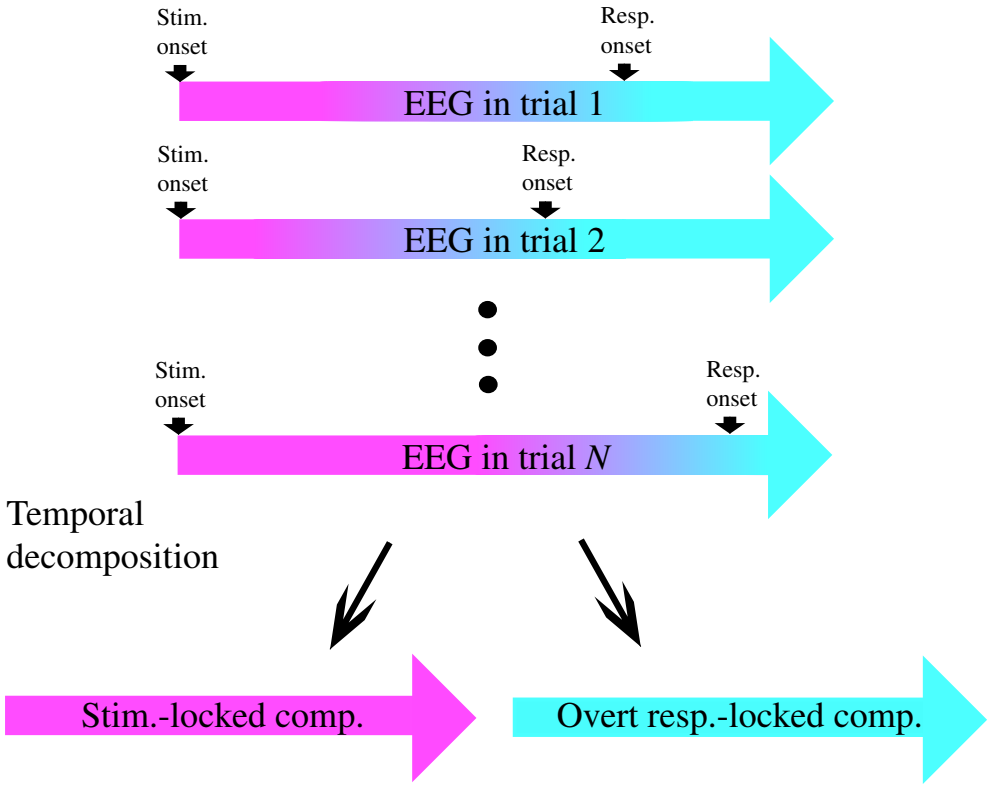

Figure 3.1: Schematic representation of the objective

By taking the discrete Fourier transform of Eq. (2.1), I obtain:

$$Y_n(\omega) = S(\omega) + \exp(-i2\pi\omega\tau_n/T)OR(\omega) + V_n(\omega) \quad \omega = 0, \cdots, T-1 \ , \tag{3.1}$$

where $Y_n(\omega)$ is the discrete Fourier transform of $y_n(t)$; $S(\omega)$ is the discrete Fourier transform of $s(t)$; $OR(\omega)$ is the discrete Fourier transform of $or(t)$; $V_n(\omega)$ is the discrete Fourier transform of $v_n(t)$. Note that the last τ_n points in $or(t)$ should be zero, because the phase shift in the Fourier domain is equal to the circular shift in the time domain. By averaging Eq. (3.1) across n, I obtain:

$$\bar{Y}(\omega) = S(\omega) + \bar{E}(\omega)OR(\omega) + \bar{V}(\omega) \ , \tag{3.2}$$

where

$$\bar{Y}(\omega) = \frac{1}{N}\sum_{n=1}^{N} Y_n(\omega); \tag{3.3}$$

$$\bar{E}(\omega) = \frac{1}{N}\sum_{n=1}^{N} \exp(-i2\pi\omega\tau_n/T); \tag{3.4}$$

$$\bar{V}(\omega) = \frac{1}{N}\sum_{n=1}^{N} V_n(\omega). \tag{3.5}$$

By solving Eqs. (3.1) and (3.2) simultaneously for $S(\omega)$ and $OR(\omega)$, I obtain:

$$\frac{\exp(-i2\pi\omega\tau_n/T)\bar{Y}(\omega) - \bar{E}(\omega)Y_n(\omega)}{\exp(-i2\pi\omega\tau_n/T) - \bar{E}(\omega)} = S(\omega) + \frac{\exp(-i2\pi\omega\tau_n/T)\bar{V}(\omega) - \bar{E}(\omega)V_n(\omega)}{\exp(-i2\pi\omega\tau_n/T) - \bar{E}(\omega)}; \tag{3.6}$$

$$\frac{Y_n(\omega) - \bar{Y}(\omega)}{\exp(-i2\pi\omega\tau_n/T) - \bar{E}(\omega)} = OR(\omega) + \frac{V_n(\omega) - \bar{V}(\omega)}{\exp(-i2\pi\omega\tau_n/T) - \bar{E}(\omega)}. \tag{3.7}$$

To prevent the denominators of Eqs. (3.6) and (3.7) from being zero, I use a function $D(n,\omega)$ instead of $\exp(-i2\pi\omega\tau_n/T) - \bar{E}(\omega)$,

$$D(n,\omega) = \begin{cases} c & \omega = 0 \\ \exp(-i2\pi\omega\tau_n/T) - \bar{E}(\omega) & \omega \neq 0 \end{cases}, \tag{3.8}$$

where c represents a constant number. By calculating Eq. (3.9) or (3.10) (see below) and from simulation results (see Appendix A), I find that only the average of extracted components depends on the parameter c. So we can set c arbitrarily. In this study, I set c to unity.

Then, by averaging across n and taking the inverse discrete Fourier transform (IDFT), I obtain:

$$\mathrm{IDFT}\left(\frac{1}{N}\sum_{n=1}^{N}\frac{\exp\left(-i2\pi\omega\tau_n/T\right)\bar{Y}\left(\omega\right)-\bar{E}(\omega)Y_n\left(\omega\right)}{D(n,\omega)}\right)$$
$$=s\left(t\right)+\mathrm{IDFT}\left(\frac{1}{N}\sum_{n=1}^{N}\frac{\exp\left(-i2\pi\omega\tau_n/T\right)\bar{V}\left(\omega\right)-\bar{E}(\omega)V_n\left(\omega\right)}{D(n,\omega)}\right)+c_s; \quad (3.9)$$

$$\mathrm{IDFT}\left(\frac{1}{N}\sum_{n=1}^{N}\frac{Y_n\left(\omega\right)-\bar{Y}\left(\omega\right)}{D(n,\omega)}\right)=or\left(t\right)+\mathrm{IDFT}\left(\frac{1}{N}\sum_{n=1}^{N}\frac{V_n\left(\omega\right)-\bar{V}\left(\omega\right)}{D(n,\omega)}\right)+c_r, \quad (3.10)$$

where c_s and c_r represent the shifts of the averages by $D(n,\omega)$.

Equations (3.9) and (3.10) show that $s(t)$ or $or(t)$ plus a noise term can be obtained by calculating the left-hand side of Eq. (3.9) or (3.10). The noise terms converge to zero as N increases, because the average of $V_n(\omega)$ converges to zero as N increases, whereas $D(n,\omega)$ varies depending on τ_n regardless of N. Let me refer to the real parts of the left-hand sides of Eqs. (3.9) and (3.10) as the extracted stimulus-locked component and the extracted overt response-locked component respectively.

Before applying the decomposition method, we need to set the parameters l_0, the number of data points before stimulus and overt response onset, and l_1, the number of data points after stimulus and overt response onset. We need to set l_1 to be adequately long so that the last data points in $or(t)$, which must be longer than the maximum τ_n, will be the baseline. In this study, I set l_0 to 100 and l_1 to 300, which correspond with 500 ms and 1500 ms respectively if the sampling rate is 200 Hz.

The Matlab codes for this decomposition method are available at: "www.p.u-tokyo.ac.jp/~takeda/decomp/".

3.2 Simulation with Artificial Data

In order to verify the performance of the proposed method, a numerical experiment was performed on a set of known artificial signals.

3.2.1 Methods

In this simulation, the original stimulus- and overt response-locked components were generated by the exponential and the cosine functions respectively. The RTs, which were randomly selected from all the subjects' RTs of the simple reaction time task (described in Chapter 4), were used as τ_n ($n = 1, \cdots, N = 100$), and white noise [standard deviation (SD) = 0.5] was used as $v_n(t)$ (Fig. 3.2, A). The simulated data $y_n(t)$ was generated from $s(t)$, $or(t)$, τ_n and $v_n(t)$ according to Eq. (2.1) (Fig. 3.2, B). Then, I extracted the stimulus- and overt response-locked component by Eqs. (3.9) and (3.10) respectively. The similarity of the extracted and original components was quantified by calculating the correlation coefficient between these two waveforms.

Further, to evaluate the residual errors between the extracted and original stimulus-/overt response-locked components, I repeated the above procedure 500 times using different sets of white noise and τ_n. The averages of the residual errors across time were adjusted to zero. To examine whether the residual errors fluctuate randomly around zero, the time courses of the mean and SD of the 500 residual errors were plotted (Fig. 3.3, B1, C1). To examine the frequency characteristics of the residual errors (Fig. 3.3, B1, C1), I calculated the amplitude spectrum (Fig. 3.3, B2, C2):

$$AP(\omega) = \frac{1}{500} \sum_{p=1}^{500} |RE_p(\omega)|, \tag{3.11}$$

where $RE_p(\omega)$ represents the Fourier transform of the p-th residual error re_p of the 500 repetitions. Finally, I examined how the noise level in the extracted stimulus-/overt response-locked components decreased as the number of trials increased (Fig. 3.3, B3, C3). The noise level $NL(N)$ was obtained by calculating the variance of the residual error as follows:

$$NL(N) = \frac{1}{500} \sum_{p=1}^{500} \left[\frac{1}{T-1} \sum_{t=0}^{T-1} re_{p,N}(t)^2 \right], \tag{3.12}$$

where $re_{p,N}(t)$ represents the p-th residual error obtained from the simulation data consisting of N trials. The variance was fitted by a function $y = a/x$ by the least square method. Further, in order to compare the noise level in the component obtained by the proposed method with that by the averaging procedure, the noise used in the above repeated simulations was simply averaged

across trials, and examined in the same manner as the residual errors (Fig. 3.3, A1–3).

By comparing the parameter a of the fitting function of the extracted components with that of the averaged noise, we can estimate the number of trials the proposed method needs in order to achieve the same noise level as the averaging procedure. Let me refer to the coefficient a obtained from the extracted component as a_c, and that obtained from the averaged noise as a_n. The equality of the variance of the residual errors to that of the averaged noise leads to the following equation:

$$\frac{a_c}{x_c} = \frac{a_n}{x_n}, \tag{3.13}$$

where x_c and x_n represent the number of trials used for the decomposition and the averaging respectively. Eq. (3.13) can be rewritten as:

$$x_c = \frac{a_c}{a_n} x_n. \tag{3.14}$$

Eq. (3.14) means that the decomposition method requires a_c/a_n times as many trials as the averaging procedure in order to achieve the same noise level.

3.2.2 Results

I extracted the original components used for the simulation with the artificial data from the simulated data (Fig. 3.2). The extracted and original stimulus-locked components are highly correlated [$r_s = 0.93$ (r_s: the correlation coefficient between the extracted and original stimulus-locked components)], as are the extracted and original overt response-locked components [$r_r = 0.90$ (r_r: the correlation coefficient between the extracted and original overt response-locked components)] (Fig. 3.2, C).

Figure 3.3 shows the detailed property of the residual errors between the extracted and original components. The time courses of the mean and SD of the residual errors are almost constant (Fig. 3.3, B1, C1), indicating that the residual errors have no temporal modulation patterns and fluctuate randomly. Note that the SD of the residual errors [0.091 ± 0.0025 (mean $\pm$SD)] is larger than that of the averaged noise (0.050 ± 0.0016), indicating that the noise level of the components extracted by the proposed method is larger than that obtained by the averaging procedure. The

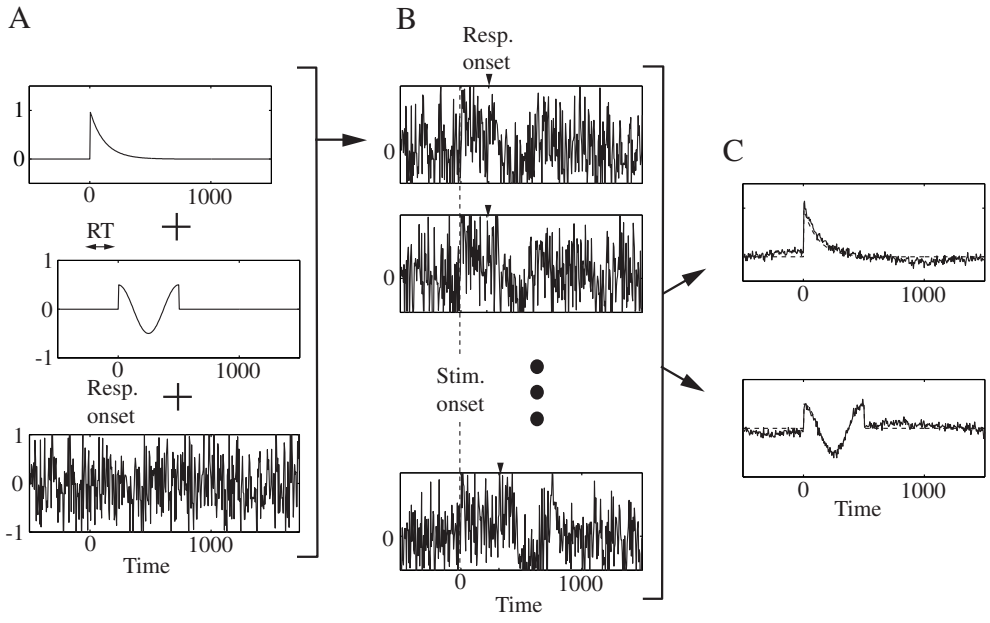

Figure 3.2: Simulations with artificial data. **A**: The original stimulus-locked component (top), overt response-locked component (middle), and noise (bottom). **B**: The simulated data obtained by Eq. (2.1) and the RTs from which the stimulus- and overt response-locked components are extracted. **C**: The extracted (solid line) and original (dotted line) stimulus-locked component (top); the extracted (solid line) and original (dotted line) overt response-locked component (bottom).

large amplitude spectra of the residual errors at low frequencies (Fig. 3.3, B2, C2) indicate that the larger residual errors are attributable to amplified slow waves in the noise. The variance of the residual errors is inversely proportional to the number of trials N, in the same way as the averaged noise (Fig. 3.3, A–C3), indicating that the noise level of the extracted components decreases as the number of trials increases. The coefficient is $a_n = 0.25$ for the averaged noise, while $a_c = 0.80$ for the extracted stimulus-locked component and $a_c = 0.83$ for the extracted overt response-locked component. Thus, the ratios a_c/a_n in Eq. (3.14) are 3.2 and 3.3 for the stimulus- and overt response-locked components respectively. This indicates that the proposed method needs about 3.3 times as many trials as the averaging procedure in order to achieve the same noise level, when the noise is white.

3.3 Simulation with EEG Data

In order to test the performance of the method for more EEG-like data, an additional numerical experiment was performed using real EEG data (Fig. 3.4).

3.3.1 Methods

In this simulation, an auditory evoked potential (AEP)[1] and a movement-related potential (MRP)[2] were used as the original stimulus- and overt response-locked components respectively, and the RTs, which were randomly selected from all the subjects' RTs of a simple reaction time task (described in Chapter 4), were used as τ_n ($n = 1, \cdots, N = 400$). The EEG data related to neither the stimulus nor the overt response were used as the noise; I randomly selected them from EEG in the interval of 2500–500 ms before the stimulus onset during the simple reaction time task of all the subjects. As the simulation with the artificial data suggested the need to apply a high-pass filter before decomposing real EEG involving non-negligible slow waves, I applied three kinds of filters to the noise EEG data: no filtering, bandpass of 1–40 Hz and bandpass of 2–40 Hz (described in Chapter 4). By using the AEP, MRP, RTs and noise EEG data, I generated the

[1]The average EEG during the passive hearing of an auditory stimulus (described in Chapter 4).
[2]The average EEG during self-paced voluntary movements (described in Chapter 4).

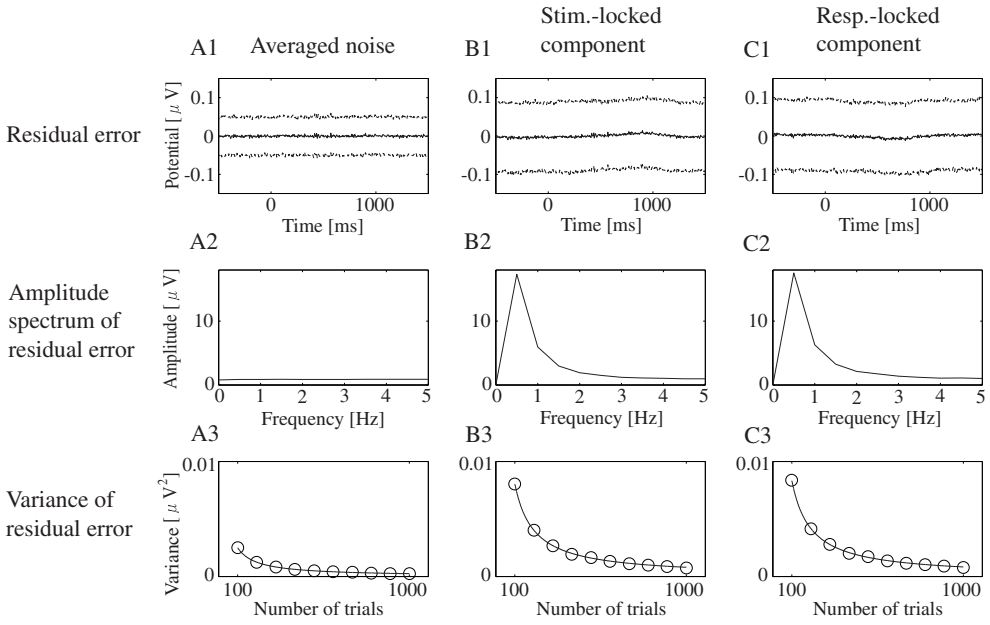

Figure 3.3: Residual errors between the original and extracted stimulus-/overt response-locked components for simulated artificial data. **A**–**C1**: Means (solid lines) and means ±SD (dotted lines) of the averaged noise (A1) and of the residual errors across 500 repeated simulations as in Fig. 3.2 (B1, C1). **A**–**C2**: Amplitude spectra of the averaged noise (A2) and of the residual errors (B2, C2). **A**–**C3**: Variance of the averaged noise (A3) and of the residual errors (B3, C3) as a function of the total number of trials N (circle). The solid lines represent fitting curves in the form of $y = a/x$. **A1**–**3**: Results for the averaged noise across trials. **B1**–**3**: Results for the residual errors for the extracted stimulus-locked component. **C1**–**3**: Results for the residual errors for the extracted overt response-locked component.

simulated EEG data according to Eq. (2.1).

Then, I extracted the stimulus- and overt response-locked components from the simulated EEG data (Fig. 3.4, A–C1, A–C2). To examine the residual errors between the extracted and original components, I repeated the above procedure 100 times using different sets of the noise and τ_n. The averages of the residual errors across time were adjusted to zero. To examine whether the residual errors fluctuate randomly around zero, the time course of the mean and SD of the residual errors across the repeated procedures were plotted (Fig. 3.4, A–C3). Then, I examined how the noise level decreased as the number of trials N increased (Fig. 3.4, A–C4, diamond). The noise level $NL(N)$ was obtained by calculating the variance of the residual errors as follows:

$$NL(N) = \frac{1}{100 \times 2} \sum_{p=1}^{100} \left[\frac{1}{T-1} \sum_{t=0}^{T-1} re_{p,N,s}(t)^2 + \frac{1}{T-1} \sum_{t=0}^{T-1} re_{p,N,r}(t)^2 \right], \tag{3.15}$$

where $re_{p,N,s}(t)$ and $re_{p,N,r}(t)$ respectively represent the p-th residual errors of the extracted stimulus- and overt response-locked components obtained from the simulation data consisting of N trials. The variance was fitted by a function $y = a/x$ by the least square method. Further, in order to compare the noise level in the components extracted by the proposed method with that obtained by the averaging procedure, the noise EEG data used in the above repeated simulations were simply averaged across trials, and examined in the same manner as the residual errors (Fig. 3.4, A–C4, circle).

3.3.2 Results

I extracted the original stimulus-/overt response-locked components used for this simulation from the simulated data (Fig. 3.4). The baseline fluctuations of the components extracted from the simulated EEG without filtering are large (Fig. 3.4, A1, A2), whereas those obtained from the filtered EEG are well suppressed (Fig. 3.4, B1, B2, C1, C2). Indeed, the correlation coefficient between the extracted and original components is low for the EEG without filtering ($r_s = 0.52, r_r = 0.30$), whereas it is much higher for the filtered EEG ($r_s = 0.79, r_r = 0.51$ for the EEG filtered with 1–40 Hz; $r_s = 0.85, r_r = 0.54$ for the EEG filtered with 2–40 Hz). This is because the remaining slow waves in the EEG without filtering are amplified by the decomposition. The time courses

	EEG (no filter)	EEG (1–40 Hz)	EEG (2–40 Hz)?@
a_c	6241	407	127
a_n	125	98	80
a_c/a_n	50	4.2	1.6

Table 3.1: Coefficients a of a fitting function $y = a/x$ for an error level y as a function of the number of trials x. a_c: Coefficients obtained from the components extracted by the proposed method. a_n: Coefficients obtained from the averaged noise.

of the mean and SD of the residual errors are almost constant, indicating that the residual errors have no temporal modulation patterns and fluctuate randomly regardless of the filter properties.

The variance of the residual errors is inversely proportional to the number of trials, in the same way as the averaged noise (Fig. 3.4, A–C4), but the coefficients a_c for the extracted components are consistently greater than the a_n for the averaged noise. These coefficients are presented in Table 3.1, and it is shown that the proposed method needs 1.6 times as many trials as the averaging procedure in order to achieve the same noise level when slow waves in the EEG lower than 2 Hz are eliminated.

3.4 Discussion

In the proposed method, the stimulus- and overt response-locked components are extracted by calculating the left-hand side of Eqs. (3.9) and (3.10) respectively. The equations are obtained by solving Eqs. (3.1) and (3.2) simultaneously. On the other hand, we are able to define other sets of simultaneous equations to obtain the extracted stimulus- and overt response-locked components. For example, we are able to use the equation:

$$Y_{n'}(\omega) = S(\omega) + \exp(-i2\pi\omega\tau_{n'}/T)R(\omega) + V_{n'}(\omega) \quad \tau_n \neq \tau_{n'}, \tag{3.16}$$

instead of Eq. (3.2). Like Eq. (3.2), Eq. (3.16) is different from Eq. (3.1) in that the RTs are different ($\tau_n \neq \tau_{n'}$), and we can solve Eqs. (3.1) and (3.16) for $s(t)$ and $or(t)$. However, in that case the denominator of the solved equations frequently tends to be zero, making the decomposition difficult. I also tried some other simultaneous equations instead of Eqs. (3.1) and

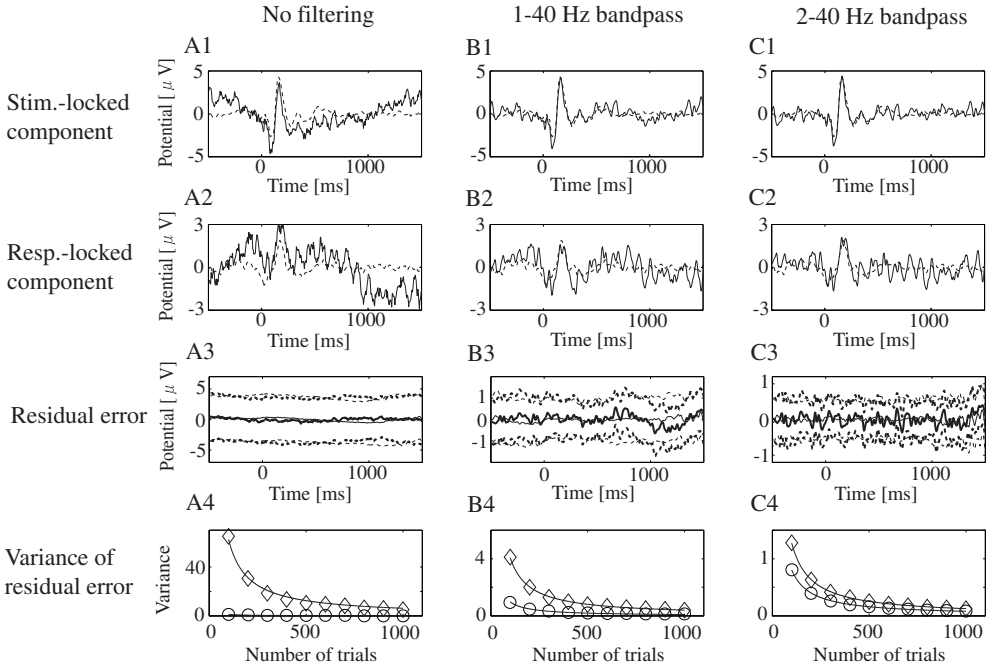

Figure 3.4: Simulations with EEG data. **A**–**C1**: Extracted stimulus-locked components (solid lines) and the original AEP data used for the simulation (dotted lines). **A**–**C2**: Extracted overt response-locked components (solid lines) and the original MRP data used for the simulation (dotted lines). **A**–**C3**: Residual errors between the extracted and original stimulus-/overt response-locked components. Thick and thin solid lines represent the means of the residual errors across the repeated simulations for the stimulus- and overt response-locked components respectively. The thick and thin dotted lines represent the means ±SD of the residual errors across the repeated simulations for the stimulus- and overt response-locked components respectively. **A**–**C4**: Variance of the residual errors between the extracted and original components (diamonds) and that of the averaged noise across trials (circles) as a function of the total number of trials N. The solid lines represent fitting curves in the form of $y = a/x$. **A1**–**4**: Results for the simulations in which pre-stimulus EEG without filtering was used as the noise. **B1**–**4**: Results for the simulations in which pre-stimulus EEG filtered with 1–40 Hz was used as the noise. **C1**–**4**: Results for the simulations in which pre-stimulus EEG filtered with 2–40 Hz was used as the noise.

(3.2). Among these trials, Eqs. (3.1) and (3.2) are the best in that the denominators of the solved equations rarely become zero, and the calculation for the decomposition is simple. Even if the denominators of Eqs. (3.9) and (3.10) do become zero, we have a solution: adjust T $(= l_0 + l_1)$ so that the denominator does not become zero.

The proposed method non-parametrically decomposes single-channel EEG into the stimulus- and overt response-locked components using a discrete Fourier transform. An alternative would be to identify parametric models of evoked potentials (for example, [15–17]). In my preliminary study, indeed, I was also able to identify these components parametrically using a Finite Impulse Response model (see Appendix B). Another alternative would be applying Woldorff's method [18], called the Adjacent Response (Adjar) technique. In the time domain, the Adjar removes the distortion due to the overlap of the consecutive event-related potentials in short inter-stimulus intervals. Although originally developed to extract only the stimulus-locked component, the Adjar could also be used to extract not only the stimulus-locked component but also the overt response-locked component [9]. As far as comparable performance is obtained, I believe the proposed method is better because it does not require a priori knowledge of parametric models themselves, and its rationale and procedure are quite simple and clear.

The simulation results show that the noise level of the components extracted by the proposed method is larger than that of the stimulus/overt response-triggered average. The amplitude spectra of the residual errors (Fig. 3.3, B2, C2) indicate that this is because the absolute value of $1/D(n, \omega)$ is higher at low frequencies ($\sim$ 1 Hz) if the observed RTs are used as τ_n; that is, slow waves ($\sim$ 1 Hz) in the noise are amplified by the decomposition. In other words, the larger noise in the extracted stimulus-/overt response-locked components is attributable to the decomposition itself rather than to the other data operations, such as the data segmentation strategy. On the other hand, the simulation results also show that the noise level of the extracted components decreases as the number of trials increases. These results lead to solutions for this methodological limitation: increasing the number of trials and/or applying a high-pass filter to the EEG before the decomposition. The number of trials required for each filter property is

shown in Table 3.1.

Generally speaking, a higher cut-off frequency of EEG leads to a smaller number of trials, but that would also result in the attenuation of slower potentials of interest. To prevent this, employing a higher number of trials with minimally filtered EEG would be a choice, but the noise level for this is substantially greater than that for the simple averaging. The averaging procedure, then, is not capable of perfectly separating temporally overlapping components when a stimulus and an overt response are temporally closer, as shown in Chapter 2. Thus, one would need to balance one choice against the others, depending on the phenomenon of interest and practical limitations of the research settings.

3.5 Conclusions

In this chapter, I propose a method temporally to decompose EEG into the stimulus- and overt response-locked components. The simulation results indicate the feasibility of the proposed method for artificial and EEG data. In the next chapter, I apply the method to the EEG during a simple reaction time task and extract the stimulus- and overt response-locked components.

Chapter 4

Application to EEG during a Simple Reaction Time Task

In this chapter, I apply the method proposed in the previous chapter to human surface EEG data during the simple reaction time task with an auditory stimulus (SR-task). To examine the effect of the temporal smearing by the averaging procedure, the extracted stimulus-/overt response-locked components are compared with the stimulus-/overt response-triggered average EEG during the simple reaction time task. Furthermore, I compare the extracted stimulus-locked component with an auditory evoked potential (AEP) obtained by averaging the EEG during the passive hearing of an auditory stimulus (S-task), and also compare the overt response-locked component with a movement-related potential (MRP) obtained by averaging the EEG during self-paced voluntary movement (M-task).

4.1 Methods

4.1.1 Experimental Procedures

Thirteen healthy adults aged between 20 and 31 years old constituted the experimental population. All the subjects gave their informed consent, and the local ethics committee approved the experimental procedure.

The subjects were seated comfortably in a chair with their eyes closed and right index finger placed on a button. The behavioral experiment consisted of 6 sessions. In each of the sessions, the

subjects were instructed to perform three kinds of tasks in the following order: a simple reaction time task (SR-task), a stimulus task (S-task) and a movement task (M-task). In the SR-task, the subjects were instructed to press the button as soon as possible after hearing an auditory stimulus (75 dB SPL, 2 ms duration, 3500 Hz). The auditory stimulus was presented via earphones. The inter-stimulus interval was randomized from 4 to 7 s. In the S-task, the subjects were instructed passively to hear the same auditory stimulus. The inter-stimulus interval was randomized from 2 to 3 s. In the M-task, the subjects were instructed to press the button repeatedly at an interval of about 4 s in the same manner as the SR-task. In total, about 300 trials were collected for each task from each of the subjects.

During the tasks, surface EEG was recorded from 19-ch tin electrodes, mounted in a cap (Electro-Cap International, Inc., Eaton, Ohio, USA) according to the International 10-20 system, referred to a tin electrode placed on AFz. The EEG was amplified on a Nihon Kohden EEG-1100 with a time constant of 0.3 s. Because I expected that large EEG activity related to the task execution would not appear around the earlobes [19], I placed Ag/AgCl electrodes on both earlobes and recorded their potentials separately. Their averaged potentials were subtracted from the EEG data off-line. For monitoring eye movements, an electrooculogram (EOG) was recorded with a pair of Ag/AgCl electrodes placed above and below the left eye. The sampling rate of the EEG and EOG was 1000 Hz.

4.1.2 Data Analyses

In an offline analysis, I resampled the EEG data at a rate of 200 Hz. The simulation results (Figs. 3.3 and 3.4) gave rise to the need to reduce slow waves in the EEG by a digital filter before the decomposition (see Chapter 3). Therefore, the EEG data was filtered with the bandpass of 1–40 Hz and of 2–40 Hz by using three kinds of finite impulse (FIR) filters: a high-pass of 1 Hz (600-point, -20 dB at 0.5 Hz), a high-pass of 2 Hz (300-point, -26 dB at 1 Hz) and a low-pass of 40 Hz (15-point, -45 dB at 50 Hz). Then, I segmented the filtered EEG data into 2 s epochs from -500 to 1500 ms after the stimulus onset for the SR- and S-task, or after the button push onset for the M-task.

Reaction times were defined as the intervals between the stimulus onset and the button push signal onset. In the following analysis, I used the 19-ch EEG epochs of the trials in which RTs were within 100–400 ms and EOG were within ± 100 μV. In addition, an artifact criterion of ± 100 μV was used for each of the channels to reject trials with excess electromyographic activity or measurement noise. Because huge measurement noise was included in one subject's EEG data, I excluded his/her data from the analysis.

The stimulus- and overt response-locked components were obtained by Eqs. (3.9) and (3.10) respectively from each set of the EEG epochs and the RTs during the SR-task. The extracted stimulus-locked components were then compared with the stimulus-triggered average EEG during the SR-task and with the AEP obtained by averaging the EEG epochs during the S-task triggering the stimulus onset. I set the baseline at the interval from 100 to 0 ms before the stimulus onset, and subtracted the average potentials during the interval from these three potentials for individual channels. The extracted overt response-locked components were compared with the overt response-triggered average EEG during the SR-task and with the MRP obtained by averaging the EEG epochs during the M-task triggering the response onset. I set the baseline at the interval from 500 to 400 ms before the response onset, and subtracted the average potentials during the interval from these three potentials for individual channels.

In the extracted stimulus-locked components (Fig. 4.1, A), negative peaks around 100 ms (N100), positive peaks around 160 ms (P200), positive peaks around 315 ms (P300) and negative peaks around 410 ms (N400) were observed. In the extracted overt response-locked components (Fig. 4.1, B), negative peaks around -40 ms (N-40), positive peaks around 160 ms (P160) and negative peaks around 500 ms (N500) were observed. Since I expected that the effects of the temporal smearing would be large in the late parts of the stimulus-triggered average EEG and in the early parts of the overt response-triggered average EEG (see Fig. 2.5, C), in this study, I only examined the scalp distributions of the P300, N400, N-40 and P160. Indeed, I confirmed that the peak amplitudes, latencies, and scalp distributions of the other potentials earlier than the P300 or later than the P160 were not substantially different depending on the methods used

(see Appendix C).

For the stimulus-locked component and the stimulus-triggered average EEG during the SR-task, the peak latencies of the P300 and N400 were measured from the extracted stimulus-locked components at Cz as the time points of the largest positive and negative peaks within 250–350 and 300–500 ms. For the AEP, its peak latencies were measured from the AEP at Cz in the same manner. For the overt response-locked component and the overt response-triggered average EEG during the SR-task, the peak latencies of the N-40 and P160 were measured from the extracted overt response-locked components at Cz as the time points of the largest negative and positive peaks within −100–100 and 50–250 ms. For the MRP, its peak latencies were measured from the MRP at Cz in the same manner. Then, scalp distributions were obtained from the 19-ch potentials at these latencies and compared with each other.

To confirm that the differences of the scalp distributions between the extracted stimulus-/overt response-locked components and the conventional stimulus-/overt response-triggered average EEG during the SR-task are attributable to the temporal overlapping with each other, I reconstructed stimulus-/overt response-triggered average EEG by overlapping both of the extracted stimulus- and overt response-locked components with the delays of the individual RTs according to Eq. (2.1).

The similarities of the scalp distributions by different methods were quantified by a dot product (dp). I normalized the 19-dimensional EEG vectors to unit vectors with a magnitude of 1, and calculated a dot product between the vectors, where the dot product of 1 represents perfect similarity of the distributions. A two-tailed Wilcoxon signed-rank test was conducted to test the null hypothesis that the dot products obtained from each of the subjects did not differ from zero. Also, peak amplitudes in different waveforms were compared by means of the two-tailed Wilcoxon signed-rank test. An alpha level of 0.05 was used for the statistical test.

4.2 Results

4.2.1 Decomposition of Observed EEG (1–40 Hz)

I obtained 256.8±34.7 trials per subject for the SR-task. The mean and SD of all the RTs are 221.0 ms and 57.8 ms respectively. I first decomposed the EEG filtered with 1–40 Hz during the SR-task. Figure 4.1 shows the stimulus- and overt response-locked components extracted from each/all of the subjects' EEG at Cz, and the RTs. The extracted stimulus-locked component at Cz exhibits the N100, P200, P300 and N400 (Fig. 4.1, A). The extracted overt response-locked component at Cz exhibits the N-40, P160 and N500 (Fig. 4.1, B).

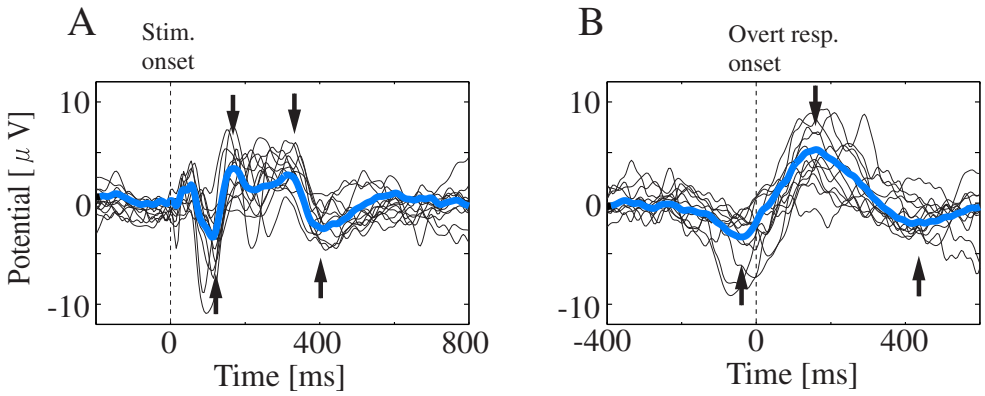

Figure 4.1: Extracted stimulus- and overt response-locked components at Cz. **A**: Extracted stimulus-locked components. The arrows indicate, from left to right, the N100, P200, P300 and N400. **B**: Extracted overt response-locked components. The arrows indicate, from left to right, the N-40, P160 and N500. The blue lines represent the components extracted from all the subjects' EEG and RTs; the black lines represent the components extracted for each subject. In this figure, the average of each wave is adjusted to zero.

Extracted Stimulus-locked Component

Figure 4.2 shows the extracted stimulus-locked components, the stimulus-triggered average EEG during the SR-task and the AEP obtained from all the subjects' EEG data. The AEP was obtained from 269.8±36.4 trials per subject during the S-task. Figure 4.4, A shows the scalp distributions of the P300 and N400 in each of the waveforms.

At around the P300, the waveforms of the extracted stimulus-locked components shift frontally as compared to those of the stimulus-triggered average EEG during the SR-task; the amplitudes of the P300 in the extracted stimulus-locked components are large at around Fp1 and Fp2, whereas those in the stimulus-triggered average EEG during the SR-task are large at around Cz (Fig. 4.2). However, the *dp* of the P300 between both waves are significantly greater than zero ($dp = 0.74 \pm 0.26, p < 0.05$) (Fig. 4.4, A). This result indicates that the differences between the extracted stimulus-locked component and the stimulus-triggered average EEG appear to exist at around the P300, but is not reflected in the (global) *dp* measure.

In the AEP, clear P300 waveforms are not observed (Fig. 4.2), although the *dp* of the P300 between the AEP and the extracted stimulus-locked components are significantly greater than zero ($dp = 0.69 \pm 0.22, p < 0.05$) (Fig. 4.4, A).

At around the N400, the waveforms of the extracted stimulus-locked components are clearly different from those of the stimulus-triggered average EEG during the SR-task; the amplitudes of the N400 in the extracted stimulus-locked components are large at around Cz, whereas those in the stimulus-triggered average EEG during the SR-task are large at around Fp1 and Fp2 (Fig. 4.2). The *dp* of the N400 between both waves are not significantly greater than zero ($dp = 0.13 \pm 0.38, p > 0.05$) (Fig. 4.4, A). It is of note that the amplitudes of the N400 in the reconstructed stimulus-triggered average EEG are large at around Fp1 and Fp2, in the same way as the observed stimulus-triggered average EEG, and the *dp* between them approach 1.0 ($dp > 0.99$ for all the subjects) (Fig. 4.4, A). This result indicates that the differences in the N400 amplitudes between the extracted stimulus-locked components and the stimulus-triggered average EEG disappear by overlapping the extracted overt response-locked components on the extracted stimulus-locked components, suggesting that the differences are attributable to the overlap of the overt response-locked components.

In the AEP, the amplitudes of the N400 are large at around Cz, as are those in the extracted stimulus-locked components (Fig. 4.2), and the *dp* of the N400 between them are significantly greater than zero ($dp = 0.37 \pm 0.44, p < 0.05$) (Fig. 4.4, A).

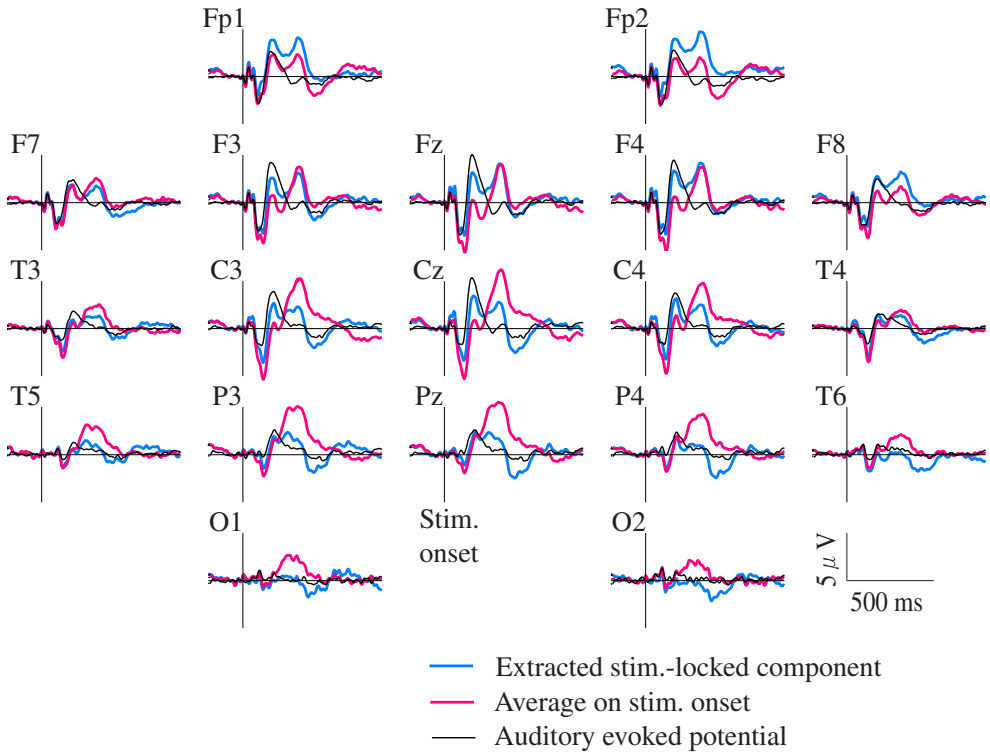

Figure 4.2: Extracted stimulus-locked components, stimulus-triggered average EEG during the SR-task and the AEP obtained from all the subjects' EEG.

Extracted Overt Response-locked Component

Figure 4.3 shows the extracted overt response-locked components, the overt response-triggered average EEG during the SR-task and the MRP obtained from all the subjects' EEG data. The MRP was obtained from 236.8±32.3 trials per subject during the M-task. Figure 4.4, B shows the scalp distributions of the N-40 and P160 in each of the waveforms.

The amplitudes of the N-40 in the extracted overt response-locked components are large at around Cz, as is the overt response-triggered average EEG during the SR-task (Fig. 4.3), and the dp of the N-40 between both waves are significantly greater than zero ($dp = 0.72 \pm 0.18, p < 0.05$) (Fig. 4.4, B).

In the MRP, clear N-40 waveforms are not observed, in contrast to the extracted overt response-locked component (Fig. 4.3), although the dp of the N-40 between them are significantly greater than zero ($dp = 0.54 \pm 0.43, p < 0.05$) (Fig. 4.4, B).

The amplitudes of the P160 in the extracted overt response-locked components are large at around Cz, as is the overt response-triggered average EEG during the SR-task (Fig. 4.3), and the dp of the P160 between both waves are significantly greater than zero ($dp = 0.75 \pm 0.20, p < 0.05$) (Fig. 4.4, B).

In the MRP, the amplitudes of the P160 are large at around Cz, as are those in the extracted overt response-locked components (Fig. 4.3), and the dp of the P160 between them are significantly greater than zero ($dp = 0.60 \pm 0.41, p < 0.05$) (Fig. 4.4, B).

On the other hand, the N-40 and P160 amplitudes of the extracted overt response-locked components do not exhibit significant differences between C3 and C4 (-4.1 ± 4.6 and -4.0 ± 3.4, respectively, $p > 0.05$ for the N-40; 4.8 ± 2.5 and 3.5 ± 2.8, respectively, $p > 0.05$ for the P160), although the overt response-triggered average EEG does exhibit significant differences (-4.4 ± 2.4 and -3.7 ± 1.9, respectively, $p < 0.05$ for the N-40; 5.1 ± 2.2 and 4.2 ± 1.9, respectively, $p < 0.05$ for the P160).

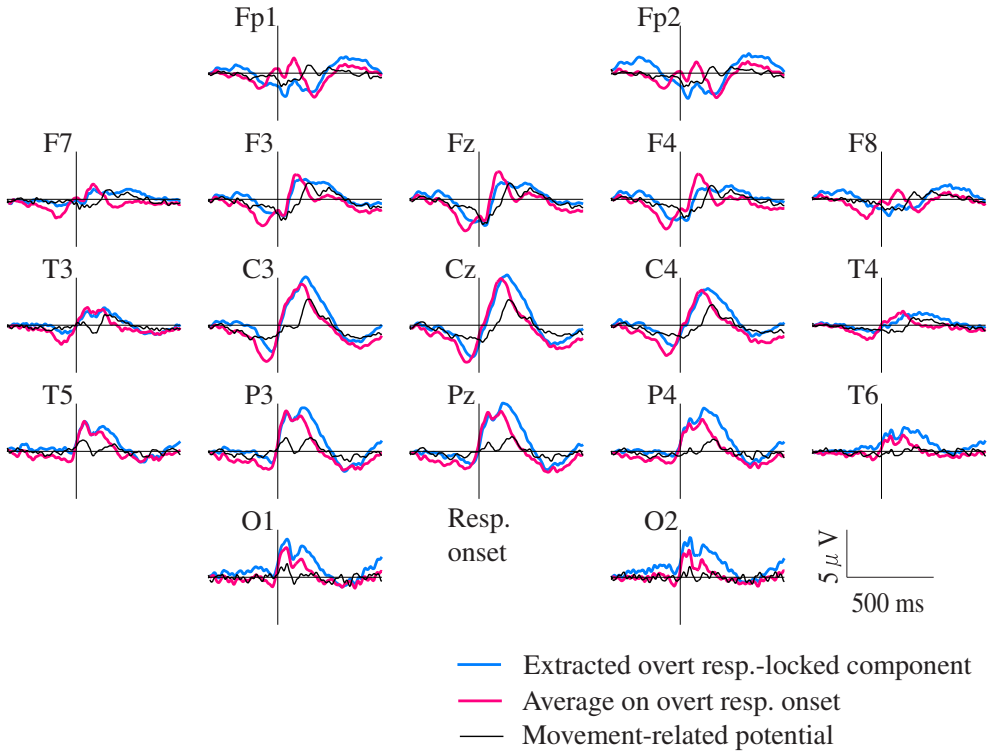

Figure 4.3: Extracted overt response-locked components, overt response-triggered average EEG during the SR-task and the MRP obtained from all the subjects' EEG.

4.2.2 Decomposition of Observed EEG (2–40 Hz)

I also decomposed the EEG filtered with 2–40 Hz during the SR-task. Figure 4.5 shows the extracted stimulus-/overt response-locked components and the stimulus-/overt response-triggered average EEG during the SR-task obtained from all the subjects' data.

The extracted stimulus-locked component at Cz exhibits the P300 and N400 in the same way as that extracted from the EEG filtered with 1–40 Hz (Fig. 4.5, A). In contrast to the EEG filtered with 1–40 Hz, however, the stimulus-triggered average EEG at Cz has the P300 and N400 peaks in the same way as the extracted stimulus-locked component (Fig. 4.5, A). The amplitudes of the P300 and N400 in the stimulus-triggered average EEG are large at around Fz in the same way as the extracted stimulus-locked components (Fig. 4.5, B), and the dp of the P300 and N400 between them are significantly greater than zero ($dp = 0.91 \pm 0.14, p < 0.05$ for the P300; $dp = 0.91 \pm 0.12, p < 0.05$ for the N400). These results indicate that, in the case of the EEG filtered with 2–40 Hz, the effect of the temporal smearing by the overt response-locked components is not so large as to change these scalp distributions significantly.

Similar to the EEG filtered with 1–40 Hz, both the extracted overt response-locked component and the overt response-triggered average EEG at Cz exhibit the N-40 and P160 (Fig. 4.5, C). The amplitudes of the N-40 and P160 in the overt response-triggered average EEG are large at around Cz in the same way as the extracted overt response-locked components (Fig. 4.5, D), and the dp of the N-40 and P160 between them are significantly greater than zero ($dp = 0.87 \pm 0.11, p < 0.05$ for the N-40; $dp = 0.92 \pm 0.067, p < 0.05$ for the P160). On the other hand, the amplitudes of the N-40 and P160 at Cz in the overt response-locked components are significantly smaller than those in the overt response-locked components extracted from the EEG filtered with 1–40 Hz (-2.63 ± 1.07 and -4.82 ± 3.44, respectively, $p < 0.05$ for the N-40; 4.03 ± 1.07 and 5.31 ± 2.27, respectively, $p < 0.05$ for the P160). This result suggests that the above-mentioned small effect of the temporal smearing by the overt response-locked components is due to the attenuated peaks in the overt response-locked components.

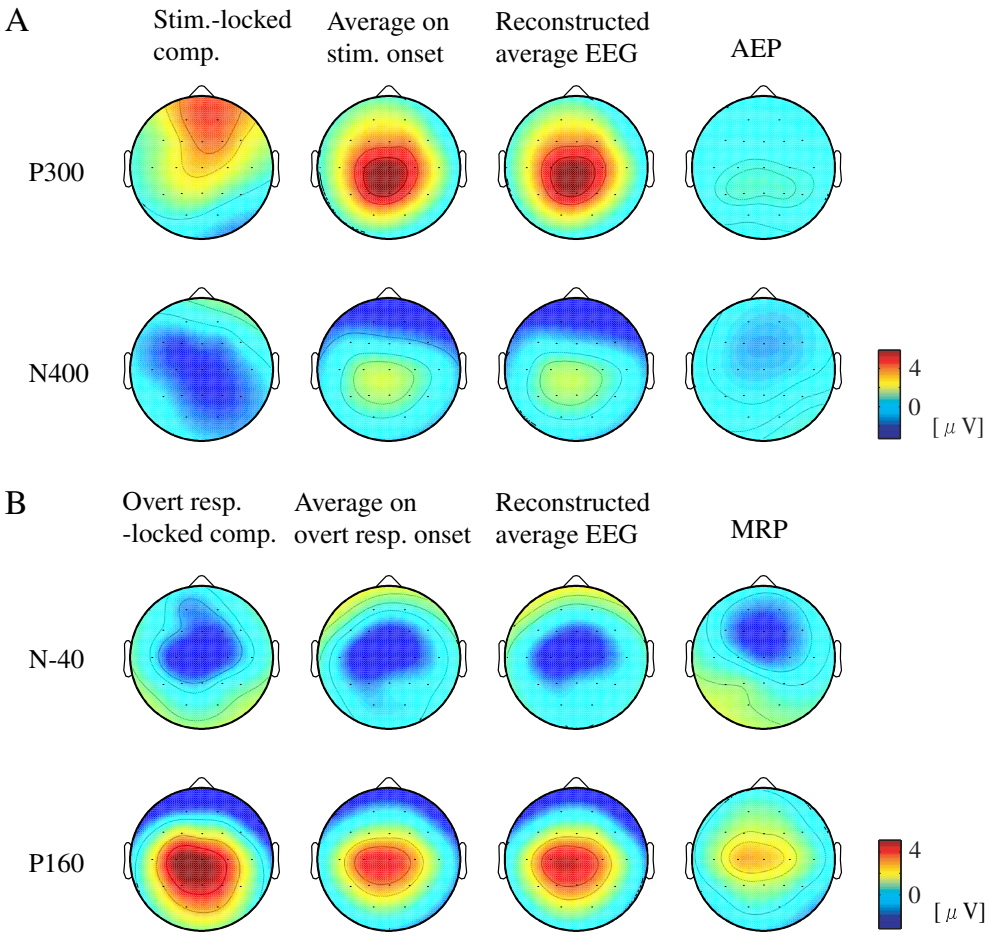

Figure 4.4: Scalp distributions of the P300, N400, N-40 and P160. **A**: The P300 and N400 in the extracted stimulus-locked components, the stimulus-triggered average EEG, the reconstructed stimulus-triggered average EEG and the AEP obtained from all the subjects' EEG. **B**: The N-40 and P160 in the extracted overt response-locked components, the overt response-triggered average EEG, the reconstructed overt response-triggered average EEG and the MRP obtained from all the subjects' EEG.

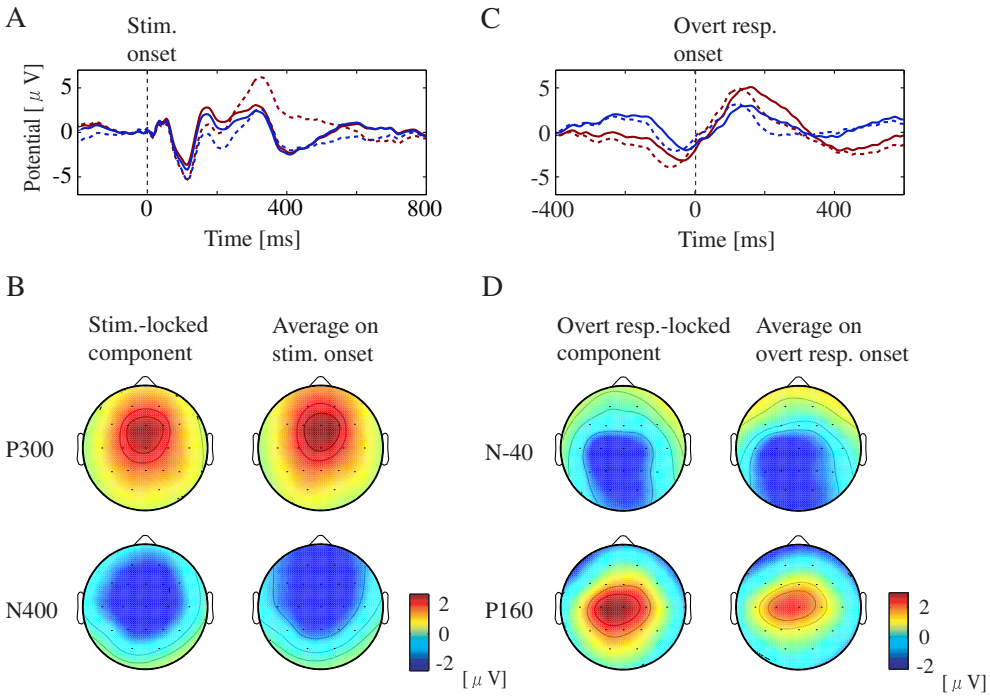

Figure 4.5: Decomposition of EEG (2–40 Hz) during the SR-task. **A**: Extracted stimulus-locked component at Cz (solid blue line) and stimulus-triggered average EEG during the SR-task at Cz (dotted blue line). For comparison, the stimulus-locked component at Cz and the stimulus-triggered average EEG at Cz obtained from the EEG filtered with 1–40 Hz are superimposed (solid red and dotted red lines respectively). **B**: Scalp distributions of the P300 and N400 in the extracted stimulus-locked components and the stimulus-triggered average EEG during the SR-task. **C**: Extracted overt response-locked component at Cz (solid blue line) and overt response-triggered average EEG during the SR-task at Cz (dotted blue line). For comparison, the overt response-locked component at Cz and the overt response-triggered average EEG at Cz obtained from the EEG filtered with 1–40 Hz are superimposed (solid red and dotted red lines respectively). **D**: Scalp distributions of the N-40 and P160 in the extracted overt response-locked components and the overt response-triggered average EEG during the SR-task.

4.3 Discussion

4.3.1 Stimulus-locked EEG Component

I extract the stimulus-locked components by Eq. (3.9) from the EEG data during the SR-task. The extracted stimulus-locked components exhibit the N100, P200, P300 and N400. The existence of the N100 and P200 is in agreement with previous studies which have examined EEG during simple reaction time tasks [20,21]. In this study, I evaluate the effect of the temporal overlapping at the late peaks: the P300 and N400.

As for the P300, the scalp distributions between the extracted stimulus-locked components and the stimulus-triggered average EEG appear to be different in the case of the EEG filtered with 1–40 Hz. However, the effect of the temporal smearing by the overt response-locked components is not so large as to change the global scalp distributions (measured by the *dp*) significantly. The local difference between the stimulus-locked P300 and the stimulus-triggered average P300, the former showing more frontal topology, should be studied further.

On the contrary, at the N400, the significant difference of the scalp distributions between the extracted stimulus-locked components and the stimulus-triggered average EEG is observed.

As for the EEG filtered with 1–40 Hz, the N400 amplitudes in the extracted stimulus-locked components are large in the central region. The validity of the central N400 in the extracted stimulus-locked components is supported by a previous study which reports a stimulus-locked, centro-parietal N400 during audio-visual cognitive tasks with overt responses [22]. The result that the AEP, which is thought to reflect only a stimulus-related brain process, also has a centrally distributed N400 could also be evidence supporting the validity of the N400 in the extracted stimulus-locked components.

The scalp distributions of the N400 in the extracted stimulus-locked components are different from those in the stimulus-triggered average EEG. However, when the extracted overt response-locked components are overlapped on the stimulus-locked components, the difference in the N400 between them disappears. This suggests that the difference is attributable to the overlapping of the overt response-locked components.

As for the EEG filtered with 2–40 Hz, the N400 appears at around Cz even in the stimulus-triggered average EEG in the same way as the extracted stimulus-locked components. This is likely because, in the case of the EEG filtered with 2–40 Hz, the overt response-locked components are attenuated by the high-pass filter, and the resultant small effect of the temporal smearing discloses the original N400 in the stimulus-triggered average EEG. Its scalp distributions are similar across subjects; the dot product between a subject's vector and the other subjects' average vector is calculated for each subject and compared with zero by the Wilcoxon signed-rank test ($dp = 0.83 \pm 0.20, p < 0.05$). Then again, the N400 which appears in the EEG filtered with 2–40 Hz additionally confirms the existence of the N400 in the stimulus-locked components extracted from the EEG filtered with 1–40 Hz.

The above results indicate that the differences between the stimulus-locked components and the stimulus-triggered average EEG can be attributed to the temporal overlapping of the overt response-locked components, and the effects of the temporal overlapping are different between the filter properties used, because the waveforms of the overlapping components vary depending on the filter properties.

On the other hand, although the auditory stimuli are the same during the SR-task and the S-task, the waveforms of the late parts in the extracted stimulus-locked components and the AEP are different; the AEP does not exhibit the clear P300 in contrast to the stimulus-locked components (Fig. 4.2). This indicates that even the "pure" stimulus-related activity is modulated depending on whether the overt response is required or not. In another task requiring no motor responses, different P300 evoked by the same stimuli in different instructions have also been reported [23]. These results might reflect the context-dependent modulation of the stimulus-related EEG activity.

4.3.2 Overt Response-locked EEG Component

In many studies which examine movement-related potentials, slow components of averaged EEG have been discussed (for example, [24–27]). However, in this study, such slow components are cut by the high-pass filter of 1 or 2 Hz because of the methodological limitation (see Chapter 3).

Therefore, in the present study I cannot easily deal with classical slow components, such as the Bereitshaftspotential [25, 27].

I extract the overt response-locked components by Eq. (3.10) from the EEG data during the SR-task. The extracted overt response-locked components exhibit the three distinct peaks: the N-40, P160 and N500. The existence of these peaks is in agreement with a previous study which examined EEG during cued movements [26]. In this study, I evaluate the effect of the temporal overlapping at the earlier peaks: the N-40 and P160.

In the EEG filtered with both 1–40 and 2–40 Hz, the scalp distributions of the N-40 and P160 in the extracted overt response-locked components are similar to those in the overt response-triggered average EEG during the SR-task. This suggests that the distributions of the overt response-locked components are less smeared by the temporal overlapping of the stimulus-locked components. This is because the stimulus-locked components do not have large slow waves in comparison with the overt response-locked components and, by the averaging procedure, are easily diminished as a result of phase cancellations of fast waves.

The MRP do not exhibit the clear N-40, in contrast to the overt response-locked components and the overt response-triggered average EEG. By the averaging procedure, some studies [24, 26] have also revealed different EEG activity during self-paced movements and cued movements. The similarity of the overt response-locked component and the overt response-triggered average EEG suggests that the differences in the overt response-triggered average EEG between the tasks observed in this and previous studies are due not to the temporal overlapping of the stimulus-locked components but to the context-dependent modulation of overt response-related EEG activity.

Although the subjects responded with their right index fingers, significant asymmetry is not observed for the N-40 and P160 in the extracted overt response-locked components, in contrast to the overt response-triggered average EEG and to previous studies (for example, [25]). This is because the noise amplified by the decomposition makes the inter-subject variability of the N-40 and P160 distributions large and the p-values become higher.

4.4 Conclusions

In conclusion, the results presented in this chapter confirm the feasibility and usefulness of the frequency domain decomposition of EEG data into stimulus- and overt response-locked components during a reaction time task, and show that the contamination by the temporal overlapping is large especially in the late part of the stimulus-triggered average EEG during the SR-task when slow waves remain in the EEG data.

It should be noted that the effect of the temporal smearing shown in this study may not hold true for every reaction time task. This is because the effect of the temporal smearing is determined by the distribution of RTs and the waveform of the stimulus- or overt response-locked components [see Eqs. (2.2) and (2.3)]; that is, the contamination is task-dependent and cannot be examined directly without the decomposition. Therefore, to examine the brain activity during reaction time tasks in detail, the decomposition is required eventually, regardless of which components we use and whether they are obtained by the averaging procedure or by the proposed method.

Chapter 5

EEG during Tasks with Covert Responses

In this chapter, I firstly introduce reports on the brain activity during tasks which require covert responses. Then, based on the reports, I mathematically formulate the EEG during the tasks with covert responses. Finally, I discuss the previous methods for extracting the stimulus- and covert response-locked components from the EEG, and discuss the necessity of a novel method for extracting the two components.

5.1 Brain Activity during Tasks with Covert Responses

As stated in Chapter 2, when a subject makes an overt response to a stimulus, stimulus- and overt response-locked brain activities occur. Similarly, when a subject makes a covert response to a stimulus, such as the perception of ambiguous figures or the solving of complex problems, it is considered that stimulus- and covert response-locked brain activities occur [28–32].

Indeed, studies by Tallon-Baudry et al. [31, 32] suggest the presence of the covert response-locked component in addition to the stimulus-locked component in EEG during cognitive tasks. They examined the EEG during the viewing of illusory (Kanizsa) triangles (Fig. 5.1, A) by time-frequency analysis, showed that the gamma activity which is not time-locked to the stimulus onset was induced when the subject perceived the triangles, and suggested the role of the induced

gamma activity[1] in the construction of a coherent representation of objects and the rehearsal of the representation in the memory. This report indicates that some brain activities related to perception and memory recall are not time-locked to the stimulus onsets but to the covert response onsets.

5.2 Mathematical Formulation

Like the EEG during tasks with overt responses, the EEG during tasks with covert responses is assumed to consist of a stimulus-locked component, a covert response-locked component shifted by the delay of an individual trial, and noise. Therefore, the EEG is expressed by:

$$y_n(t) = s(t) + cr(t - \tau_n) + v_n(t) \quad (t = 0, \cdots, T-1;\ n = 1, \cdots, N), \tag{5.1}$$

where $y_n(t)$: observed EEG data in trial n; $s(t)$: stimulus-locked component; $cr(t)$: covert response-locked component; τ_n: delay of $cr(t)$ in trial n; $v_n(t)$: noise in trial n. This implies that ongoing EEG activity and trial-to-trial variability of stimulus- and covert response-locked activity are included in $v_n(t)$. Note that, in this case, τ_n is unknown, in contrast to tasks with overt responses.

5.3 Previous Methods

While the stimulus-locked component has been extracted by the stimulus-triggered averaging procedure, the covert response-locked component cannot be extracted by the averaging procedure, or even by the method proposed in Chapter 3, because its delays in individual trials are of unknown length.

5.3.1 Time-frequency Analyses

As mentioned above, using time-frequency analyses, some studies have examined the induced EEG activity, or covert response-locked EEG activity [28,29,31–33]. A time-frequency analysis is

[1] They call EEG activity not time-locked to stimulus onset "induced" activity. In contrast, I define the covert response-locked component as being the EEG component not time-locked to stimulus onset (see Chapter 1). Therefore, their term "induced" corresponds to the term "covert response-locked" used in this thesis.

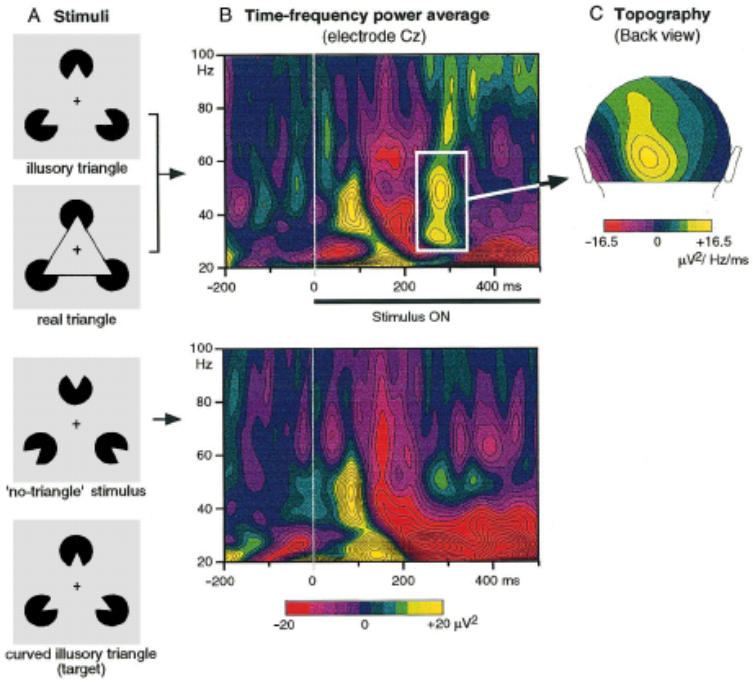

Figure 5.1: Induced gamma activity. **A**: The subjects were presented with four different stimuli. Both the illusory (Kanizsa) and the real triangles were coherent stimuli, leading to a coherent percept through a bottom-up feature binding process. The "no-triangle" stimulus served as a control. Subjects had silently to count the occurrences of the target stimulus, a curved illusory triangle, and to report this number at the end of each recording block. This task, when correctly performed, ensured that the subjects perceived correctly the illusory triangles and remained attentive throughout the whole recording session. **B**: Time-frequency power of the EEG at electrode Cz, in response to the illusory triangle (top) and to the no-triangle stimulus (bottom). Two successive bursts of oscillatory activities were observed. A first burst occurred at about 100 ms and 40 Hz; it was a stimulus-locked response peaking at electrode Cz. It showed no difference between stimulus types, and thus cannot reflect the spatial feature-binding process required to perceive the triangles. The second burst, around 280 ms and between 30 and 60 Hz, was not stimulus-locked, and most prominent in response to coherent stimuli. There was no statistical difference in the gamma range between the responses to the illusory and real triangles. Induced gamma could thus reflect the spatial binding of the elementary features of the picture into a coherent representation of the triangle. It should be noted that no component of the stimulus-locked response discriminated between coherent and non-coherent stimuli. (Adapted from [31])

a method for mapping a one-dimensional signal of time into a two-dimensional function of time and frequency by a time-frequency transform, such as the short-time Fourier transform and the continuous wavelet transform [34]. Because the stimulus-triggered averaging procedure canceled out the induced EEG activity (Fig. 5.2, B), in these studies [28,29,31–33], time-frequency analyses were used before applying the averaging procedure as follows. First, time-frequency analyses were applied to individual single-trial EEG epochs, and time-frequency powers were estimated (Fig. 5.2, D). Then, the time-frequency powers were averaged across trials (Fig. 5.2, E). Tallon-Baudry and Bertrand [32] stated that this approach can identify non-phase-locked activity as long as the signal-to-noise ratio is high enough and the jitter does not exceed the wavelet duration used in the time-frequency transform.

However, the limitation of the time-frequency analyses is that this method only identifies the power and average delay of the covert response-locked component. To obtain more detailed information on the covert response-locked components, their waveforms and delays of individual trials, we need to use another method rather than the time-frequency analyses.

5.3.2 Peak Picking, Woody's Method, and Pham et al.'s Method

Hitherto, the waveforms and delays of the covert response-locked components have been obtained by peak picking, Woody's method and Pham et al.'s method [35–43]. In peak picking, EEG is low-pass filtered, and the individual delay of the covert response-locked component is estimated by detecting the largest positive/negative deflection in a predefined time window. In Woody's method [43], cross-correlation is calculated between a template that resembles the waveform of the covert response-locked component and the low-pass filtered EEG. The individual delay is defined as the time lag by which the template should be shifted to obtain the maximal cross-correlation. In Pham et al.'s method [40], the individual delays are estimated by the maximum likelihood approach employing iterative Fisher-scoring.

A critical problem of these methods is their underlying assumption. These methods implicitly or explicitly assume that only one component, the covert response-locked component, appears

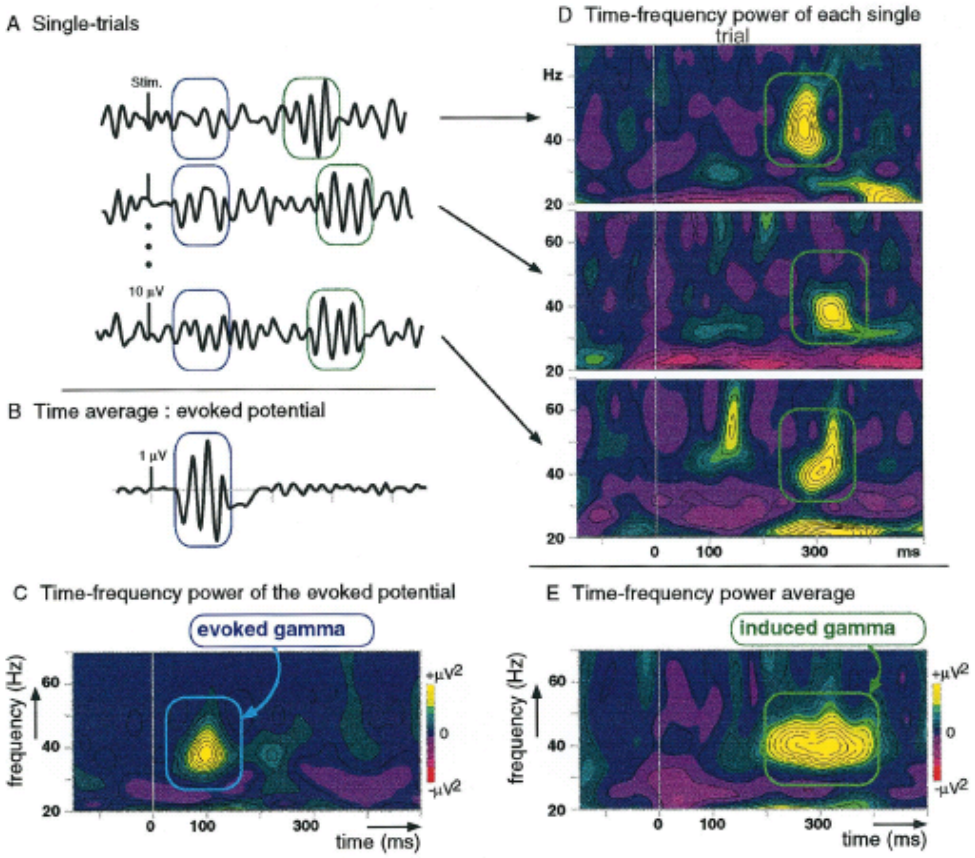

Figure 5.2: Identification of induced activity (covert response-locked activity) by time-frequency analyses. (Adapted from [32])

after stimulus onsets; that is, these methods model the EEG by:

$$y_n(t) = cr(t - \tau_n) + v_n(t), \tag{5.2}$$

being obviously different from Eq. (5.1). In my assumption of Eq. (5.1), there are two components and the two components can be temporally overlapping. The temporal overlapping of the two unknown components makes the problem quite difficult because the two components contaminate each other, and the appearance of the two components varies from trial to trial (see Fig. 2.5, B). For example, it is possible that a negative peak in the stimulus-locked component averages out a positive peak in the covert response-locked component and both of the components appear not to have the peaks. Because methods which assume only one component do not consider such a contamination effect, they cannot be used when two components are temporally overlapping.

5.4 Conclusions

From the previous studies on the EEG during cognitive tasks, it is suggested that, even when a subject does not respond overtly to a stimulus, EEG activity can exhibit two components: the stimulus- and covert response-locked components. To extract the two components, time-frequency analyses, peak picking, Woody's Method, and Pham et al.'s Method have been used. However, these methods are not adequate. Therefore, it is necessary to propose a novel method for extracting the stimulus- and covert response-locked components. In the next chapter, I propose such a method.

Chapter 6

Proposed Method for Covert Responses

In the previous chapter, I describe the necessity of a novel method for temporally decomposing EEG into the stimulus- and covert response-locked components without knowledge of the individual delays of the covert response-locked component. In this chapter, I propose a non-parametric method for the temporal decomposition.

6.1 Decomposition Method

I assume that the EEG activity consists of the stimulus- and covert response-locked components and is expressed by Eq. (5.1). Here, the objective is to obtain $s(t)$, $cr(t)$ and τ_n only from $y_n(t)$ $(n = 1, \cdots, N)$ (Fig. 6.1).

Once a set of delays $\boldsymbol{\tau} = [\tau_1, \tau_2, \cdots, \tau_N]$ is determined, the waveforms of $s(t)$ and $cr(t)$ are determined by the proposed method for overt responses (see Chapter 3). In the method for overt responses, $s(t)$ and $cr(t)$ extracted by using $\boldsymbol{\tau}$ are respectively expressed by:

$$s_{\boldsymbol{\tau}}(t) = \mathrm{IDFT}\left[\frac{1}{N}\sum_{n=1}^{N}\frac{\exp\left(-i2\pi\omega\tau_n/T\right)\bar{Y}\left(\omega\right) - \bar{E}(\omega)Y_n\left(\omega\right)}{D(n,\omega)}\right], \tag{6.1}$$

$$cr_{\boldsymbol{\tau}}(t) = \mathrm{IDFT}\left[\frac{1}{N}\sum_{n=1}^{N}\frac{Y_n\left(\omega\right) - \bar{Y}\left(\omega\right)}{D(n,\omega)}\right]. \tag{6.2}$$

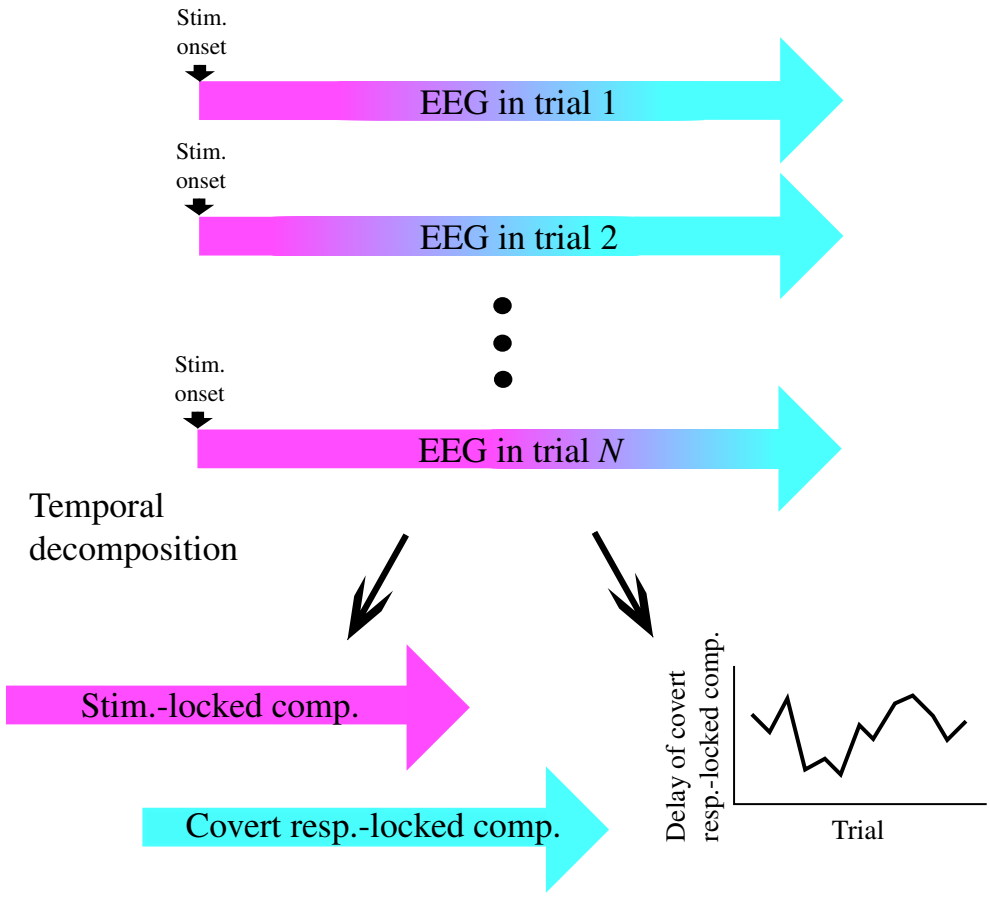

Figure 6.1: Schematic representation of the objective.

I estimate true $\boldsymbol{\tau}$ under a certain assumption. Figure 6.2 shows the simulation results on which the assumption is based. If $\boldsymbol{\tau}$ is true, the waveforms of $s_{\boldsymbol{\tau}}(t)$ and $cr_{\boldsymbol{\tau}}(t)$ are close to those of $s(t)$ and $cr(t)$ (Fig. 6.2, C), and the waveform of $s_{\boldsymbol{\tau}}(t) + cr_{\boldsymbol{\tau}}(t - \tau_n)$ becomes close to $y_n(t)$ (Fig. 6.2, E). In contrast, if $\boldsymbol{\tau}$ is wrong, the waveforms of $s_{\boldsymbol{\tau}}(t)$ and $cr_{\boldsymbol{\tau}}(t)$ are not close to those of $s(t)$ and $cr(t)$ (Fig. 6.2, D), and the waveform of $s_{\boldsymbol{\tau}}(t) + cr_{\boldsymbol{\tau}}(t - \tau_n)$ does not become close to $y_n(t)$ (Fig. 6.2, F). Based on these simulation results, I assume that sets of nearly true delays provide better approximations of the observed EEG data than sets of wrong delays. Under this assumption, I estimate the true $\boldsymbol{\tau}$ by solving an optimization problem of:

$$\textbf{Minimize} \quad o_{\boldsymbol{\tau}} = \sum_{t=t_1}^{t_2} \sum_{n=1}^{N} \{y_n(t) - s_{\boldsymbol{\tau}}(t) - cr_{\boldsymbol{\tau}}(t - \tau_n)\}^2$$

$$\textbf{Subject to} \quad \boldsymbol{\tau} \subset \mathbf{N}.$$

In this study, t_1 and t_2 were respectively set at 0 and 1000 ms after the stimulus onset.

To select algorithms for solving this optimization problem, by using simulated data, I checked the structure of the objective function by changing τ_k (k was fixed) one step at a time (an example is shown in Fig. 6.3). Consequently, as the objective function seemed to have many local minima (Fig. 6.3), hill-climbing methods [44], such as the steepest descent method [44], are not suitable because these methods are easily trapped in a local minimum. Stochastic algorithms, such as simulated annealing [44–46], are thus considered suitable because these methods can escape from a local minimum and find a global minimum.

Among the algorithms I tested, a random search [44, 46, 47] is the best in the point that this algorithm achieves speedy convergence to a global minimum with a high probability. The procedure of the random search is as follows:

1. Generate a set of delays $\boldsymbol{\tau}$ by random numbers, and set the index of the delays k to 1.
2. Obtain $o_{\boldsymbol{\tau}}$.
3. Make $\boldsymbol{\tau}'$ by changing τ_k in $\boldsymbol{\tau}$ randomly.
4. Obtain $o_{\boldsymbol{\tau}'}$.

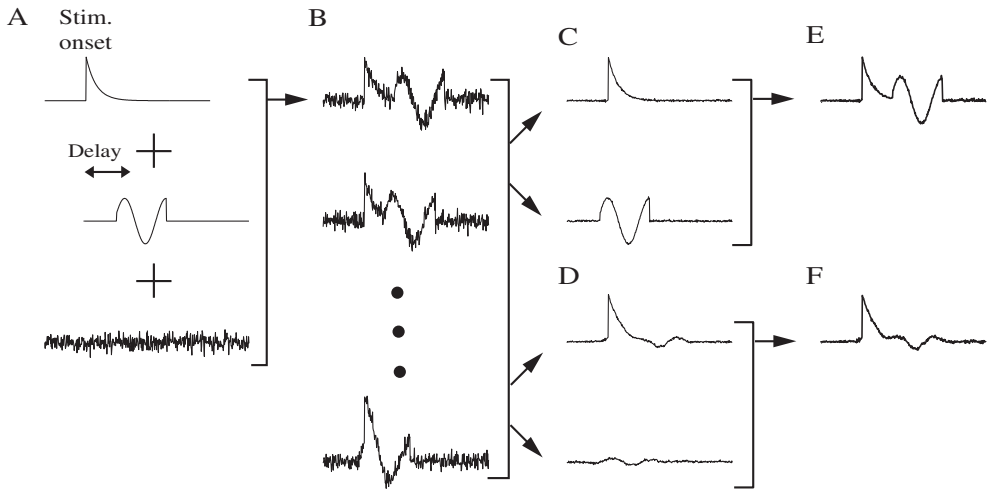

Figure 6.2: Simulation results on which the proposed method is based. **A**: Original stimulus-locked component (top), covert response-locked component (middle), and noise (bottom). **B**: Simulated data obtained by Eq. (5.1). **C**: Stimulus-locked component (top) and covert response-locked component (bottom) extracted using the true $\boldsymbol{\tau}$ by the method for overt responses. The waveforms of these components are similar to those of the original ones. **D**: Stimulus-locked component (top) and covert response-locked component (bottom) extracted using a wrong $\boldsymbol{\tau}$ by the method for overt responses. The waveforms of these components are different from those of the original ones. **E**: Reconstructed data from the components extracted by the true $\boldsymbol{\tau}$. Its waveform is similar to that of the simulated data (top row in **B**). **F**: Reconstructed data from the components extracted by the wrong $\boldsymbol{\tau}$. Its waveform is different from that of the simulated data (top row in **B**).

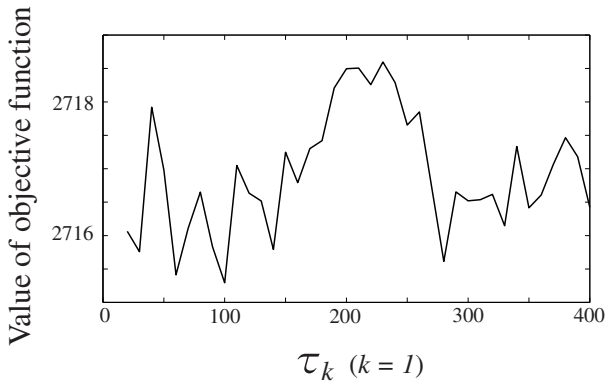

Figure 6.3: Value of objective function for each value of τ_k $(k = 1)$ obtained from simulated data. The other τ_k $(k \neq 1)$ are fixed at random numbers.

5. Replace $\boldsymbol{\tau}$ and $o_{\boldsymbol{\tau}}$ by $\boldsymbol{\tau}'$ and $o_{\boldsymbol{\tau}'}$ respectively if $o_{\boldsymbol{\tau}'}$ is smaller than $o_{\boldsymbol{\tau}}$.

6. Return to step 3 with increasing k by 1 (k returns to 1 if k becomes larger than N).

This procedure is different from the so-called general random search [44,46,47] in the point that, at step 3 in each iteration, this procedure does not change all of the τ_n $(n = 1, \cdots, N)$, but only one τ_k, where k circulates from 1 to N as the iteration number increases.

By using $y_n(n = 1, \cdots, N)$ shown in Fig. 6.2, B, I demonstrate the performance of the random search in Fig. 6.4. Figure 6.4, A, shows how the values of the objective function decrease within the same computational time (10 s) by the following four algorithms: the random search, a more general random search [47] where the procedure is the same as one I used except for making $\boldsymbol{\tau}'$ by random numbers at step 3, a genetic algorithm [48] and simulated annealing [45]. The convergence of the random search is the fastest among these (Fig. 6.4, A). Figure 6.4, B, shows the converged points by 2000 [$= 20 \times N$ $(N = 100)$] iterations of the random search, taking about 13 s by a personal computer [Dell XPS M1210 Intel(R) Core(TM)2 CPU T7200 @ 2.00GHz]. The 2000 iterations were repeated 100 times with different initial $\boldsymbol{\tau}$ at step 1. Among the 100 converged points, 54 points (encircled points in Fig. 6.4, B) reached values smaller than 200, and the correlation coefficients between the estimated and original delays were higher than 0.94. This indicates that the random search achieves convergence to a global minimum with a probability of about 0.5, being adequately high for practical use.

In the optimization, I firstly repeated $20 \times N$ iterations of the random search 50 times, and obtained 50 sets of $\boldsymbol{\tau}$ and $o_{\boldsymbol{\tau}}$. Then, I started $20 \times N$ iterations from the $\boldsymbol{\tau}$ which had the smallest $o_{\boldsymbol{\tau}}$ among the 50 sets.

During the optimization, I monitored the variance across n of $y_n(t) - s_{\boldsymbol{\tau}}(t) - cr_{\boldsymbol{\tau}}(t - \tau_n)$, which became smaller and smaller as the optimization proceeded, and stopped the optimization if the variance became smaller than those of the prestimulus level. This is because $y_n(t) - s_{\boldsymbol{\tau}}(t) - cr_{\boldsymbol{\tau}}(t - \tau_n)$ is considered as the extracted background noise and the level of original background noise is considered not to decrease after stimulus onsets.

After the optimization, I adjusted the average of the obtained $\boldsymbol{\tau}$. This adjustment is re-

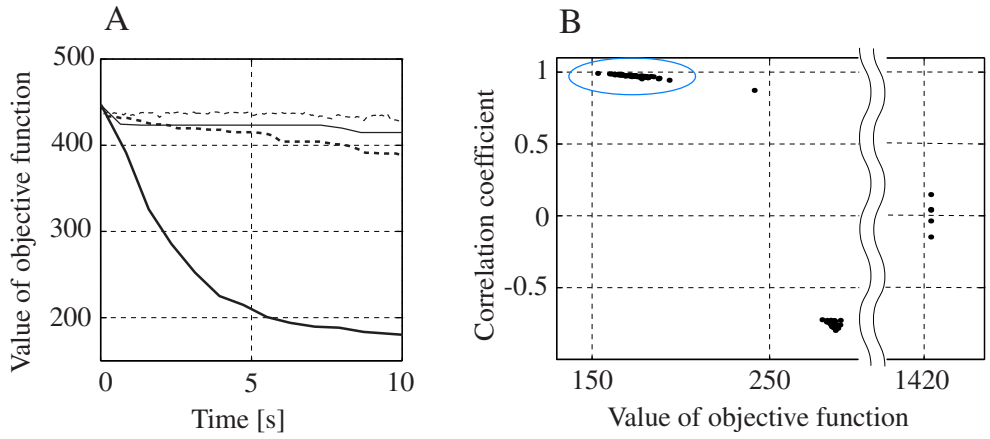

Figure 6.4: Performance of a random search. **A**: Decay of the values of the objective function by the restricted random search proposed (thick solid line), complete random search (thin solid line), genetic algorithm (thick dotted line), and simulated annealing (thin dotted line). **B**: Scatter plots of the converged values of the objective function and the correlation coefficients between the estimated and original delays by the restricted random search. Encircled dots indicate the converged points whose values of the objective function are lower than 200.

quired because the average of $\boldsymbol{\tau}$ varies depending on the time point defined as the onset of the covert response-locked component and the onset is arbitrarily determined in the optimization. For example, I adjusted the average of $\boldsymbol{\tau}$ obtained from the EEG during NoGo trials so that the maximum peaks in the extracted covert response-locked components became their onsets (described in Chapter 7). I then called the adjusted $\boldsymbol{\tau}$ the estimated delays.

6.2 Simulation Test with Artificial Data

In order to verify the performance of the proposed method, a numerical experiment was performed on a set of known artificial signals.

6.2.1 Methods

In this simulation, original $s(t)$ and $cr(t)$ were generated by the exponential and the cosine functions respectively (Fig. 6.2, A). Gaussian random numbers [mean = 270 ms, standard deviation (SD) = 50 ms] were used as $\boldsymbol{\tau}$, and white noise was used as $v_n(t)$. To examine

the relation between the accuracy of the estimated $\boldsymbol{\tau}$ and noise level, I generated 11 sets of $y_n(t)(n = 1, \cdots, 100)$ with different signal to noise ratio (SNR) of $-10, -9, \cdots, 0$ by adjusting SD of $v_n(t)$ to $0.56, 0.50, 0.45, 0.39, 0.36, 0.32, 0.28, 0.25, 0.22, 0.20, 0.18$, respectively. The SNR was defined as $10 \log_{10}(\sum_{t=0}^{T-1} cr(t)^2 / \sum_{t=0}^{T-1} v_n(t)^2)$.

Because the proposed method uses a stochastic algorithm (the random search), the estimation results should vary more or less in every estimation. To examine the robustness of the estimation results, I applied the proposed method to each set of $y_n(t)(n = 1, \cdots, 100)$ for 10 times, and obtained 10 sets of $\boldsymbol{\tau}$, $s_{\boldsymbol{\tau}}(t)$ and $cr_{\boldsymbol{\tau}}(t)$ for each set. Because the averages of $\boldsymbol{\tau}$ were arbitrarily determined in the optimization, the averages of the estimated $\boldsymbol{\tau}$ were adjusted to those of the original $\boldsymbol{\tau}$. The accuracy of the estimated $\boldsymbol{\tau}$ was quantified by the correlation coefficient between the estimated and original $\boldsymbol{\tau}$ (Figs. 6.5, D). Also, the similarity of the extracted component to the original one was quantified by the correlation coefficient between them, corresponding to the cross correlation between them at the lag of zero.

6.2.2 Results

Figure 6.5 shows the results of the simulation test with artificial data. Examples of the extracted components and estimated delays from the simulated data with a SNR of 0 are shown in Fig. 6.5, A–C. The extracted stimulus-locked components are highly correlated with the original one ($r = 0.96$) (Fig. 6.5, A), as are the extracted covert response-locked components ($r = 0.93$) (Fig. 6.5, B). The estimated delays are significantly correlated with the original ones ($r = 0.99$, $p < 0.05$, $slope = 0.96$) (Fig. 6.5, C). This indicates that the performance of the method is adequately accurate when the SNR is 0. The correlation coefficients between the original and estimated delays from the simulated data with a SNR of $-10, \cdots, 0$ are shown in Fig. 6.5, D. For a SNR ≥ -7 (SD of the noise ≤ 0.39), the correlation coefficients are high in all the repeated estimations (Fig. 6.5, D), indicating that the estimation is adequately accurate and robust when the SNR is high. In contrast, for a SNR < 7 (SD of the noise > 0.39), the correlation coefficients are low and variable across the repeated estimations (Fig. 6.5, D), indicating that the estimation is neither accurate nor robust when the SNR is low.

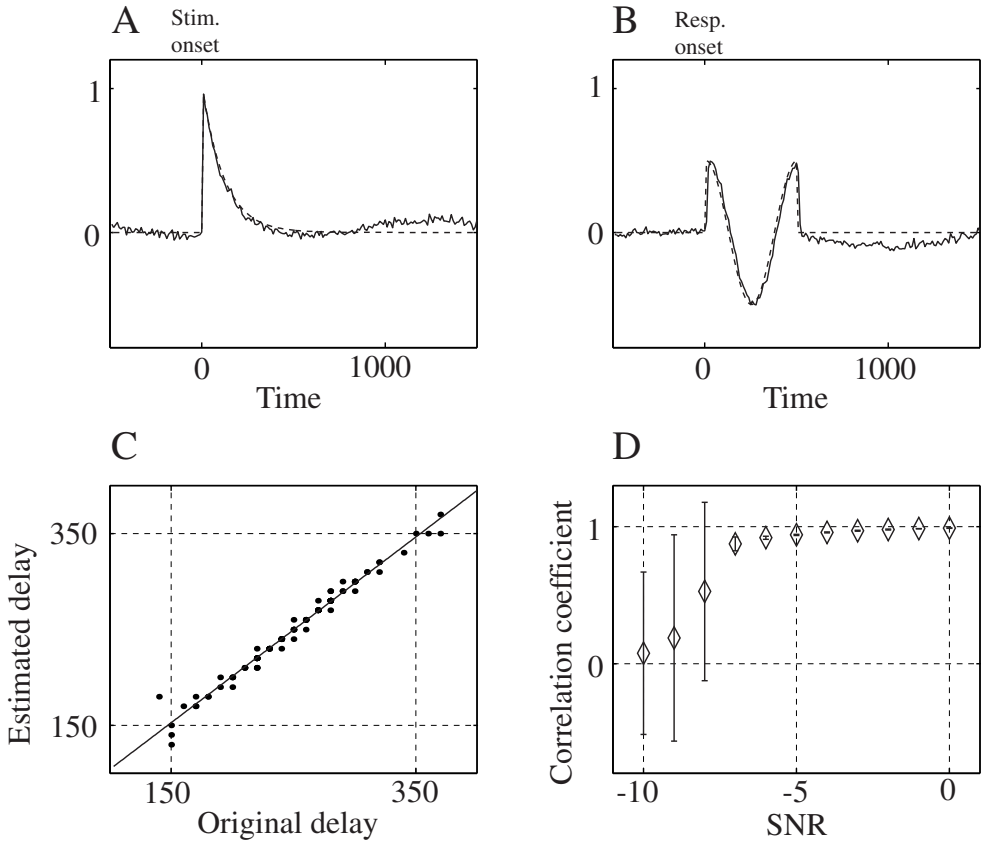

Figure 6.5: Simulation with artificial data. **A**–**C**: Examples of the extracted components and the estimated delays when the SNR is set to zero. **A**: Extracted stimulus-locked component (solid line) and original one (dotted line). **B**: Extracted covert response-locked component (solid line) and original one (dotted line). The horizontal axis represents relative time to the defined onsets of the covert response-locked component. **C**: Scatter plot of the estimated and original delays. **D**: Correlation coefficients between the estimated and original delays for each SNR. The diamonds and error bars respectively represent the means and SDs of the correlation coefficients.

6.3 Simulation Test with EEG Data

In order to test the performance of the method for more EEG-like data, an additional numerical experiment was performed using real EEG data.

6.3.1 Methods

In this simulation, the stimulus- and overt response-locked components extracted by the method for overt responses (see Chapter 3) from all the subjects' EEG and RTs during Go trials in the Go/NoGo task (described in Chapter 7) were used as $s(t)$ and $cr(t)$ respectively, and the RTs, which were randomly selected from all the subjects' RTs during Go trials, were used as $\boldsymbol{\tau}$. Noise $v_n(t)(n = 1, \cdots, 100)$ was obtained from all the subjects' EEG during a passive viewing task (described in Chapter 7) in the following way. The averaged EEG across trials were subtracted from each of the sets of EEG data, and the resultant EEG was discrete Fourier transformed and new sweeps were constructed by randomizing the phase information of the transformed EEG, while keeping their distributions constant (see [49], for a detailed description). From the sweeps obtained, I randomly selected 100 sweeps, and used them as $v_n(t)(n = 1, \cdots, 100)$. To examine the relation between the accuracy of the estimated $\boldsymbol{\tau}$ and the noise level, I generated 11 sets of $y_n(t)(n = 1, \cdots, 100)$ with different SNR of $-10, -9, \cdots, 0$ by adjusting the SD of $v_n(t)$ to $2.6, 2.3, 2.0, 1.8, 1.6, 1.4, 1.3, 1.2, 1.0, 0.91, 0.81$, respectively. Without the adjustment, the SD of $v_n(t)$ was 6.8 and the SNR was -18.

As in the simulation test with artificial data, I applied the proposed method to each set of $y_n(t)(n = 1, \cdots, 100)$ 10 times, and obtained 10 sets of $\boldsymbol{\tau}$, $s_{\boldsymbol{\tau}}(t)$ and $cr_{\boldsymbol{\tau}}(t)$ for each set. Because the averages of $\boldsymbol{\tau}$ were arbitrarily determined in the optimization, the averages of the estimated $\boldsymbol{\tau}$ were adjusted to those of the original $\boldsymbol{\tau}$. The accuracy of the estimated $\boldsymbol{\tau}$ was quantified by the correlation coefficient between the estimated and original $\boldsymbol{\tau}$ (Figs. 6.6, D). Also, the similarity of the extracted component to the original one was quantified by the correlation coefficient between them, corresponding to the cross correlation between them at a lag of zero.

6.3.2 Results

Figure 6.6 shows the results of the simulation test with EEG data. Examples of the extracted components and estimated delays from the simulated data with a SNR of 0 are shown in Fig. 6.6, A–C. The extracted stimulus-locked components are highly correlated with the original one ($r = 0.94$) (Fig. 6.6, A), as are the extracted covert response-locked components ($r = 0.89$) (Fig. 6.6, B). The estimated delays are significantly correlated with the original ones ($r = 0.94$, $p < 0.05$, *slope* $= 0.78$) (Fig. 6.6, C). This indicates that the performance of the method is adequately accurate when the SNR is 0. The correlation coefficients between the original and estimated delays from the simulated data with a SNR of $-10, \cdots, 0$ are shown in Fig. 6.6, D. For a SNR ≥ -4 (SD of the noise ≤ 1.3), the correlation coefficients are high in all the repeated estimations (Fig. 6.6, D), indicating that the estimation is adequately accurate and robust when the SNR is high. In contrast, for a SNR < -4 (SD of the noise > 1.3), the correlation coefficients are low and variable across the repeated estimations (Fig. 6.6, D), indicating that the estimation is neither accurate nor robust when the SNR is low.

6.4 Discussion

The simulation tests show that the proposed method can obtain the delays of the covert response-locked component even from noisy data, the SNR of which is lower than zero but higher than -6 (for artificial data) or -3 (for EEG data) (Figs. 6.5 and 6.6, D). Here, the SNR lower than zero means that the level of the noise is larger than that of the signal. Generally speaking, when the noise is larger than the signal, it is quite difficult, or impossible, to estimate the variable delays of the signal from single-trial data. The proposed method deals with the difficulty in a paradoxical way. To estimate the delays of "individual" trials, the method uses data epochs of "all" the trials in calculating the objective function. That is, I use all the trials for individual trials. This strategy is an essential point in the feasibility of the proposed method for noisy data, such as EEG data.

The simulation tests also show that the estimation results become inaccurate when the SNR

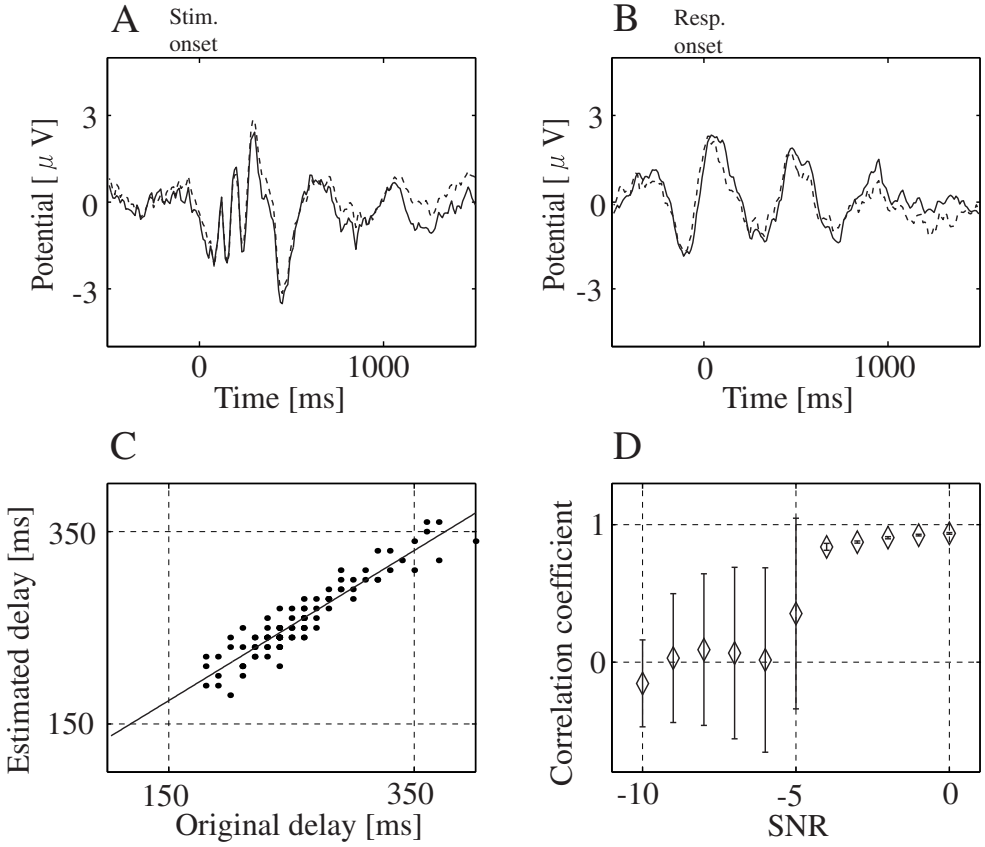

Figure 6.6: Simulation with EEG data. **A**–**C**: Examples of the extracted components and the estimated delays when the SNR is set to zero. **A**: Extracted stimulus-locked component (solid line) and original one (dotted line). **B**: Extracted covert response-locked component (solid line) and original one (dotted line). The horizontal axis represents relative time to the defined onsets of the covert response-locked component. **C**: Scatter plot of the estimated and original delays. **D**: Correlation coefficients between the estimated and original delays for each SNR. The diamonds and error bars respectively represent the means and SDs of the correlation coefficients.

is lower than -7 (for artificial data) or -4 (for EEG data) (Figs. 6.5 and 6.6, D). It is of note that these results hold true only when the number of trials N is 100, and the accuracy of the estimation depends on the number of trials. When the number of trials is smaller, the waveforms of the components extracted by using true delays become less accurate. This indicates that the estimated delays obtained by searching for the delays which minimize the value of the objective function become less accurate. In contrast, when the number of trials is larger, the waveforms of the components extracted by using true delays become more accurate. As a result, the true delays decrease the value of the objective function more adequately, and the estimated delays obtained by searching for the delays which minimize the value of the objective function become more accurate. In fact, in my simulation tests (see Appendix D), as the number of trials increases, the correlation coefficients between the estimated and original delays become greater. Therefore, as long as the optimization problem can be solved, the proposed method can overcome a higher noise level by increasing the number of trials.

In the optimization, I search for the set of the delays which minimizes the objective function. I adopt the random search for the optimization, because it achieves speedy convergence to a global minimum with a high probability. Generally speaking, a complete random search is a very slow algorithm when the number of trials N is large (see Fig. 6.4, A, thin solid line). This is because, as N increases, the size of the search space increases exponentially and the probability of finding an optimal set of delays decreases exponentially. I overcome this problem by searching for the delays sequentially. That is, I reduce the dimension of the search space from N to 1 by searching for the delays with respect to individual trials, and increase the probability to find a better set of delays. This is the reason why the convergence of the *restricted* random search I used is fast (Fig. 6.4, A, thick solid line), with a high probability of convergence to a global minimum (Fig. 6.4, B).

Because the random search is a stochastic algorithm, the estimated delays and the extracted components should vary more or less in each repeated estimation. The repeated simulation tests show that, when the SNR is high, the accuracy of the estimation is high and almost the same

across the repetitions (Figs. 6.5 and 6.6, D), indicating that the estimation is robust when it is accurate. When the SNR is low, the accuracy of the estimation is low and variable across the repetitions (Figs. 6.5 and 6.6, D), indicating that the estimation is not robust when it is not accurate. From these results, it is suggested that the robustness can be an index of the accuracy of the estimation.

On the other hand, the proposed method has a limitation. In calculating the objective function, this method uses the method for overt responses proposed in Chapter 3. This method has the technical limitation that slow waves ($\sim$ 1 Hz) in noise are amplified by the decomposition. Because of this limitation, the proposed method cannot easily deal with slow components, such as the contingent negative variation [50]. To extract slow components by the proposed method, we need to increase the number of trials at the expense of the calculation time for the optimization.

6.5 Conclusions

In this chapter, I propose a method for obtaining the stimulus-locked component, the covert response-locked component, and its delays of individual trials. The simulation results indicate the feasibility of the proposed method for artificial and EEG data. In the next chapter, I apply the proposed method to the EEG during NoGo trials of a Go/NoGo task.

Chapter 7

Application to EEG during NoGo Trials of a Go/NoGo Task

In this chapter, I apply the method proposed in the previous chapter to the EEG during NoGo trials of a Go/NoGo task, in which subjects are instructed to withhold a response. Although the subjects do not response overtly in NoGo trials, it is expected that the subjects response covertly in their brains, and the proposed method can extract the covert response-locked components together with the stimulus-locked components.

7.1 Methods

7.1.1 Experimental Procedure

Nine healthy adults (age 28.4 ± 3.7 years) constituted the experimental population. All the subjects gave their informed consent and the local ethics committee approved the experimental procedure.

The subjects were comfortably seated on a chair in a dimly lit, electrically shielded room. At about 50 cm in front of the subjects' eyes, red and green light-emitting diodes (LEDs) for imperative signals were vertically arrayed 1.5 cm apart on a black panel. The subjects were instructed to perform two kinds of tasks in the following order: a Go/NoGo task, and a passive viewing task. In the Go/NoGo task, the subjects undertook four experimental blocks, each consisting of 50 trials. The subjects were instructed to push a button immediately after a "Go"

signal (green LED) or not to push it after a "NoGo" signal (red LED). The green or red LED was illuminated in random order with almost equal probability. In two blocks, the subjects had to respond with their right index finger, and in the other two blocks with their left index finger. In an off-line analysis, the data from the blocks of right and left fingers were mixed. In the passive viewing task, the subjects undertook two experimental blocks, each consisting of 50 trials. The subjects were instructed passively to view the same stimulus as in the Go/NoGo task. In both tasks, each trial began with a warning signal (a beep), followed, after a variable delay of 1.8–2.2 s, by the imperative signals (duration: 500 ms). Inter-trial intervals were randomized from 3.5 to 7.5 s.

During the tasks, surface EEG was recorded from 19-ch Tin electrodes, mounted in a cap (Electro-Cap International, Inc., Eaton, Ohio, USA) according to the International 10-20 system, referred to a Tin electrode placed on AFz. The EEG was amplified on a Nihon Kohden EEG-1100 with a time constant of 0.3 s. Because I expected that large EEG activity related to the task execution would not appear around the earlobes, I placed Ag/AgCl electrodes on both earlobes and recorded their potentials separately. Their averaged potentials were subtracted from the EEG data off-line. For monitoring eye movements, an electrooculogram (EOG) was recorded with a pair of Ag/AgCl electrodes placed above and below the left eye. The sampling rate of the EEG and EOG was 1000 Hz.

7.1.2 Data Analyses

In an off-line analysis, I resampled the EEG data at a rate of 100 Hz. Because the proposed method has the technical limitation that slow waves ($\sim$ 1 Hz) in the background EEG activity are amplified by the decomposition (see Chapter 6), the EEG data were filtered with a bandpass of 2–40 Hz by using two kinds of finite impulse response (FIR) filters: a high-pass of 2 Hz (300-point, -26 dB at 1 Hz) and a low-pass of 40 Hz (15-point, -45 dB at 50 Hz). Then, the filtered EEG data were segmented into 2 s epochs from -500 to 1500 ms after stimulus onsets.

Reaction times of Go trials were defined as the intervals between the stimulus onset and the button push signal onset. I excluded Go trials with the RT either shorter than 100 ms or longer

than 400 ms, and excluded NoGo trials with responses. An artifact criterion of ± 50 μV was used for the EEG and EOG to reject trials with excess ocular artifacts or measurement noise. The numbers of trials obtained per subject were 77 ± 12 for Go trials, 87 ± 13 for NoGo trials, and 78 ± 25 for the passive viewing task.

Application to EEG during Go Trials

Because the EEG during Go trials consists of the stimulus- and overt response-locked components, it is expected that the EEG during Go trials satisfies the assumption of the proposed method for covert responses and the proposed method can estimate the RTs of Go trials, i.e., the delays of the overt response-locked component. To test this, I applied the proposed method to the individual subject's EEG data at Cz during Go trials for 10 times, and obtained 10 sets of estimated RTs. In estimating the RTs, I set the range of the RTs at the width of 300 ms. The accuracy of the estimated RTs was quantified by the correlation coefficient between the estimated and real RTs.

Check for Existence of Covert Response-locked Component in EEG during NoGo Trials

Although the proposed method assumes that EEG activity consists of the stimulus- and covert response-locked components, the validity of this assumption, especially the existence of the covert response-locked component, is not always guaranteed at least for the EEG during NoGo trials of the Go/NoGo task. As an alternative assumption, we might also consider that the EEG during NoGo trials includes only the stimulus-locked component. Therefore, in order to check whether the EEG included the covert response-locked component or not, I examined the time course of the EEG variance across trials.

Suppose that the background noise is a stationary process, from the assumption of Eq. (5.1), the EEG variance across trials $\mathrm{Var}[y(t)]$ is approximately expressed by:

$$\mathrm{Var}[y(t)] \approx \frac{1}{N}\sum_{n=1}^{N}[cr(t-\tau_n) - \frac{1}{N}\sum_{n=1}^{N} cr(t-\tau_n)]^2 + \mathrm{Var}[v], \tag{7.1}$$

where $\mathrm{Var}[v]$ represents the variance of noise across trials. From Eq. (7.1), if the covert response-

locked component does not exist, the EEG variance is expressed by:

$$\mathrm{Var}[y(t)] \approx \mathrm{Var}[v]. \tag{7.2}$$

Equations (7.1) and (7.2) indicate that the time courses of the EEG variance are qualitatively different depending on whether the covert response-locked component exists or not. If the covert response-locked component exists, the variance should increase and decrease after stimulus onset because of the trial-to-trial variability in its delays. In contrast, if the covert response-locked component does not exist, the variance should be constant. We can confirm this fact by the simulation results shown in Fig. 7.1. When the simulated data includes the covert response-locked component (Fig. 7.1, A), the variance across trials of the simulated data shows a transient increase after stimulus onset (Fig. 7.1, C). In contrast, when the simulated data does not include the covert response-locked component (Fig. 7.1, B), the variance across trials of the simulated data is almost constant (Fig. 7.1, D). Therefore, I checked the existence of the covert response-locked components by examining the time course of the EEG variance across trials (Fig. 7.2).

Application to EEG during NoGo Trials

Because the variance of the EEG during NoGo trials at C3, C4, Fz and Cz showed a transient increase (Fig. 7.2), I applied the proposed method to these EEG data. I obtained the stimulus-locked components, the covert response-locked components and the delays for each subject and each channel. In estimating the delays, I set their range at the width of 400 ms, because the EEG variance was significantly greater than the pre-stimulus level for about 400 ms after the stimulus onset ($p < 0.05$, Wilcoxon signed-rank test).

To examine the robustness of the estimated delays, I repeated the estimation of the delays 10 times for the same EEG data, and obtained 10 sets of delays. The robustness was checked in the following way. First, I calculated the correlation coefficient between each set and the average of the other sets, and obtained the 10 correlation coefficients. Then, I conducted a two-tailed Wilcoxon signed-rank test to assess the null hypothesis that the correlation coefficients did not differ from zero. If the null hypothesis was not rejected at the alpha level of 0.05, I regarded the

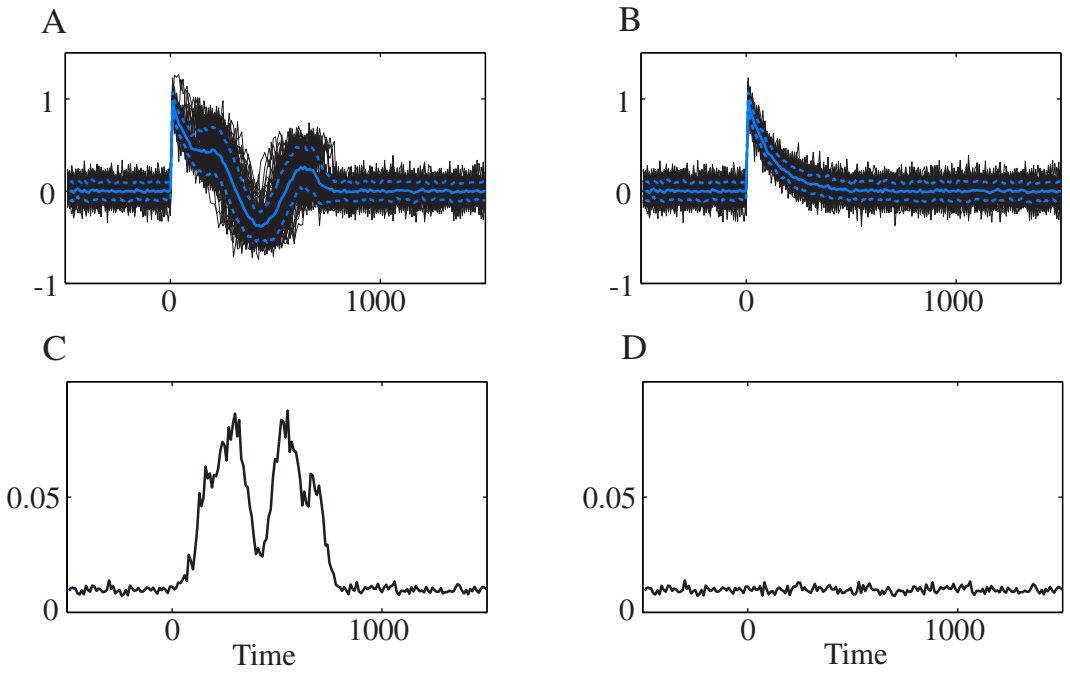

Figure 7.1: Time course of variance of simulated data. **A**: Simulated data, consisting of the stimulus- and covert response-locked components. **B**: Simulated data, consisting of only the stimulus-locked components. In **A** and **B**, the black lines represent the simulated data of individual trials, the blue solid lines represent the means of the simulated data, and the blue dotted lines represent the mean ±SD of the simulated data. **C**: Variance across trials of the simulated data in **A**. **D**: Variance across trials of the simulated data in **B**.

SNR of the EEG not to be high enough to estimate the delays robustly and excluded the EEG data from the following analyses. If the null hypothesis was rejected, I regarded the estimation results to be robust and, in the following analyses, used the set of delays whose correlation coefficient was the highest. As a result, I obtained the delays of 6 sets for C3, 6 sets for C4, 7 sets for Fz, and 6 sets for Cz, from the 9 subjects' EEG data during NoGo trials.

I adjusted the averages of the estimated delays so that the estimated delays represented latencies of the same peaks in the extracted covert response-locked components across subjects. First, I set a subject's covert response-locked components as references, and shifted the other subjects' delays and the covert response-locked components so that their values of the cross-correlations with the references became maximum at the lag of zero. Then, I shifted all the subjects' delays so that the delays represented latencies of the maximum peaks in the average covert response-locked components of all the subjects.

After the estimation, to examine the validity of the estimated delays, I formed time-trial images [7] of the EEG during NoGo trials sorted by the estimated delays (Fig. 7.3). In these images, all the subjects' EEG epochs were smoothed vertically with a 15-trial moving average, and the potential fluctuations were shown as color-coded horizontal lines. If the estimated delays are valid, both the stimulus- and estimated delay-locked fluctuations should appear, whereas, if the estimated delays are wrong, only the stimulus-locked fluctuations should appear, as shown in the left panel in Fig. 7.3. Therefore, I examined whether the estimated delay-locked fluctuations appeared or not in the time-trial images of the EEG sorted by the estimated delays.

The similarity of the extracted components across subjects was quantified by calculating the correlation coefficient between a subject's component and the other subjects' average component for each subject, corresponding to the cross-correlation between the two waveforms at a lag of zero. As for the stimulus-locked components, the similarity of the extracted component to the stimulus-triggered average EEG was also quantified by the correlation coefficient between them. A two-tailed Wilcoxon signed-rank test was conducted to assess the null hypothesis that the correlation coefficients obtained from individual subjects did not differ from zero. An alpha level

Table 7.1: Correlation coefficients (r) between the estimated and real RTs in Go trials.

	Subj. 1	Subj. 2	Subj. 3	Subj. 4	Subj. 5
r	-0.39 ± 0.061	0.017 ± 0.092	0.042 ± 0.15	0.37 ± 0.16	0.69 ± 0.043
	Subj. 6	Subj. 7	Subj. 8	Subj. 9	
r	-0.097 ± 0.11	-0.22 ± -0.25	0.17 ± 0.23	-0.018 ± 0.11	

Values are mean ± SD for 10 estimations.

of 0.05 was used for the statistical tests.

7.2 Results

7.2.1 Estimation of RTs in Go Trials

Table 7.1 shows the correlation coefficients between the real and estimated RTs from the individual subjects' EEG at Cz during Go trials by the proposed method. For Subjs. 4 and 5, the estimated RTs are highly correlated with the real RTs (Table 7.1). For the other subjects, however, the estimated RTs are not correlated with the real RTs (Table 7.1).

7.2.2 Testing Assumption for EEG during NoGo Trials

Figure 7.2 shows the time courses of the EEG variance during NoGo trials of the Go/NoGo task obtained from all the subjects' EEG. The variance of the EEG at C3, C4, Fz and Cz during NoGo trials shows transient increases during 300–500 ms after the stimulus onset (Fig. 7.2). In contrast, the variance is almost constant for the EEG during the passive viewing task (Fig. 7.2). This suggests that the EEG at these channels during NoGo trials includes the covert response-locked component, whereas the EEG during the passive viewing of the same stimulus does not. Therefore, I apply the proposed method to the EEG at C3, C4, Fz and Cz during NoGo trials.

7.2.3 Decomposing EEG during NoGo Trials

Then, I obtain the stimulus-locked components, covert response-locked components and the delays for individual EEG channels and individual subjects. The estimated delays, representing the

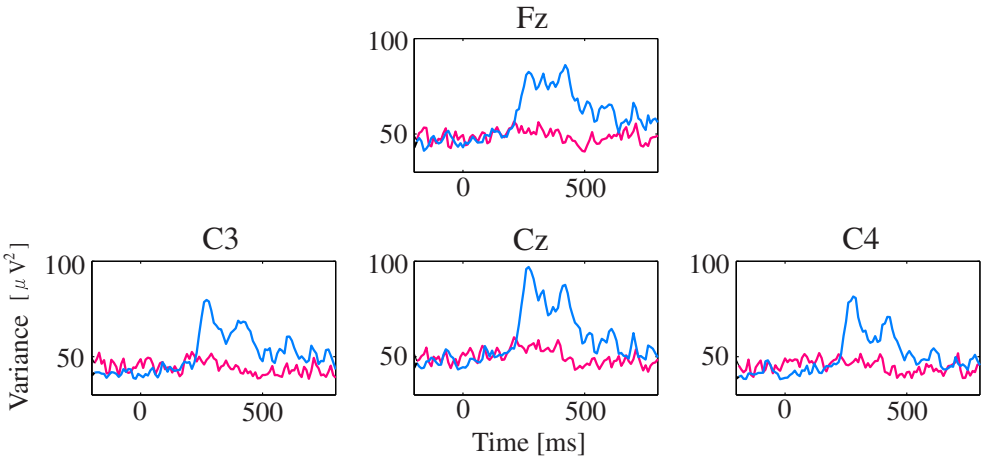

Figure 7.2: Time course of the EEG variance across trials at C3, C4, Fz and Cz obtained from all the subjects' EEG. The blue lines represent the EEG variance during NoGo trials; the red lines represent the EEG variance during the passive viewing task.

latencies of the positive peaks in the covert response-locked components, are 403 ± 76 ms for C3, 360 ± 66 ms for C4, 292 ± 78 ms for Fz, and 336 ± 69 ms for Cz, and these are much longer than the RTs of Go trials (269 ± 50 ms).

Figure 7.3 shows the time-trial images obtained from all the subjects' EEG at Cz. When the EEG epochs are randomly sorted, only the stimulus-locked fluctuations appear (Fig. 7.3, left). However, when the EEG epochs are sorted by the estimated delays, not only the stimulus-locked but also the estimated delay-locked fluctuations appear (Fig. 7.3, right), suggestive of the validity of the estimated delays.

Figure 7.4, A, shows the extracted stimulus-locked components for each EEG channel. The extracted components exhibit negative peaks at around 240 ms (N200) and positive peaks at around 370 ms (P300) after the stimulus onset for all the 4 channels. The correlation coefficients between the extracted components of individual subjects and the averaged components of the other subjects are significantly larger than zero ($r = 0.54 \pm 0.26, p < 0.05$ for C3; $r = 0.42 \pm 0.31, p < 0.05$ for C4; $r = 0.66 \pm 0.15, p < 0.05$ for Fz; $r = 0.43 \pm 0.31, p < 0.05$ for Cz), indicating that the extracted components exhibit similar patterns across subjects. The correlation coefficients between

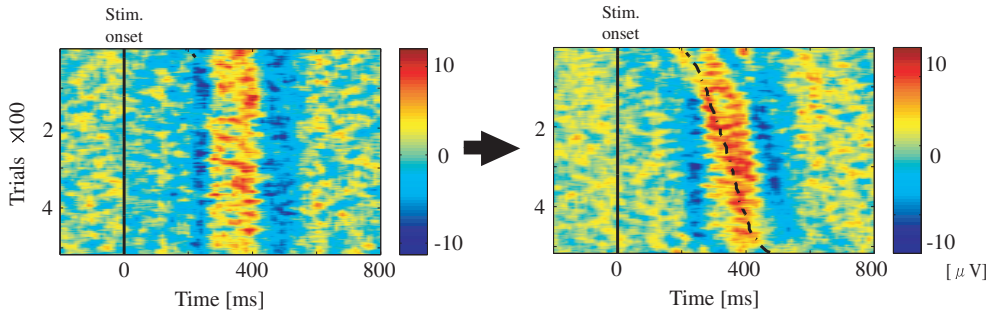

Figure 7.3: Time-trial images of all the subjects' EEG at Cz during NoGo trials. In the left image, the EEG epochs are randomly sorted. In the right image, the EEG epochs are sorted by the estimated delays. The solid lines represent the stimulus onsets, and the dotted line represents the estimated delays.

the extracted components and the stimulus-triggered average EEG are significantly larger than zero ($r = 0.90 \pm 0.049, p < 0.05$ for C3; $r = 0.87 \pm 0.12, p < 0.05$ for C4; $r = 0.94 \pm 0.050, p < 0.05$ for Fz; $r = 0.89 \pm 0.10, p < 0.05$ for Cz), indicating that the extracted stimulus-locked components exhibit similar patterns to the stimulus-triggered average EEG.

Conventionally, EEG activity related to a response inhibition is examined by using the NoGo−Go subtracting waveforms of the stimulus-triggered average EEG (for example, [20, 51–53]). However, the stimulus-triggered average EEG is more or less contaminated by the temporal overlapping of the response-locked components (see Chapter 2). From the above-mentioned similarity between the extracted stimulus-locked component and the stimulus-triggered average EEG, it is expected that the difference in the stimulus-triggered average EEG between Go and NoGo trials comes from that of the stimulus-locked components. To confirm this expectation, I compare the NoGo−Go subtracting waveforms of the stimulus-triggered average EEG with those of the stimulus-locked components. The stimulus-locked components of Go trials are extracted from the EEG and real RTs of Go trials by the method for overt responses. The NoGo−Go subtracting waveforms of the stimulus-triggered average EEG appear to be almost the same as those of the stimulus-locked components (Fig. 7.4, B), and the squared correlation coefficients between them are high ($r^2 = 0.59$ for C3; $r^2 = 0.70$ for C4; $r^2 = 0.94$ for Fz; $r^2 = 0.83$ for Cz).

Therefore, it is suggested that, at around Fz and Cz, the differences of the stimulus-triggered average EEG between Go and NoGo trials are mainly (about 83–94%) attributable to those of the stimulus-locked components.

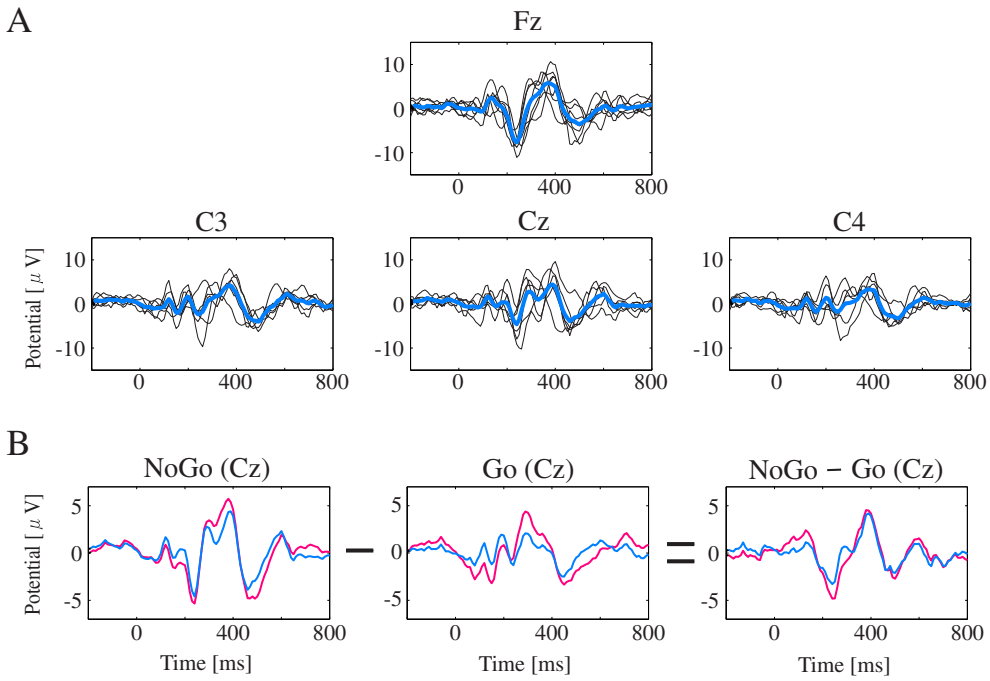

Figure 7.4: Extracted stimulus-locked components at C3, C4, Fz and Cz. **A**: Stimulus-locked components extracted from the EEG during NoGo trials. The black lines represent the extracted stimulus-locked components of individual subjects, and the blue lines represent the averaged components across subjects. **B**: Differences of the extracted stimulus-locked components between Go and NoGo trials at Cz. The left panel shows the stimulus-locked component (blue line) and the stimulus-triggered average (red line) of NoGo trials. The middle panel shows the stimulus-locked component (blue line) and the stimulus-triggered average (red line) of Go trials. The right panel shows the NoGo−Go subtracting waveforms of the stimulus-locked component (blue line) and that of the stimulus-triggered average EEG (red line).

Figure 7.5 shows the extracted covert response-locked components for each EEG channel. The extracted covert response-locked components exhibit positive peaks, whose magnitudes are comparable with those in the extracted stimulus-locked components. The correlation coefficients between the extracted components of individual subjects and the averaged components of the

other subjects are significantly larger than zero ($r = 0.67 \pm 0.097, p < 0.05$ for C3; $r = 0.67 \pm 0.24, p < 0.05$ for C4; $r = 0.56 \pm 0.27, p < 0.05$ for Fz; $r = 0.67 \pm 0.17, p < 0.05$ for Cz), indicating that the extracted covert response-locked components exhibit similar patterns across subjects.

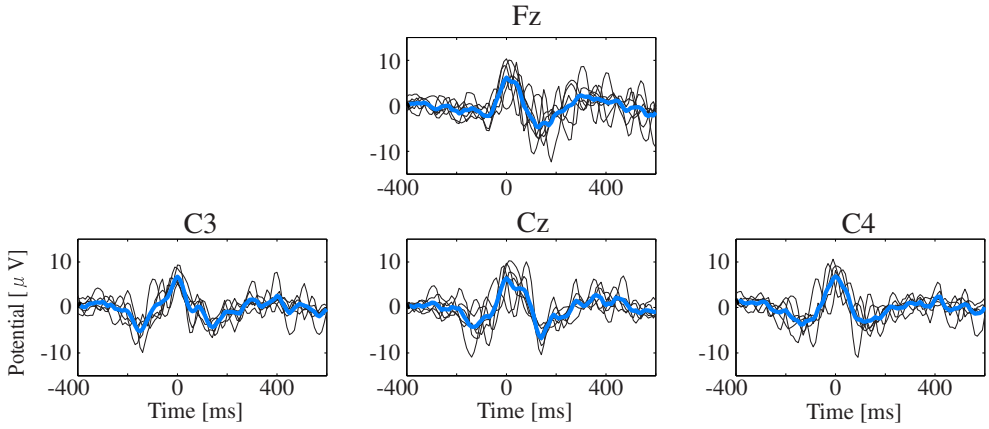

Figure 7.5: Extracted covert response-locked components from the EEG at C3, C4, Fz and Cz during NoGo trials. The black lines represent the extracted covert response-locked components of individual subjects, and the blue lines represent the averaged components across subjects. The horizontal axes represent relative time to the time points of the maximum peaks in the average covert response-locked components.

7.3 Discussion

7.3.1 Estimated RTs from EEG during Go Trials

By applying the proposed method to the EEG during Go trials, the RTs of Go trials are successfully estimated for Subjs. 4 and 5, but are not for the other subjects (Table 7.1). The successes of the estimation support the feasibility of the method for real EEG data. On the other hand, the failures of the estimation are partially due to the low SNR of EEG during Go trials and to the fact that the stimulus-unlocked components are not necessarily time-locked to the motor responses. As for the latter, Verleger et al. [54] examined the EEG during choice reaction time tasks by the stimulus- and response-triggered averaging procedures, and reported that the P3b is time-locked to neither stimulus nor motor response onsets. Considering that the Go/NoGo

task is a choice reaction time task, it is possible that the EEG during Go trials also includes the components time-locked to neither stimulus nor motor response onsets and the method extracts such components instead of the overt response-locked components.

7.3.2 Extracted Components from EEG during NoGo Trials

The proposed method assumes that the EEG activity consists of a stimulus-locked component and a covert response-locked component. However, the existence of a covert response-locked component is less evident than a stimulus-locked component, which appears with the use of the stimulus-triggered averaging procedure. Therefore, to check the validity of the assumption, I examine whether the EEG variance across trials increases after the stimulus onset. Although one might argue that the changes in the EEG variance are attributable to the variability of the waveform of the stimulus-locked component rather than the covert response-locked component and its variable delays, from the relatively constant EEG variance during the passive viewing task, I believe that the variability of the waveform of the stimulus-locked component is not so large as to generate a drastic change in the variance of the EEG during NoGo trials (Fig. 7.2). Therefore, I apply the proposed method to the EEG during NoGo trials, and extract the stimulus- and covert response-locked components.

The waveforms of the extracted stimulus-locked components are almost the same as those of the stimulus-triggered average EEG. This indicates that the covert response-locked components are almost cancelled out by the stimulus-triggered averaging procedure. The extracted stimulus-locked components exhibit the N200 and P300 as well as the stimulus-triggered average EEG. This indicates that the N200 and P300, which are the classical peaks of the EEG during NoGo trials [20, 51, 53, 55, 56], are stimulus-locked. We can visually confirm this fact by the stimulus-locked fluctuations at around 240 and 370 ms in the time-trial images (Fig. 7.3). At around Fz and Cz, the differences in the stimulus-locked components between Go and NoGo trials largely account for those in the stimulus-triggered average EEG (Fig. 7.4, B). This result suggests that, in the fronto-central region, the conventional differences in the EEG between Go and NoGo trials are mainly attributable to those in the stimulus-locked components rather than the contamination effects by

the covert response-locked components. Further, the different waveforms of the stimulus-locked component between Go and NoGo trials indicate that the stimulus-related brain processes are different between Go and NoGo trials.

As for the extracted covert response-locked components, its magnitudes are comparable with those of the stimulus-locked components (Figs. 7.4 and 7.5). The presence of the extracted covert response-locked components and the validity of the estimated delays are confirmed by the results that the time-trial images show the fluctuations time-locked to the estimated delays and that the waveforms of the extracted components are similar across subjects.

The average delays of the positive peaks in the covert response-locked components are almost the same as the P300 latency in the stimulus-locked component (363 ± 26 ms), indicating that the positive peaks mainly overlap with the P300 in the stimulus-locked components (see Fig. 7.3, right). From this result, I consider that the proposed method for the first time decomposes the conventional P300 of NoGo trials, which appears by the stimulus-triggered averaging procedure, into the stimulus-locked P300 and the covert response-locked P300.

7.4 Conclusions

The proposed method successfully extracts a covert response-locked component and its delays from the EEG during NoGo trials. In the brain, internal and subjective events related to cognitive functions seem to occur, not with precisely constant delays, but with various delays from trial to trial after stimulus onset. Since the proposed method can extract such brain activity, the method will provide a new tool to look into complex and implicit brain functions.

Chapter 8

General Discussion

In this thesis, I propose two methods for decomposing EEG into the stimulus- and response-locked components: the method for overt responses and the method for covert responses.

The method for overt responses is used when responses are observable. This method decomposes EEG into the stimulus- and overt response-locked components using RTs by the discrete Fourier transform (Chapter 3). I apply the method to the EEG during a simple reaction time task, and show that the contamination by the temporal overlapping is large especially in the late part of the stimulus-triggered average EEG when slow waves remain in the EEG data (Chapter 4).

The method for covert responses is used when responses are not observable. This method obtains the individual delays of the covert response-locked component together with the stimulus- and covert response-locked components. In this method, I initially set random values for the delays and extract uncontaminated stimulus- and covert response-locked components using the preset delays by the method for overt responses. Then, I reconstruct the EEG by overlapping the extracted components with the preset delays, and calculate the residual errors between the reconstructed and original EEG. This procedure is repeated by updating the delays until the residual errors become adequately small (Chapter 6). I apply the method to the EEG during NoGo trials of a Go/NoGo task, and extract the covert response-locked components, the magnitudes of which are comparable with those of the stimulus-locked components (Chapter 7).

In this chapter, I discuss the remaining problems and possible applicability of these methods, and show the further development of the methods.

8.1 Method for Overt Responses

In Chapter 3, I propose the method for decomposing EEG into the stimulus- and overt response-locked components using RTs.

This method has the limitation that the slow waves ($\sim$ 1 Hz) in the noise are amplified by the decomposition. This is due to the fact that the absolute values of $1/D(n,\omega)$ in Eqs. (3.9) and (3.10) tend to be high at low frequencies when τ_n is RTs. To overcome this limitation, I propose two solutions: increase the total number of trials, and apply a highpass filter to the EEG before the decomposition. At the same time, it is necessary to improve the method itself to eliminate the limitation. Originally, the source of the limitation, $1/D(n,\omega)$, arises from the simultaneous equations (3.1) and (3.2). It is possible that another set of simultaneous equations may solve the limitation. Therefore, we need to try various sets of simultaneous equations to improve the method itself.

On the other hand, this method has the practical advantage of requiring only single-channel EEG data. This advantage makes it possible to apply the method in clinical use, because the single-channel recording is more easily applied. To date, several EEG studies have attempted to investigate the relation between stimulus-/overt response-related brain activity and movement disorders by the averaging procedure (for example, [57, 58]). However, the average EEG does not reflect pure stimulus- or overt response-related brain activity due to the temporal smearing. By using the proposed method, we are able to extract more detailed information about stimulus- and overt response-related brain activities, and to identify which process, the stimulus- or the overt response-related process, is responsible for the disorders. The proposed method can be used as an alternative to the averaging procedure to investigate stimulus- and overt response-related brain activities during various cognitive tasks with stimulus-overt response paradigms.

8.2 Method for Covert Responses

In Chapter 6, I propose a method for estimating the individual delays of the covert response-locked component and extracting the stimulus- and covert response-locked components from only single-channel EEG epochs.

The delays are estimated by solving the optimization problem. The limitation of this method is the calculation cost for solving this optimization problem. Suppose the number of trials is N and the delay is within M ms. We need to search for the optimal set of delays from M^N sets. When N and M are large, this is quite a difficult problem and it takes a lot of time to solve it. There are two approaches to overcome this limitation: 1) to make the optimization problem easy, and 2) to improve the optimization algorithm. For 1), I reduce N by decreasing the number of trials and M by using a priori information about the range of the delays derived from the time course of EEG variance, and make M^N as small as possible. For 2), I test various optimization algorithms, and adopt the best algorithm, the random search, which achieves speedy convergence to the optimal delays. Although these attempts work well for the EEG during NoGo trials of the Go/NoGo task, to apply this method to various noisy data, it is necessary to propose more powerful solutions to the limitation. Especially, there is plenty of room for improving the optimization algorithm, because the random search used is so simple and seems to be brute force.

On the other hand, the advantage of this method is, of course, its ability to extract the covert response-locked component, which has hardly been extracted owing to its variable delays. Then, what will be gained by applying this method to other EEG data (and possibly to other brain signals)?

Tallon-Baudry et al. [31, 32] showed evidence for a role for induced gamma activity, whose phase is not time-locked to stimulus onset, in the construction of a coherent representation of objects and the rehearsal of the representation in memory. This suggests that some brain activity related to perception and memory recall is not time-locked to stimulus onset. Also, the brain activity related to solving problems, or the "Aha!" experience [59], is not time-locked to the presentation of problems. Until now, the time points of solving problems have been estimated

from the onset of the subject's response claiming to have solved the problem (for example, [59]). However, the relation between the onset of the solving of a problem and that of the subject's response is not clear. Considering the large variability of RTs even during "simple" reaction time tasks, it is possible that the interval between the two onsets also has large variability. If so, we cannot extract pure brain activity related to problem solving from the response onset. By applying this method to EEG during these kinds of cognitive tasks, we can obtain more detailed information, the pure EEG waveform and its onsets, on the brain activity involved in such complex functions.

The advantages of this method are not only to extract the covert response-locked component but also to extract the uncontaminated stimulus-locked component. Conventionally, the stimulus-triggered average EEG has been thought to reflect the stimulus-locked EEG component in the hope that the covert response-locked component, even if it exists, would be cancelled out by the stimulus-triggered averaging procedure. However, whether this premise is well satisfied or not is unclear unless uncontaminated components are disclosed. This is because the effect of the contamination is determined by the waveform of the covert response-locked component and its delays, which were unknown before the application of this method. In Chapter 7, I reveal that the contamination is small in the fronto-central region by comparing the NoGo−Go subtracting waveforms of the stimulus-triggered average EEG with those of the stimulus-locked components. By applying the proposed method, we can obtain the uncontaminated stimulus-locked component and examine the level of contamination by the covert response-locked component.

8.3 Further Development of Proposed Methods

The essential strategies on which the proposed two methods based are as follows.

1. Separate components by solving simultaneous equations in the Fourier domain.

2. Estimate delays by searching for the delays which give the optimal approximation of EEG.

The method for overt responses is based on the first strategy, and the method for covert responses is based on the second strategy in addition to the first one. Based on these strategies, it is possible

easily to propose another method which is used for more complicated problems.

For example, I can propose a method for extracting the three components: the stimulus-locked component, the covert response-locked component and the overt response-locked component (Fig. 8.1). The three components may exist in daily complex stimulus-response situations. For example, let us consider a situation in which you are presenting your research. Someone asks you a question, and you have to answer it as soon as possible. In such a situation, it is possible that listening to the question evokes stimulus-locked activity, solving the question evokes covert response-locked activity, and answering the question evokes overt response-locked activity in your brain.

The method for decomposing the three components is proposed as follows. The EEG including the three components is expressed by:

$$y_n(t) = s(t) + cr(t - \tau_n) + or(t - rt_n) + v_n(t) \quad (t = 0, \cdots, T-1;\ n = 1, \cdots, N), \tag{8.1}$$

where $y_n(t)$: observed EEG data in trial n; $s(t)$: stimulus-locked component; $cr(t)$: covert response-locked component; $or(t)$: overt response-locked component; τ_n: delay of $cr(t)$ in trial n; rt_n: RT in trial n; $v_n(t)$: noise in trial n.

To separate $s(t)$, $cr(t)$ and $or(t)$, according to strategy 1, I take the discrete Fourier transform of Eq. (8.1), generate two more equations, and solve the equations simultaneously for $s(t)$, $cr(t)$ and $or(t)$ as follows. The discrete Fourier transform of Eq. (8.1) is expressed by:

$$Y_n(\omega) = S(\omega) + \exp(-i2\pi\omega\tau_n/T)CR(\omega) + \exp(-i2\pi\omega rt_n/T)OR(\omega) + V_n(\omega) \quad (\omega = 0, \cdots, T-1), \tag{8.2}$$

where $Y_n(\omega)$ is the discrete Fourier transform of $y_n(t)$; $S(\omega)$ is the discrete Fourier transform of $s(t)$; $CR(\omega)$ is the discrete Fourier transform of $cr(t)$; $OR(\omega)$ is the discrete Fourier transform of $or(t)$; $V_n(\omega)$ is the discrete Fourier transform of $v_n(t)$. I make the following two equations by averaging Eq. (8.2) across trials with fast RTs and across trials with slow RTs respectively.

$$\bar{Y}_f(\omega) = S(\omega) + \bar{E}c_f(\omega)CR(\omega) + \bar{E}o_f(\omega)OR(\omega) + \bar{V}_f(\omega)\ , \tag{8.3}$$

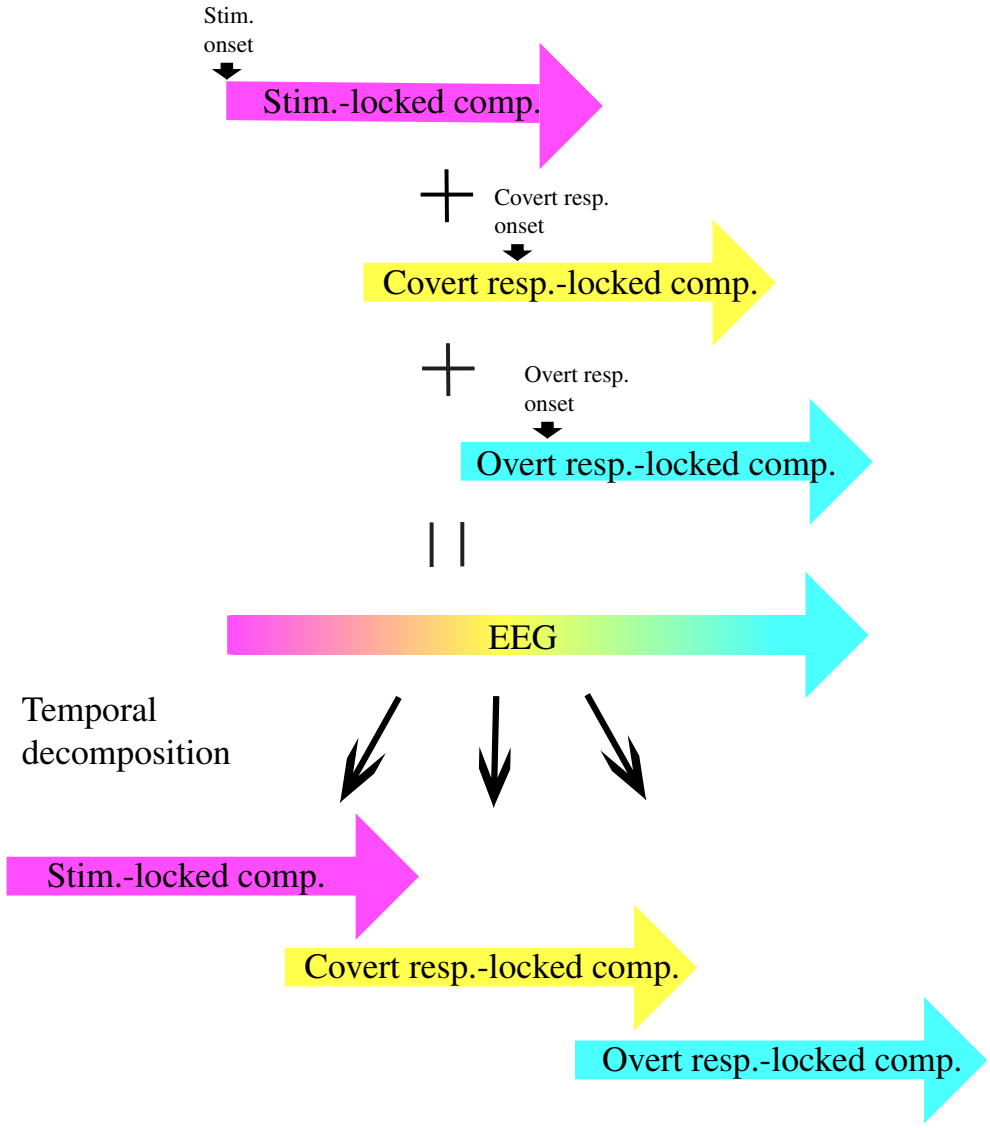

Figure 8.1: Schematic representation of the EEG including the three components: the stimulus-locked component, the covert response-locked component and the overt response-locked component. I propose a method for temporally decomposing the EEG into the three components.

$$\bar{Y}_s(\omega) = S(\omega) + \bar{Ec}_s(\omega)CR(\omega) + \bar{Eo}_s(\omega)OR(\omega) + \bar{V}_s(\omega) \ , \tag{8.4}$$

where

$$\bar{Y}_f(\omega) = \frac{1}{2N}\sum_{n\in n_f} Y_n(\omega); \tag{8.5}$$

$$\bar{Y}_s(\omega) = \frac{1}{2N}\sum_{n\in n_s} Y_n(\omega); \tag{8.6}$$

$$\bar{Ec}_f(\omega) = \frac{1}{2N}\sum_{n\in n_f} \exp(-i2\pi\omega\tau_n/T); \tag{8.7}$$

$$\bar{Ec}_s(\omega) = \frac{1}{2N}\sum_{n\in n_s} \exp(-i2\pi\omega\tau_n/T); \tag{8.8}$$

$$\bar{Eo}_f(\omega) = \frac{1}{2N}\sum_{n\in n_f} \exp(-i2\pi\omega rt_n/T); \tag{8.9}$$

$$\bar{Eo}_s(\omega) = \frac{1}{2N}\sum_{n\in n_s} \exp(-i2\pi\omega rt_n/T); \tag{8.10}$$

$$\bar{V}_f(\omega) = \frac{1}{2N}\sum_{n\in n_f} V_n(\omega); \tag{8.11}$$

$$\bar{V}_s(\omega) = \frac{1}{2N}\sum_{n\in n_s} V_n(\omega), \tag{8.12}$$

and n_f is the trial with fast RTs, n_s is the trial with slow RTs. Equations (8.2), (8.3) and (8.4) are rewritten by:

$$\begin{pmatrix} Y_n(\omega) \\ \bar{Y}_f(\omega) \\ \bar{Y}_s(\omega) \end{pmatrix} = A \begin{pmatrix} S(\omega) \\ CR(\omega) \\ OR(\omega) \end{pmatrix} + \begin{pmatrix} V_n(\omega) \\ \bar{V}_f(\omega) \\ \bar{V}_s(\omega) \end{pmatrix}, \tag{8.13}$$

where

$$A = \begin{pmatrix} 1 & \exp(-i2\pi\omega\tau_n/T) & \exp(-i2\pi\omega rt_n/T) \\ 1 & \bar{Ec}_f(\omega) & \bar{Eo}_f(\omega) \\ 1 & \bar{Ec}_s(\omega) & \bar{Eo}_s(\omega) \end{pmatrix}. \tag{8.14}$$

By multiplying Eq (8.13) by A^{-1}, I obtain:

$$A^{-1}\begin{pmatrix} Y_n(\omega) \\ \bar{Y}_f(\omega) \\ \bar{Y}_s(\omega) \end{pmatrix} = \begin{pmatrix} S(\omega) \\ CR(\omega) \\ OR(\omega) \end{pmatrix} + A^{-1}\begin{pmatrix} V_n(\omega) \\ \bar{V}_f(\omega) \\ \bar{V}_s(\omega) \end{pmatrix}. \tag{8.15}$$

Then, by averaging across n and taking the inverse discrete Fourier transform (IDFT), I obtain:

$$\text{IDFT}\left[\frac{1}{N}\sum_{n=1}^{N} A^{-1}\begin{pmatrix} Y_n(\omega) \\ \bar{Y}_f(\omega) \\ \bar{Y}_s(\omega) \end{pmatrix}\right] = \begin{pmatrix} s(t) \\ cr(t) \\ or(t) \end{pmatrix} + \text{IDFT}\left[\frac{1}{N}\sum_{n=1}^{N} A^{-1}\begin{pmatrix} V_n(\omega) \\ \bar{V}_f(\omega) \\ \bar{V}_s(\omega) \end{pmatrix}\right]. \tag{8.16}$$

Equation (8.16) shows that, if both the τ_n and rt_n are observable, we can extract $s(t)$, $cr(t)$ and $or(t)$ by calculating the left-hand side of Eq. (8.16).

Then, according to strategy 2, I estimate the unknown delays of the covert response-locked component τ_n. Let me define $s_{\boldsymbol{\tau}}(t)$, $cr_{\boldsymbol{\tau}}(t)$ and $or_{\boldsymbol{\tau}}(t)$ respectively as $s(t)$, $cr(t)$ and $or(t)$ extracted using a set of delays $\boldsymbol{\tau} = [\tau_1, \tau_2, \cdots, \tau_N]$ by calculating the left-hand side of Eq. (8.16). Under the assumption that sets of nearly true delays provide better approximations of the observed EEG data than sets of wrong delays, I estimate the true $\boldsymbol{\tau}$ by solving an optimization problem of:

$$\textbf{Minimize} \quad \sum_{t=t_1}^{t_2} \sum_{n=1}^{N} \{y_n(t) - s_{\boldsymbol{\tau}}(t) - cr_{\boldsymbol{\tau}}(t - \tau_n) - or_{\boldsymbol{\tau}}(t - rt_n)\}^2$$

$$\textbf{Subject to} \quad \boldsymbol{\tau} \subset \mathbf{N}.$$

In this method, the stimulus-locked component, the covert response-locked component and the overt response-locked component are extracted together with the delays of the covert response-locked component.

The performance of this method is examined by a simulation with artificial data (Fig. 8.2). In this simulation, the original stimulus-locked component, covert response-locked component and overt response-locked component are generated by the exponential, rectangular and cosine functions respectively (Fig. 8.2, A–C). The delays of the covert response-locked component and RTs are generated by Gaussian random numbers (180 ± 50 ms). The simulated signal $y_n(t)$ is generated from the three components according to Eq. (8.1) (Fig. 8.2, E). Then, I estimate the delays of the covert response-locked components and extract the three components by the method. The estimated delays are highly correlated with the original ones ($r = 0.96$, $p < 0.05$, $slope = 0.87$) (Fig. 8.2, H). The correlation coefficients between the original and extracted components are high for all the three components ($r = 0.99$ for the stimulus-locked component; $r = 0.95$ for the covert response-locked component; $r = 0.98$ for the overt response-locked component) (Fig. 8.2, F, G, I). These results indicate that the estimated delays and the extracted components by this method are sufficiently accurate in this simulation, suggestive of the validity of this method.

As mentioned in the "Discussion" section of Chapter 7, it is expected that the EEG during Go trials of the Go/NoGo task includes the three components: the stimulus-locked component,

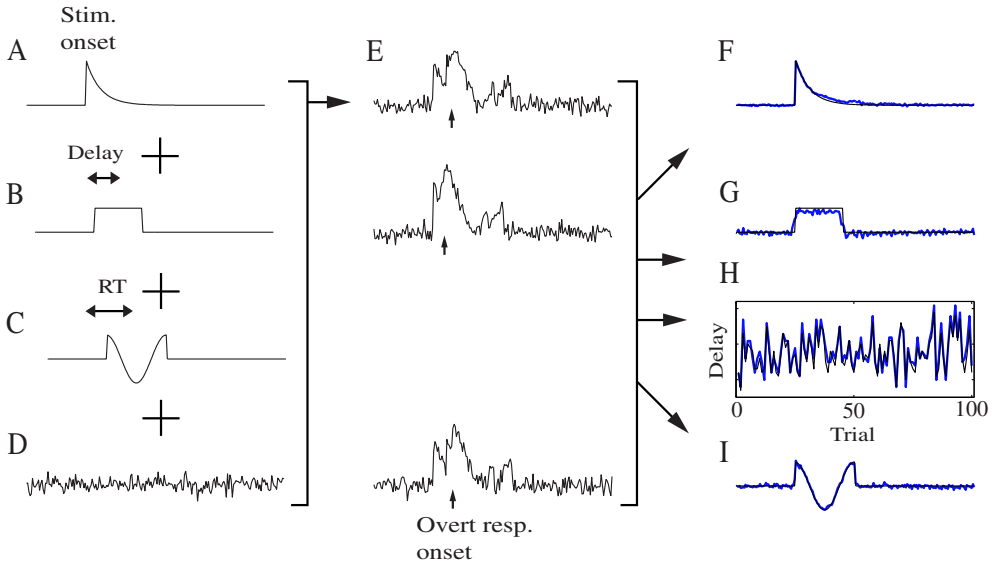

Figure 8.2: Simulation result with artificial data. **A**: Original stimulus-locked component. **B**: Original covert response-locked component shifted by an unknown delay. **C**: Original overt response-locked component shifted by a RT. **D**: Background noise. **E**: Simulated data generated according to Eq. (8.1). **F**: Extracted stimulus-locked component. **G**: Extracted covert response-locked component. **H**: Estimated delays of the covert response-locked component. **I**: Extracted overt response-locked component. The blue lines represent the extracted components and the estimated delays, and the black lines represent the original data.

the covert response-locked component, and the overt response-locked component. Therefore, I apply this method to a subject's EEG at Cz during Go trials of the Go/NoGo task. The average of the estimated delays of the covert response-locked component is adjusted so that the delays represent latencies of the largest positive peak in the extracted covert response-locked component. The estimated delays of the covert response-locked component are 311 ± 62 ms. The validity of the estimated delays is visually confirmed by the fluctuations time-locked to the delays in the time-trial image sorted by the delays (Fig. 8.3, A). The magnitude of the extracted covert response-locked component is comparable with those of the extracted stimulus- and overt response-locked components (Fig. 8.3, D). In the expectation that the covert response-locked component relates to decision making, its delays should correlate with the RTs. However, the correlation coefficient between the delays and RTs is not significantly high ($r = 0.067$, $p > 0.05$) (Fig. 8.3, B). Although I cannot identify the functional role of the extracted covert response-locked components at this time, these results indicate the feasibility of the method for EEG, and indicate the presence of the three components in the EEG during Go trials.

As shown above, based on the two strategies, it is possible to propose various decomposition methods easily. It should be worthwhile developing a family of decomposition methods which are used for broad problems.

8.4 Conclusions

The original question of this thesis is how the human brain operates in daily stimulus-response situations. As the tools to solve this question, in this thesis, I propose two data analysis methods. One is used when responses are observable and the other is used when responses are not observable. These methods decompose EEG signals into the stimulus- and response-locked components. By applying these methods, we can examine brain activity in detail, and, in the future, we will be able to answer the original question, based on the decomposed components.

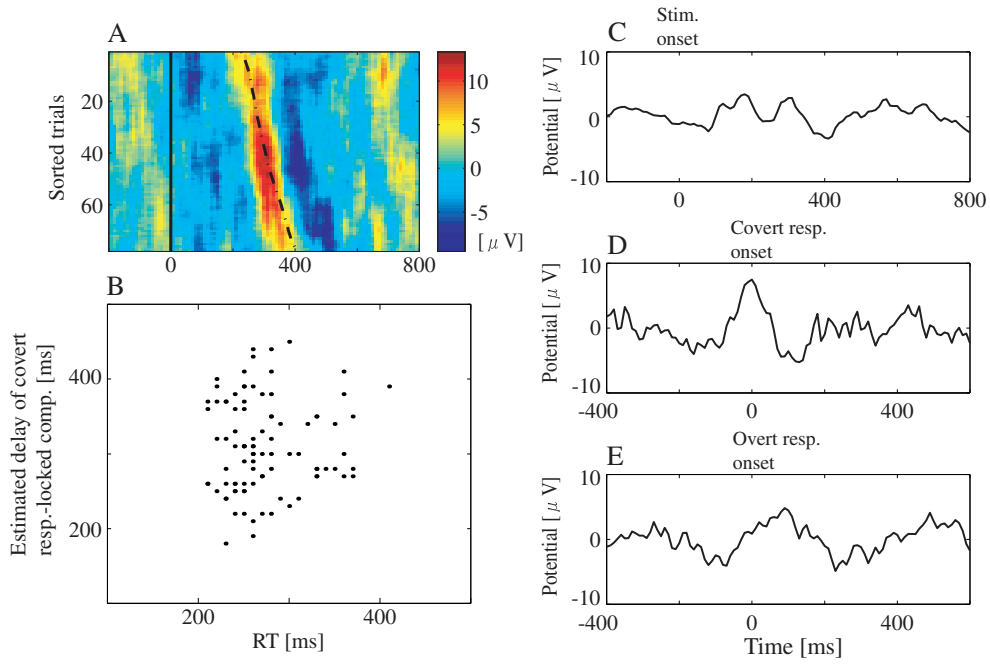

Figure 8.3: Decomposition of a subject's EEG at Cz during Go trials of Go/NoGo task into the stimulus-, covert response- and overt response-locked components. **A**: Time-trial image of the EEG sorted by the estimated delays of the covert response-locked component. The solid line represents the stimulus onsets, and the dotted line represents the estimated delays of the covert response-locked component. **B**: Scatter plot of the RTs and the estimated delays. **C**: Extracted stimulus-locked component. **D**: Extracted covert response-locked component. **E**: Extracted overt response-locked component.

Appendix A

Averages of Extracted Components Depend on c

Only the averages of extracted stimulus- and overt response-locked components vary depending on the parameter c in Eq. (3.8).

To demonstrate this, I performed a simulation test. In this simulation, I generated simulated data by the same procedure as the one in the simulation test with artificial data (Chapter 3), except for setting $v_n(t) = 0$. Then, I extracted the stimulus- and overt response-locked components using different c from the same simulated data, and obtained the residual errors between the extracted and original stimulus-/overt response-locked components. The simulation results show that only the average of the residual errors varies depending on c (Fig. A.1).

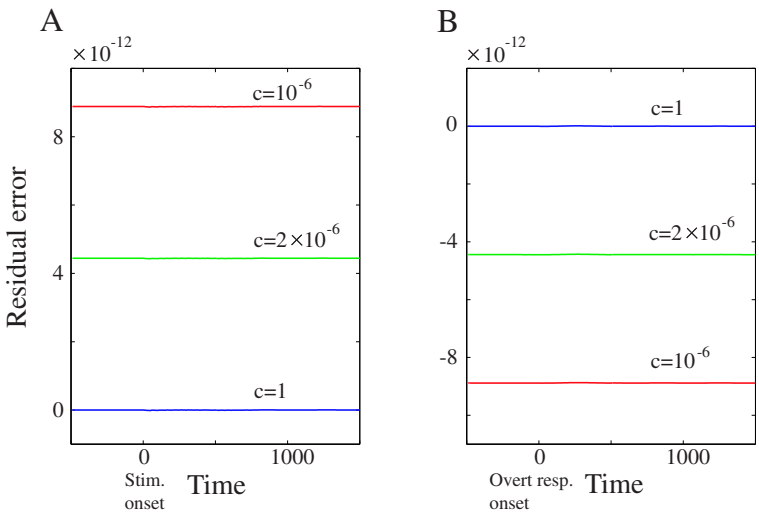

Figure A.1: Residual errors between the original and extracted components using different c. **A**: Result for the extracted stimulus-locked components. **B**: Result for the extracted overt response-locked components.

Appendix B

Parametric Method for Overt Responses

Here, I show a parametric method for obtaining the stimulus- and overt response-locked components from EEG epochs and RTs. In this method, I firstly generate three sweeps $z(t), u_s(t), u_r(t)$ from observed data, then assume a parametric model relating the three sweeps, and finally identify the model.

I generate $z(t)$ by concatenating EEG epochs, generate $u_s(t)$ by:

$$u_s(t) = \begin{cases} 1 & t = \text{Stimulus onset} \\ 0 & t \neq \text{Stimulus onset} \end{cases}, \tag{B.1}$$

and generate $u_r(t)$ by:

$$u_r(t) = \begin{cases} 1 & t = \text{Overt response onset} \\ 0 & t \neq \text{Overt response onset} \end{cases}. \tag{B.2}$$

The three sweeps generated from simulated data are shown in Fig. B.1, A.

Then, I assume that $z(t)$ is expressed by:

$$z(t) = a_1 u_s(t-1) + \cdots + a_{n_s} u_s(t-n_s) + b_1 u_r(t-1) + \cdots + b_{n_r} u_r(t-n_r) + e(t) \quad (t = 0, \cdots, J), \tag{B.3}$$

where $e(t)$ represents noise. Equation (B.3) is considered as a Finite Impulse Response (FIR) system [60,61] with double-input ($u_s(t)$ and $u_r(t)$) and single-output ($z(t)$) (Fig. B.1, A). Further, in Eq. (B.3), the stimulus- and overt response-locked components are respectively represented by

the impulse responses to the individual inputs. Therefore, we can obtain the stimulus- and overt response-locked components by identifying this FIR system.

In the least square method, the parameters in this system are identified by calculating

$$\hat{\boldsymbol{\theta}} = [\boldsymbol{\Omega}^T \boldsymbol{\Omega}]^{-1} \boldsymbol{\Omega} \boldsymbol{x}, \tag{B.4}$$

where

$$\boldsymbol{\theta} = [a_1, \cdots, a_{n_s}, b_1, \cdots, b_{n_r}]^T, \tag{B.5}$$

$$\boldsymbol{\Omega} = \begin{bmatrix} u_s(n_s-1) & \cdots & u_s(0) & u_r(n_r-1) & \cdots & u_r(0) \\ \vdots & \ddots & \vdots & \vdots & \ddots & \vdots \\ u_s(J-1) & \cdots & u_s(J-n_s) & u_r(J-1) & \cdots & u_r(J-n_r) \end{bmatrix}, \tag{B.6}$$

and

$$\boldsymbol{x} = [z(n_s+n_r), z(n_s+n_r+1), \cdots, z(J)]^T. \tag{B.7}$$

In practice, we can use system identification software, such as the System Identification Toolbox for MATLAB (The MathWorks, Inc.) [61].

Figure B.1, B and C show the simulation result obtained by identifying the system shown in Fig. B.1, A. The identified and original stimulus-locked components are highly correlated ($r = 0.97$) (Fig. B.1, B), as are the identified and original overt response-locked components ($r = 0.98$) (Fig. B.1, C). This result indicates that we can also obtain the stimulus- and overt response-locked components by the parametric method.

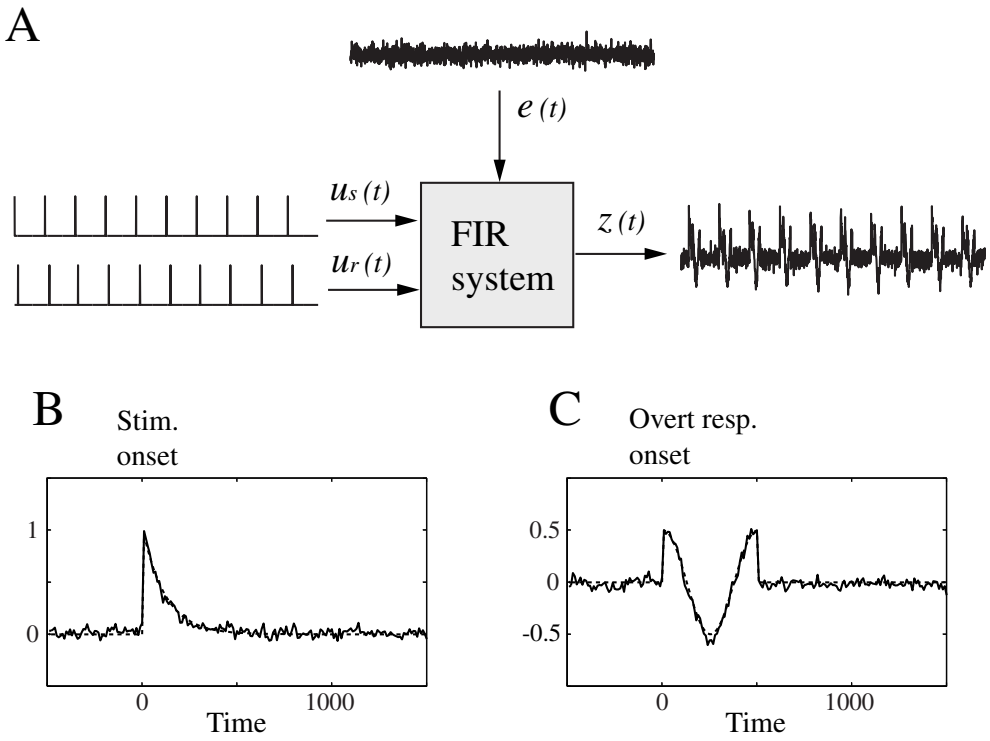

Figure B.1: Parametric method for identifying stimulus- and overt response-locked components. **A**: Schematic representation of the FIR system expressed by Eq. (B.3). **B** and **C**: Stimulus- and overt response-locked components obtained by identifying the FIR system in **A**. **B**: Identified (solid line) and original (dotted line) stimulus-locked components. **C**: Identified (solid line) and original (dotted line) overt response-locked components.

Appendix C

Scalp Distributions of Potentials Earlier than P300 and Later than P160

The scalp distributions of the potentials earlier than the P300 and later than the P160 were not substantially different depending on the methods used.

As examples, in Fig. C.1, I show the scalp distributions of the N100 in the extracted stimulus-locked components and the stimulus-triggered average EEG during the SR-task, and also show the scalp distributions of the N500 in the extracted overt response-locked components and the overt response-triggered average EEG during the SR-task.

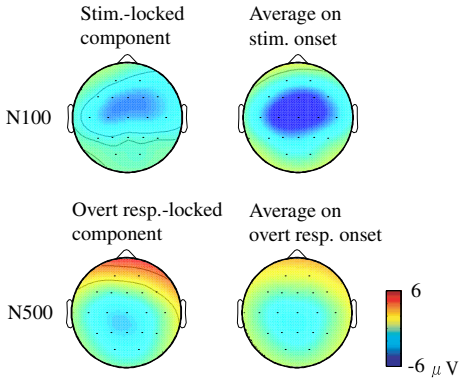

Figure C.1: Scalp distributions of the N100 and N500.

Appendix D

Accuracy of Estimation Depends on Number of Trials

The accuracy of the estimation depends on the number of trials.

To demonstrate this, I performed a simulation test. In this simulation, I generated simulated data by the same procedure as the one in the simulation test with artificial data (Chapter 6). I set the number of trials N to 10, 20, 30, 40, and the SD of noise $v_n(t)$ to 0.5. Then, I estimated the delays of the covert response-locked component from the simulated data, and obtain the correlation coefficients between the estimated and original delays. I repeated this simulation 20 times. The simulation results show that the correlation coefficients become greater as the number of trials increases (Fig. D.1).

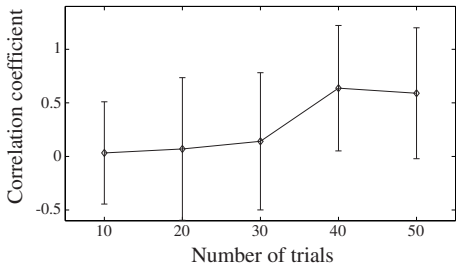

Figure D.1: Correlation coefficients between the original and estimated delays for each number of trials. The diamonds and error bars respectively represent the means and SDs of the correlation coefficients.

Bibliography

[1] Lamarre Y, Busby L, and Spidalieri G. Fast ballistic arm movements triggered by visual, auditory, and somesthetic stimuli in the monkey. i. activity of precentral cortical neurons. *J. Neurophysiol.*, Vol. 50, pp. 1343–1358, 1983.

[2] Nelson RJ. Activity of monkey primary somatosensory cortical neurons changes prior to active movement. *Brain Res.*, Vol. 406, pp. 402–407, 1987.

[3] Nelson RJ, Smith BN, and Douglas VD. Relationships between sensory responsiveness and premovement activity of quickly adapting neurons in areas 3b and 1 of monkey primary somatosensory cortex. *Exp. Brain Res.*, Vol. 84, pp. 75–90, 1991.

[4] Perfiliev SN. Responses in the motor cortex time-locked to the sensory stimuli conditioning target-reaching in the cat. *Neurosci. Res.*, Vol. 32, pp. 273–279, 1998.

[5] Tanji J and Kurata K. Comparison of movement-related activity in two cortical motor areas of primates. *J. Neurophysiol.*, Vol. 48, pp. 633–653, 1982.

[6] Endo H, Kizuka T, Masuda T, and Takeda T. Automatic activation in the human primary motor cortex synchronized with movement preparation. *Cogn. Brain Res.*, Vol. 3, pp. 229–239, 1999.

[7] Jung TP, Makeig S, Westerfield M, Townsend J, Courchesne E, and Sejnowski TJ. Analysis and visualization of single-trial event-related potentials. *Hum. Brain Mapp.*, Vol. 14, pp. 166–185, 2001.

[8] Goodin DS, Aminoff MJ, and Mantle MM. Subclasses of event-related potentials: response-locked and stimulus-locked components. *Ann. Neurol.*, Vol. 20, pp. 603–609, 1986.

[9] CMJ Braun, Villeneuve L, and Gruzelier JH. Topographical analysis of stimulus-related and response-related electrical scalp activity and interhemispheric dynamics in normal humans. *Int. J. Psychophysiol.*, Vol. 46, pp. 109–122, 2002.

[10] Jutten C and Herault J. Blind separation of sources, part i: An adaptive algorithm based on neuromimetic architecture. *Signal Process.*, Vol. 24, pp. 1–10, 1991.

[11] Kayser J and Tenke CE. Principal components analysis of laplacian waveforms as a generic method for identifying erp generator patterns: I. evaluation with auditory oddball tasks. *Clin. Neurophysiol.*, Vol. 117, pp. 348–368, 2006.

[12] Makeig S, Delorme A, Westerfield M, Jung TP, Townsend J, Courchesne E, and Sejinowski TJ. Electroencephalographic brain dynamics following manually responded visual targets. *PLos Biol.*, Vol. 2, pp. 747–762, 2004.

[13] 村田昇. 入門　独立成分分析. 東京電機大学出版局, 2004.

[14] 甘利俊一, 村田昇. 独立成分分析　多変量データ解析の新しい手法. サイエンス社, 2002.

[15] Cerutti S, Baselli G, Liberati D, and Pavesi G. Single sweep analysis of visual evoked potentials through a model of parametric identification. *Biol. Cybern.*, Vol. 56, pp. 111–120, 1987.

[16] Jensen EW, Lindholm P, and Henneberg SW. Autoregressive modeling with exogenous input of middle-latency auditory-evoked potentials to measure rapid changes in depth of anesthesia. *Meth. Inform. Med.*, Vol. 35, pp. 256–260, 1996.

[17] Litvan H, Jensen EW, Galan J, Lund J, Rodriguez BE, Henneberg SW, Caminal P, Villar, and Landeira JM. Comparison of conventional averaged and rapid averaged, autoregressive-based extracted auditory evoked potentials for monitoring the hypnotic level during propofol induction. *Anesthesiology*, Vol. 97, pp. 351–358, 2002.

[18] Woldorff MG. Distortion of erp averages due to overlap from temporally adjacent erps: analysis and correction. *Psychophysiology*, Vol. 30, pp. 98–119, 1993.

[19] 柳澤信夫, 柴崎浩. 神経生理を学ぶ人のために. 医学書院, 2002.

[20] Falkenstein M, Hoormann J, and Hohnsbein J. Erp components in go/nogo tasks and their relation to inhibition. *Acta Psychologica*, Vol. 101, pp. 267–291, 1999.

[21] Hohnsbein J, Falkenstein M, Hoormann J, and Blanke L. Effects of crossmodal divided attention on late erp components. i. simple and choice reaction tasks. *Electroencephalogr. Clin. Neurophysiol*, Vol. 78, pp. 438–446, 1991.

[22] Cummings A, Čeponienė R, Koyama A, Saygin AP, Townsend J, and Dick F. Auditory semantic networks for words and natural sounds. *Brain Res.*, Vol. 1115, pp. 92–107, 2006.

[23] Verleger R and Berg P. The waltzing oddball. *Psychophysiology*, Vol. 28, pp. 468–477, 1991.

[24] Jankelowitz SK and Colebatch JG. Movement-related potentials associated with self-paced, cued and imagined arm movements. *Exp. Brain Res.*, Vol. 147, pp. 98–107, 2002.

[25] Neshige R, Lüders H, and Shibasaki H. Recording of movement-related potentials from scalp and cortex in man. *Brain*, Vol. 111, pp. 719–736, 1988.

[26] Papa SM, Artieda J, and Obeso JA. Cortical activity preceding self-initiated and externally triggered voluntary movement. *Mov. Disord.*, Vol. 6, pp. 217–224, 1991.

[27] Shibasaki H, Barrett G, Halliday E, and Halliday AM. Components of the movement-related cortical potential and their scalp topography. *Electroencephalogr. Clin. Neurophysiol.*, Vol. 111, pp. 719–736, 1980.

[28] David O, Kilner JM, and Friston KJ. Mechanisms of evoked and induced responses in meg/eeg. *NeuroImage*, Vol. 31, pp. 1580–1591, 2006.

[29] Haenschel C, Baldeweg T, Croft RJ, Whittington M, and Gruzelier J. Gamma and beta frequency oscillations in response to novel auditory stimuli: A comparison of human electroencephalogram (eeg) data with in vitro models. *Proc. Natl. Acad. Sci. USA*, Vol. 97, pp. 7645–7650, 2000.

[30] Schürmann M and Başar E. Functional aspects of alpha oscillations in the eeg. *Int. J. Psychophysiol.*, Vol. 39, pp. 151–158, 2001.

[31] Tallon-Baudry C, Bertrand O, Delpuech C, and Pernier J. Stimulus specificity of phase-locked and non-phase-locked 40 hz visual responses in human. *J. Neurosci.*, Vol. 16, pp. 4240–4249, 1996.

[32] Tallon-Baudry C and Bertrand O. Oscillatory gamma activity in humans and its role in object representation. *Trends Cogn. Sci.*, Vol. 3, pp. 151–162, 1999.

[33] Kirmizi-Alsan E, Bayraktaroglu Z, Gurvit H, Keskin YH, Emre M, and Demiralp T. Comparative analysis of event-related potentials during go/nogo and cpt: Decomposition of electrophysiological markers of response inhibition and sustained attention. *Brain Res.*, Vol. 1104, pp. 114–128, 2006.

[34] 電気学会ウェーブレット解析の産業応用に関する協同研究委員会（編）. ウェーブレット解析の産業応用. 朝倉書店, 2005.

[35] Biggins CA, MacKay S, Clark W, and Fein G. Event-related potential evidence for frontal cortex effects of chronic cocaine dependence. *Biol. Psychiatry.*, Vol. 42, pp. 472–485, 1997.

[36] Jaśkowski P and Verleger R. Amplitudes and latencies of single-trial erp's estimated by a maximum-likelihood method. *IEEE Trans. Biomed. Eng.*, Vol. 46, pp. 987–993, 1999.

[37] Jaśkowski P and Verleger R. An evaluation of methods for single-trial estimation of p3 latency. *Psychophysiol.*, Vol. 37, pp. 153–162, 2000.

[38] McGillem CD, Aunon JI, and Pomalaza CA. Improved waveform estimation procedures for event-related potentials. *IEEE Trans. Biomed. Eng.*, Vol. 32, pp. 371–379, 1985.

[39] Möcks J, Köhler W, Gasser T, and Pham DT. Novel approaches to the problem of latency jitter. *Psychophysiol.*, Vol. 25, pp. 217–226, 1988.

[40] Pham DT, Möcks J, Köhler W, and Gasser T. Variable latencies of noisy signals: estimation and testing in brain potential data. *Biometrika*, Vol. 74, pp. 525–533, 1987.

[41] Puce A, Berkovic SF, Cadusch PJ, and Bladin PF. P3 latency jitter assessed using 2 techniques. i. simulated data and surface recordings in normal subjects. *Neurophysiol.*, Vol. 92, pp. 352–364, 1994.

[42] Puce A, Berkovic SF, Cadusch PJ, and Bladin PF. P3 latency jitter assessed using 2 techniques. ii. surface and sphenoidal recordings in subjects with focal epilepsy. *Electroencephalogr. Clin. Neurophysiol.*, Vol. 92, pp. 555–567, 1994.

[43] Woody CD. Characterization of an adaptive filter for the analysis of variable latency neuroelectric signals. *Med. Biol. Eng.*, Vol. 5, pp. 539–553, 1967.

[44] 長尾智晴. 最適化アルゴリズム. 昭晃堂, 2000.

[45] Kirkpatrick S, Gelatt Jr CD, and Vecchi MP. Optimization by simulated annealing. *Science*, Vol. 220, pp. 671–680, 1983.

[46] 茨木俊秀. 離散最適化法とアルゴリズム. 岩波書店, 1993.

[47] Zhigljavsky AA. *Theory of global random search.* Kluwer Academic Publishers, 1991.

[48] Holland JH. *Adaptation in natural and artificial systems.* The Univ. Michigan Press, 1975.

[49] 合原一幸（編）. カオス時系列解析の基礎と応用. 産業図書, 2000.

[50] Walter WG, Cooper R, Aldridge VJ, Mccallum WC, and Winter AL. Contingent negative variation: an electric sign of sensori-motor association and expectancy in the human brain. *Nature*, Vol. 203, pp. 380–384, 1964.

[51] Bokura H, Yamaguch S, and Kobayashi S. Electrophysiological correlates for response inhibition in a go/nogo task. *Clin. Neurophysiol.*, Vol. 112, pp. 2224–2232, 2001.

[52] Kok A. Overlap between p300 and movement-related-potentials: a response to verleger. *Biol. Psychol.*, Vol. 27, pp. 51–58, 1988.

[53] Yamanaka K, Kimura T, Miyazaki M, Kawashima N, Nozaki D, Nakazawa K, Yano H, and Yamamoto Y. Human cortical activities during go/nogo tasks with opposite motor control paradigms. *Exp Brain Res*, Vol. 142, pp. 301–307, 2002.

[54] Verleger R, Jaśkowski P, and Wascher E. Evidence for an integrative role of p3b in linking reaction to perception. *J. Psychophysiol.*, Vol. 19, pp. 165–181, 2005.

[55] Verleger R. The true p3 is hard to see: some comments on kok's (1986) paper on degraded stimuli. *Biol. Psychol.*, Vol. 27, pp. 45–50, 1988.

[56] Verleger R, Paehge T, Kolev V, Yordanova J, and Jaśkowski P. On the relation of movement-related potentials to the go/no-go effect on p3. *Biol. Psychol.*, Vol. 73, pp. 298–313, 2006.

[57] Cunnington R, Iansek R, and Bradshaw JL. Relationships between movement initiation times and movement-related cortical potentials in parkinson ' s disease. *Hum Mov Sci*, Vol. 18, pp. 443–459, 2006.

[58] Golob EJ and Starr A. Effects of stimulus sequence on event-related potentials and reaction time during target detection in alzheimer ' s disease. *Clin Neurophysiol*, Vol. 111, pp. 1438–1449, 2000.

[59] Jung-Beeman M, Bowden EM, Haberman J, Frymiare JL, Arambel-Liu S, Greenblatt R, Reber PJ, and Kounios J. Neural activity when people solve verbal problems with insight. *Plos Biol.*, Vol. 2, pp. 500–510, 2004.

[60] 相良節夫, 中溝高好, 秋月影雄, 片山徹. システム同定. 計測自動制御学会, 1987.

[61] 足立修一. MATLAB による制御のためのシステム同定. 東京電機大学出版局, 1996.